Inaugural dissertation

for

obtaining the doctoral degree

of the

Combined Faculty of Mathematics, Engineering and Natural Sciences

of the

Ruprecht - Karls - University

Heidelberg

Presented by

M.Sc. Karina Berschneider

born in: Amberg

Oral examination: 16.03.2023

Functional and molecular characterization of the effects of *Arnica montana* L. extracts and corresponding lead compounds on primary human T cells

Referees:

Prof. Dr. Stefan Wölfl

Prof. Dr. Yvonne Samstag

„Der Unterschied zwischen dem Unmöglichen und dem Möglichen liegt in der Entschlossenheit einer Person.“

Tommy Lasorda

Abstract

Arnica montana L. (Arnica) has a long tradition of use in treating inflammation and promoting tissue regeneration after blunt injuries such as contusions or bruises. Various immune cell types, including T cells, were shown to be critically involved in the normal muscle healing process in response to trauma. They invade the injured site in a spatiotemporally controlled manner and rapidly induce a proinflammatory milieu, which is necessary for proper wound healing. Prolonged presence of T cells, however, was found to be a hallmark of delayed muscle healing. Therefore, investigating the effects of Arnica preparations on T cell functions offers the possibility to gain novel insights and explanations regarding Arnica's mode of action.

In this thesis, differentially prepared Arnica extracts and the lead compounds Thymol and Helenalin were directly compared for their immunomodulatory potential using primary human T cells. The three selected Arnica extracts as well as the lead compounds inhibited T cell activation, measured by analyzing CD25 surface expression. Similarly, all test drugs diminished the proliferative capacity of T cells. Both, a reduced production of the growth factor IL-2 as well as limited affinity of the IL-2 receptor (IL-2R) due to lacking IL-2Rα chain (CD25) can explain the decreased cell division rate. Despite similar functional effects, different molecular mechanisms underlying drug action were identified. While the tested root extract specifically inhibited DNA binding of the transcription factor NFκB (p65), the fermented aqueous extract prepared from the whole plant interfered with NFAT-dependent gene expression. In contrast, the hydroalcoholic whole plant extract diminished NFκB DNA binding as well as NFAT-dependent gene expression without reaching statistical significance. The molecular mode of action identified for the lead compounds was again different. Thymol interfered with intracellular signaling at various steps, including NFκB nuclear translocation and transcriptional activity as well as calcium signaling and NFAT-dependent gene expression. Helenalin specifically inhibited nuclear translocation of NFκB (p50).

In order to draw conclusions about which phytochemical compounds might mediate the extracts' effects, the plant extracts were analyzed by HPLC-MS/MS followed by tentative identification of extract components. This analysis provided interesting results, since Helenalin was not found at detectable levels in any of the three Arnica extracts. Instead, Caffeoylquinic acid derivatives constituted the main identified substance group. Testing isolated (Mono-, di-, and tri-) Caffeoylquinic acids, however, revealed that the effects observed upon treating T cells with Arnica extract were not mimicked by Caffeoylquinic acids.

Given the inhibitory effect on T cell functions identified in this thesis, Arnica preparations might indeed have a positive influence on restoring the normal muscle healing process in the setting of delayed tissue repair. In contrast, interfering with T cell activity too early during normal muscle regeneration might rather have detrimental effects by inhibiting the initial inflammatory phase, which is essential for normal healing.

Zusammenfassung

Arnica montana L. (Arnika) wird traditionell zur Behandlung von Entzündungen und zur Förderung der Geweberegeneration nach stumpfen Verletzungen, wie zum Beispiel Prellungen und Quetschungen, angewendet. Verschiedene Immunzelltypen, unter anderem auch T-Zellen, tragen wesentlich zur normalen Muskelheilung in Folge eines Traumas bei. Sie dringen räumlich-zeitlich kontrolliert in die verletzte Stelle ein und induzieren ein entzündliches Milieu, welches essentiell für die Wundheilung ist. Allerdings wurde eine verlängerte Anwesenheit von T-Zellen mit verzögerter Muskelheilung assoziiert. Deshalb eröffnet die Untersuchung der Wirkung von Arnika Präparaten auf T-Zellen neue Möglichkeiten, deren Wirkweise zu erklären.

In dieser Doktorarbeit wurden unterschiedlich hergestellte Arnika Extrakte sowie die Leitsubstanzen Thymol und Helenalin im direkten Vergleich auf ihr immunmodulierendes Potential untersucht, wofür primäre menschliche T-Zellen verwendet wurden. Die drei ausgewählten Arnika Extrakte sowie die beiden Leitsubstanzen inhibierten die Aktivierung von T-Zellen, was anhand der Oberflächenexpression von CD25 untersucht wurde. Ebenso verringerten alle Testsubstanzen die Zellteilungskapazität von T-Zellen. Sowohl eine verminderte Produktion des Wachstumsfaktors IL-2 sowie die eingeschränkte Affinität des IL-2 Rezeptors (IL-2R) aufgrund fehlender IL-2Rα-Kette (CD25) liefern eine Erklärung für die reduzierte Teilungsrate. Trotz ähnlicher Effekte auf funktionaler Ebene wurden unterschiedliche molekulare Wirkmechanismen der Testsubstanzen identifiziert. Während das getestete Wurzelextrakt spezifisch die DNA-Bindung des Transkriptionsfaktors NFκB (p65) inhibierte, beeinträchtigte das aus der ganzen Pflanze hergestellte und fermentierte wässrige Extrakt NFAT-abhängige Genexpression. Im Gegensatz dazu verringerte das hydroalkoholische Extrakt der ganzen Pflanze sowohl die DNA-Bindung von NFκB, als auch NFAT-abhängige Genexpression, allerdings nicht signifikant. Wiederum andere Wirkmechanismen wurden mit den Leitsubstanzen assoziiert. Thymol griff an mehreren Stellen in intrazelluläre Signalwege ein. Sowohl die Kerntranslokation und transkriptionelle Aktivität von NFκB, als auch die Calcium-Signalkaskade und NFAT-abhängige Genexpression waren verringert. Helenalin inhibierte spezifisch die Kerntranslokation von NFκB (p50).

Um Rückschlüsse über die phytochemischen Komponenten, die die Effekte der Pflanzenextrakte vermitteln, ziehen zu können, wurden die Extrakte mittels HPLC-MS/MS mit anschließender literaturbasierter Identifikation der Extrakt-Komponenten analysiert. Interessanterweise war Helenalin in keinem der drei getesteten Extrakte detektierbar. Stattdessen wurden die Derivate der Caffeoylchinasäure als Hauptkomponente identifiziert. Die Effekte von Arnika Extrakten auf T-Zellen waren jedoch mit keiner der getesteten, isolierten (Mono-, di-, oder tri-) Caffeoylchinasäure reproduzierbar.

Der in dieser Doktorarbeit charakterisierte, inhibitorische Effekt auf die Funktion von T-Zellen unterstützt den angenommenen positiven Einfluss von Arnika auf die Wiederherstellung des normalen Muskelheilungsprozesses bei bestehender verzögerter Gewebereparatur. Es ist allerdings zu beachten, dass ein zu frühes Eingreifen und damit eine Inhibition der wichtigen entzündlichen Phase zu Beginn der normalen Muskelregeneration den Heilungsprozess eher negativ beeinflussen könnte.

Table of Content

Contributions

The qPCR analysis (results see Figure 20A) was conducted by Simone Fomuki (Heidelberg University Hospital, Institute of Immunology, AG Giese). Ralph Röth (Heidelberg University Hospital, Institute of Human Genetics and nCounter Core Facility, AG Niesler) performed the nCounter run for gene expression analysis. For detailed description of his contribution, please refer to section 2.2.15. The KEGG pathway gene set enrichment analysis was done by Dr. Carsten Sticht (Heidelberg University, Medical Faculty Mannheim, NGS Core Facility). Phytochemical characterization of the plant extracts by HPLC-MS/MS and tentative identification of extract compounds was carried out by Dr. Bernhard Wetterauer (Heidelberg University, Institute of Pharmacy and Molecular Biotechnology, Pharmaceutical Biology).

1 Introduction

1.1 The human immune system

Since the human body is continuously exposed to potentially harmful organisms, the immune system has the essential function to prevent infection and fight invading pathogens. In principle, the immune system can be divided into two parts, the innate immunity and the adaptive immunity. While the innate immune system is able to react immediately but nonspecifically, adaptive immune responses are specific against a certain microorganism or antigen but require days or even weeks to be established. Another difference is that adaptive immunity, in contrast to innate immunity, can provide long-lasting protection from recurrent infection by development of a so-called immunological memory.

1.1.1 Innate immunity

By creating a natural barrier between an organism and its environment, the skin as well as mucous membranes represent the first line of defense against pathogens. These surfaces are furthermore covered with antimicrobial peptides such as lysozyme or defensins. In case a pathogen can overcome the barriers and invade the human body, the complement system will be activated. This system comprises a number of plasma proteins that are activated in a cascade to opsonize pathogens and induce inflammation to fight infection.

Innate immunity furthermore includes various effector cells like macrophages, dendritic cells (DCs), monocytes and granulocytes. These cells express pattern recognition receptors (PRRs) such as Toll-like receptors (TLRs) (1–3) to sense microorganisms and react by releasing cytokines and other inflammatory mediators. Phagocytes, including granulocytes, macrophages and DCs, have the capacity to engulf and digest foreign particles, which is important for pathogen clearance. Furthermore, macrophages and DCs fulfil the essential function of bridging innate and adaptive immunity due to their function as professional antigen-presenting cells (pAPCs). Peptides of particles digested by pAPCs are loaded on major histocompatibility complex (MHC) class II (MHC-II) molecules and presented on the cell surface. This presentation of antigens forms the basis for specific activation of adaptive immune cells.

1.1.2 Adaptive immunity

While the innate immune system includes various effector cells, B cells and T cells execute the cellular and humoral responses linked to adaptive immunity. Both lymphocyte types are derived from hematopoietic stem cells residing in the bone marrow. B cells undergo maturation in the bone marrow and are released to the periphery as mature B cells coexpressing immunoglobulin D (IgD) and immunoglobulin M (IgM) as membrane-bound antibodies. In contrast, T cell maturation takes place in the thymus.

The maturation process includes two selection steps, which ensure that released T cells are capable of binding to MHC complexes (positive selection) but not recognizing self-antigens (negative selection) to prevent autoimmunity. During thymic development, T cells furthermore undergo somatic recombination, whereby individual T cell clones expressing unique T cell receptors (TCRs) are generated. While the majority of T cells expresses an αß TCR (αß T cells), 1 – 5 % of mature T cells are bearing a γδ TCR (γδ T cells) (4). The following sections focus on the predominant αß T cells, which express α- and ß-chains of the TCR and either CD4 or CD8 as coreceptor.

Via the TCRs, T cells can recognize their cognate antigen but only when bound to MHC molecules (MHC restriction). $CD4^+$ T cells specifically bind to MHC-II, whereas $CD8^+$ T cells only recognize MHC class I (MHC-I). This is connected to the completely different function of the two T cell populations. CD8 is expressed by cytotoxic T cells that play a decisive role in the protection from intracellular pathogens and elimination of malignant cells using their lytic granules. Consistent with this, all nucleated cells of the body express MHC-I and are thus able to activate cytotoxic T cells. $CD4^+$ T cells, also called T helper cells (Th cells), fulfill important regulatory functions by shaping the immune response to pathogens. Naïve $CD4^+$ T cells are activated by peptide loaded on MHC-II, which is expressed by pAPCs. Depending on the antigen, TCR signaling strength and the surrounding cytokine milieu, differentiation into distinct Th cell subsets is initiated following activation (Figure 1) (reviewed by (5)). They can be categorized into Th1, Th2, Th9, Th17, Th22, T follicular helper (Tfh) cells and regulatory T cells (Tregs). The subsets differ in their cell surface receptors, master transcription factors and the secreted cytokines. In general, pro-inflammatory Th1, Th9 and Th17 cells can be distinguished from anti-inflammatory Th2 cells and Tregs. Th22 cells cannot be finally classified into either of the two groups. Tfh cells provide B cell help and are thus involved in antibody production (6).

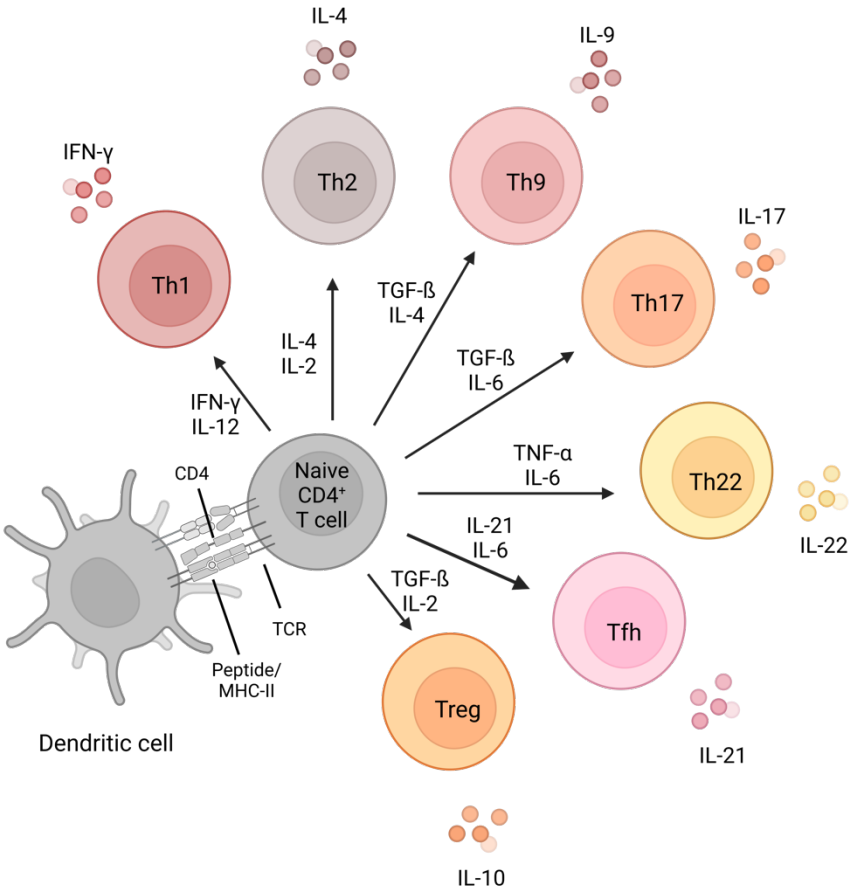

Figure 1: Th cell subset differentiation.

APCs like DCs can activate naïve $CD4^+$ T cells and induce differentiation into different Th cell subsets. Especially the surrounding cytokine milieu influences the differentiation process. The combination of IFN-γ and IL-12, for example, favors the generation of Th1 cells, which are characterized by IFN-γ secretion and are thus considered as pro-inflammatory. IL-10-producing Tregs, in contrast, are categorized as anti-inflammatory. Since each subset fulfils a defined role in cell-mediated immunity, Th subset differentiation needs to be tightly controlled. This figure was created with BioRender.com and modified from (7).

1.2 T cell activation

Naïve T cells constantly patrol the human body to search for their cognate antigen. They therefore circulate through the blood and the lymphatic system. Due to MHC restriction, T cells need to get in direct contact with pAPCs to be activated. DCs take up antigen in the periphery and subsequently migrate towards the lymph nodes. During the migration process, DCs undergo maturation and upregulate the expression of costimulatory molecules such as CD80/CD86 (reviewed by (8)). Within the lymph nodes DCs can directly interact with naïve T cells by forming a so-called immune synapse (Figure 2A). To be fully activated, T cells need to receive two independent signals. The first signal is transmitted by ligation of the TCR/CD3 complex to its cognate peptide-MHC complex. Secondly, a costimulatory signal such as ligation of CD80/CD86 to CD28 on the T cell is required. Ligation of the TCR without costimulation results in T cell anergy (9,10).

Apart from this, also the surrounding cytokine milieu influences T cell activation. Following costimulation, naïve T cells undergo clonal expansion, known as proliferation, and start to differentiate into distinct effector and memory T cell subsets.

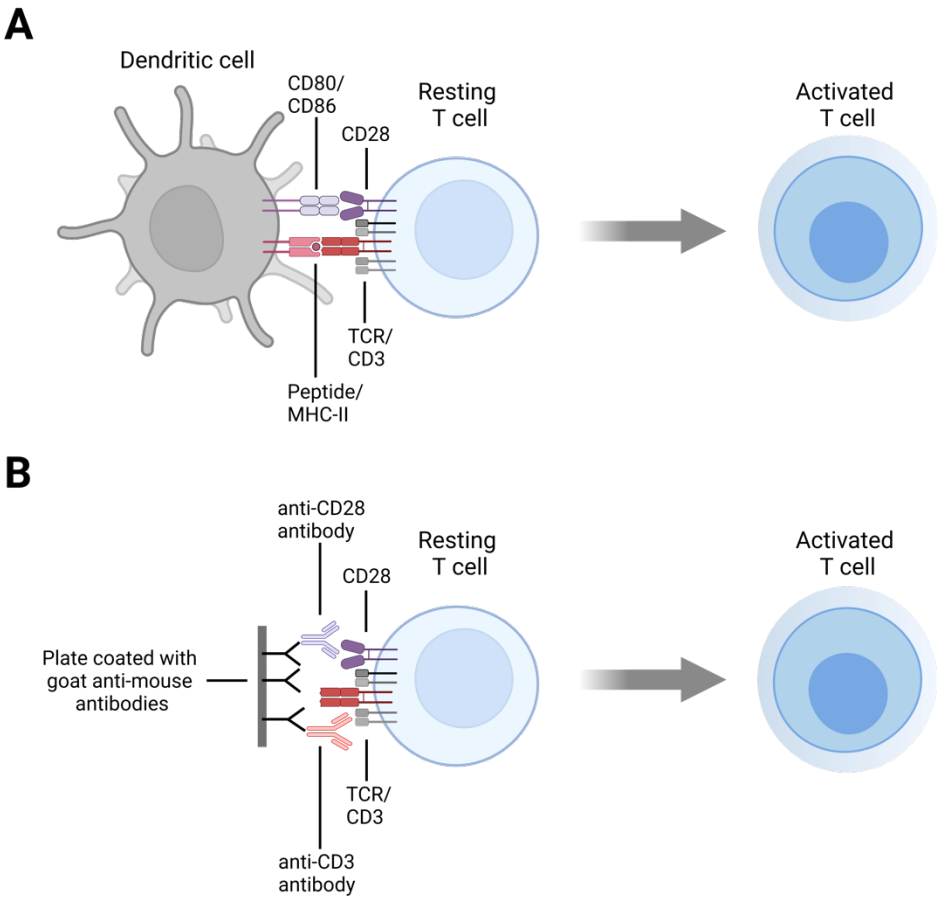

Figure 2: Physiological versus experimental activation of T cells.
(**A**) Under physiological conditions, APCs like DCs can activate resting T cells, wherefore two interactions are required. First, peptide loaded on MHC-II ligates to its cognate TCR/CD3 complex. Second, the costimulatory ligand CD80 or CD86 binds to the costimulatory receptor CD28 on T cells. Only the combination of both signals results in proper T cell activation. (**B**) *In vivo* T cell stimulation by APCs can be mimicked *in vitro* using plate-bound antibodies against CD3 and CD28. This figure was created with BioRender.com.

In vivo T cell activation by DCs can be mimicked *in vitro* using antibodies against the CD3 complex, a coreceptor noncovalently associated with the TCR, and the costimulatory receptor CD28 (Figure 2B). Therefore, plates are first coated with goat anti-mouse antibodies which can subsequently be coupled to mouse-derived anti-CD3 and anti-CD28 antibodies. This combination of antibodies closely resembles natural T cell activation and induces various T cell effector functions like proliferation and cytokine production (Figure 3).

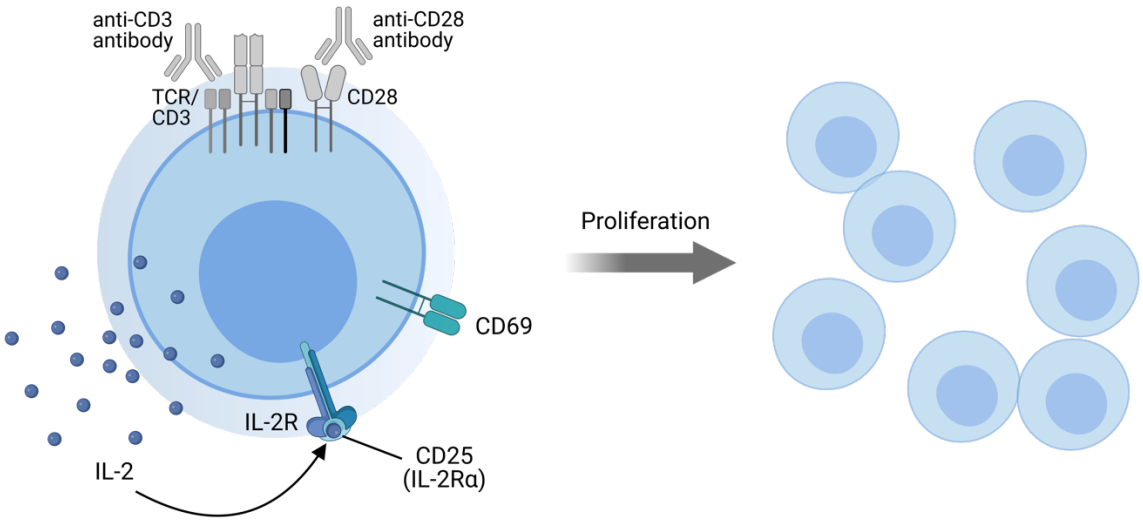

Figure 3: T cell activation via anti-CD3/CD28 antibodies induces T cell effector functions.
Comparable to T cell activation by antigen-presenting cells, *in vitro* stimulation via anti-CD3/CD28 antibodies induces T cell effector functions such as production of the cytokine IL-2. This growth factor binds in an autocrine and paracrine manner to its receptor (IL-2R) and thereby induces T cell proliferation. T cells upregulate certain surface proteins, including CD69 and CD25, upon stimulation. CD25 constitutes the IL-2Rα chain and is essential for formation of a high-affinity IL-2R. CD69 is involved in T cell migration and lymphocyte homing to the lymph nodes. This figure was created with BioRender.com.

1.3 TCR and costimulatory signaling pathways

TCR ligation induces a complex network of signaling pathways that control T cell effector functions (reviewed by (11)). An overview of the TCR signaling cascades is presented in Figure 4. An early event occurring upon TCR-mediated T cell activation is phosphorylation of the CD3 immunoreceptor tyrosine-based activation motifs (ITAMs) by lymphocyte-specific protein tyrosine kinase (LCK) (12,13). Subsequent zeta-chain-associated protein kinase 70 (ZAP70) recruitment to the TCR/CD3 complex and activation promotes downstream signaling (14,15). Phosphorylation of the linker for activation of T cells (LAT) (16) and SH2 domain-containing leukocyte protein of 76 kDa (SLP-76) (17) are among the most important functions of ZAP70 . These proteins serve as a scaffold for the recruitment of further signaling molecules such as interleukin-2-inducible tyrosine kinase (ITK) and VAV1. VAV1, a guanine nucleotide exchange factor for Rho family GTPases, activates Rac and Cdc42 and regulates rearrangement of the cytoskeleton (18,19). ITK-mediated phosphorylation of phospholipase Cγ1 (PLCγ1) induces production of the second messengers diacylglycerol (DAG) and inositol 1,4,5-trisphosphate (IP3) by hydrolysis of phosphatidylinositol 4,5-bisphosphate (PIP2) (20,21). While DAG is necessary for activation of Protein kinase Cθ (PKCθ) and the mitogen-activated protein kinase/Erk (MAPK/Erk) pathway via Ras (22–24), IP3 is critically involved in promoting calcium (Ca^{2+}) release from the endoplasmic reticulum (ER) (25,26).

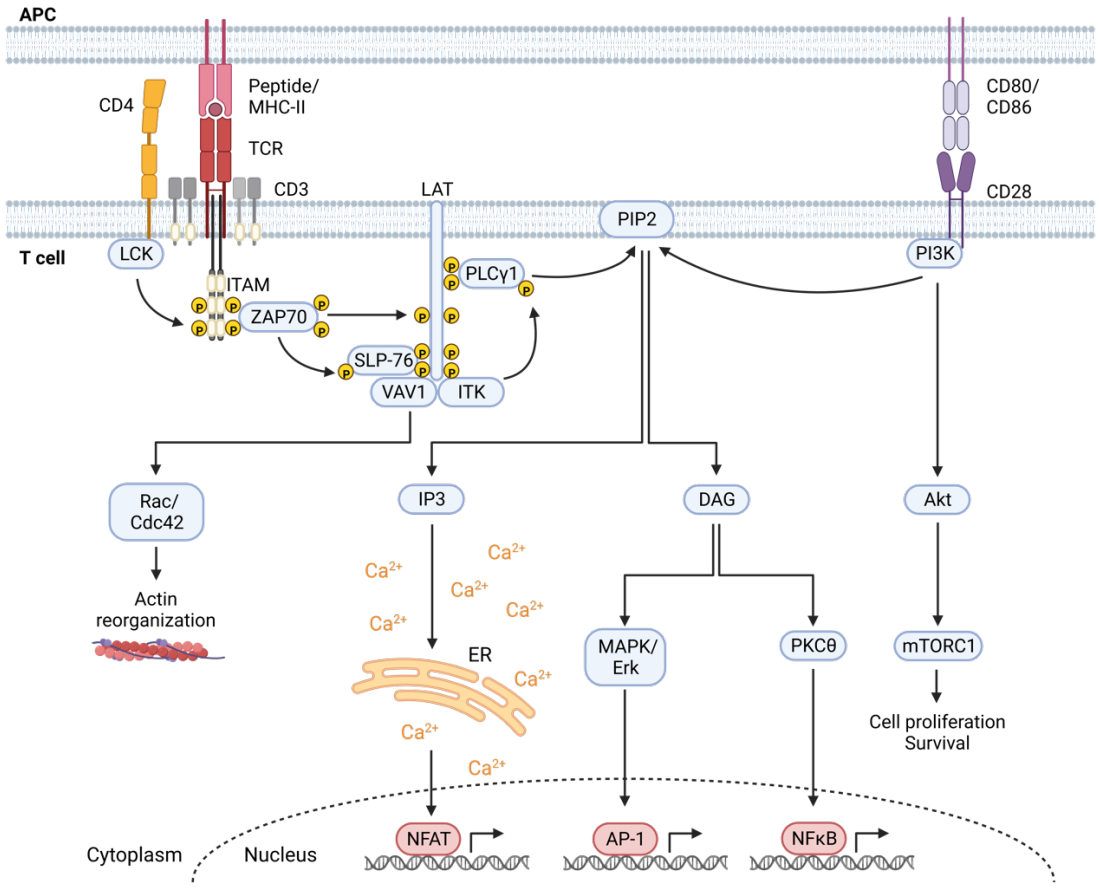

Figure 4: TCR and costimulatory signaling pathways.

Upon TCR engagement, various intracellular signaling cascades are induced. The first event consists in the phosphorylation of CD3 ITAMs by CD4-bound LCK, followed by sequential activation of further kinases. LAT and SLP-76 serve as a scaffold for the assembly of multi-protein complexes. Costimulatory signals, transmitted for example through the costimulatory receptor CD28, are required for full activation of naïve T cells. CD28-mediated signaling via PI3K not only augments TCR signaling but also promotes cell proliferation and survival via Akt and mTORC1. All in all, T cell activation results in the activation of three major transcription factor families, namely AP-1, NFκB and NFAT. Furthermore, VAV1-mediated activation of Rac/Cdc42 leads to reorganization of the actin cytoskeleton. This figure was created with BioRender.com.

Apart from TCR-mediated signaling, full T cell activation requires costimulation via costimulatory receptors such as CD28 (Figure 4). Phosphatidylinositol 3-kinase (PI3K) catalyzes the hydrolysis of PIP2 to IP3 and DAG and thereby amplifies TCR signaling. Furthermore, PI3K-mediated prolonged activation of protein kinase B (PKB or Akt) supports glucose metabolism and thus cell proliferation and survival via mammalian target of rapamycin complex 1 (mTORC1) (27). Costimulatory signals are also involved in rearrangement of the actin cytoskeleton. In this context, our group identified two important actin-remodeling proteins, namely L-plastin (LPL) and cofilin, which are activated upon T cell costimulation (28–31). The actin-bundling protein LPL is activated by ribosomal protein S6 kinase ($p90^{RSK}$)-mediated phosphorylation at serine-5 (32,33). Activation of the actin severing and depolymerization function of cofilin requires dephosphorylation at serine-3 by phosphatases such as protein

phosphatase 1 (PP1) and PP2A (34). The activity of both proteins is not only controlled by the phosphorylation state, but also by the redox state of the surrounding milieu. Oxidation of cofilin upon oxidative stress was shown to render T cells hyporesponsive due to impaired actin dynamics (35) and the activity of LPL is also limited by oxidation (36).

All in all, TCR ligation in combination with costimulation induces three major transcription factor families including activator protein 1 (AP-1), nuclear factor kappa-light-chain-enhancer of activated B cells (NFκB), and Ca^{2+}/Calcineurin/nuclear factor of activated T cells (NFAT). However, it should be considered that TCR signaling is not a linear event but rather includes complex feedback and feedforward regulation.

1.3.1 NFκB signaling pathway

NFκB constitutes a family of eukaryotic transcription factors that controls expression of a variety of immunity- and inflammation-related genes. Five members with structural similarity can be distinguished: p50 (or NFκB1), p52 (or NFκB2), p65 (or RelA), RelB and c-Rel. They form homo- and heterodimers, which is a prerequisite for DNA binding. NFκB activation can be induced either via the canonical (also called classical) (Figure 5A) or the non-canonical (also called alternative) pathway (Figure 5B).

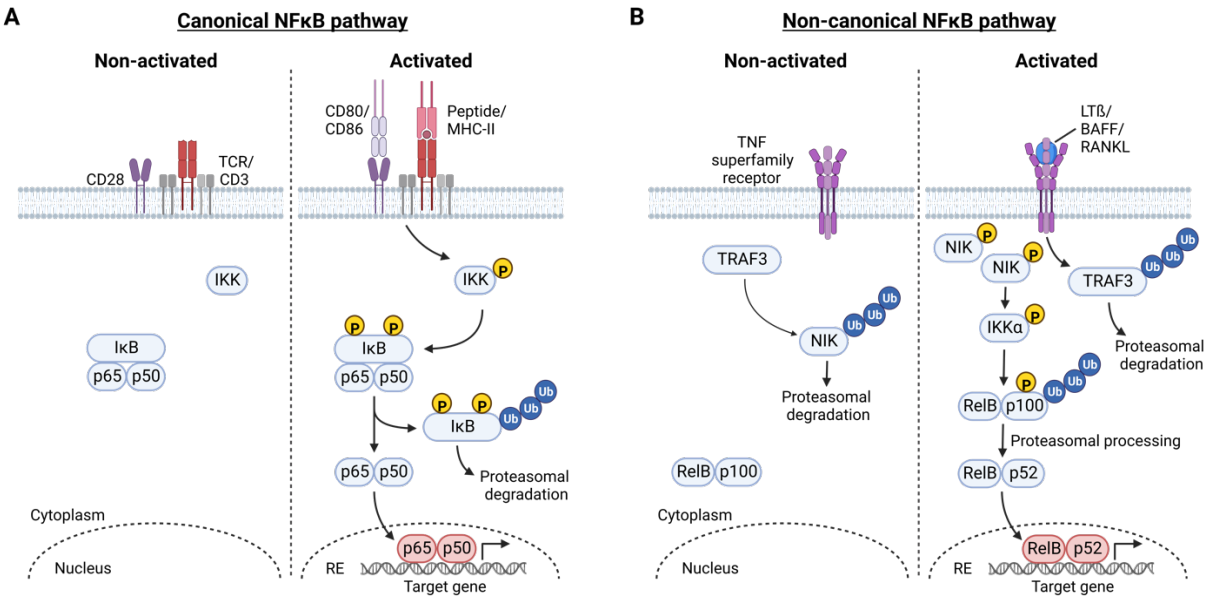

Figure 5: Canonical versus non-canonical NFκB pathway.

(**A**) Activation of the canonical NFκB pathway can be induced via different receptors, including the TCR. In unstimulated cells, NFκB p65/p50 is inactive in the cytoplasm. Upon T cell stimulation, the inhibitor IκB is subjected to proteasomal degradation. NFκB p65/p50 is released, translocates to the nucleus and induces target gene transcription. (**B**) The non-canonical NFκB pathway is specifically activated by TNF superfamily receptors. Under resting conditions, TRAF3 induces proteasomal degradation of NIK. Upon activation, NIK can accumulate and mediate proteasomal processing of RelB-bound NFκB p100 to p52. The active RelB/p52 dimer can then translocate to the nucleus and induce target gene expression. This figure was created with BioRender.com and modified from (37).

Most abundant and best studied is the NFκB heterodimer p65/p50 that is activated via the canonical pathway. In unstimulated cells, the inhibitor IκB is bound to NFκB and retains the transcription factor in the cytoplasm (38). As it is already present in an inactive form in resting cells, NFκB p65/p50 can be quickly activated without the need for new protein synthesis. The canonical pathway integrates signals initiated by cell surface receptors, including the TCR, B cell receptor, PRRs or cytokine receptors. All these stimuli result in activation of the IκB kinase (IKK) complex, which phosphorylates IκB and induces its degradation (39). Thereby, NFκB is released and can translocate to the nucleus via its nuclear localization sequence. Interestingly, PP1 activity, which is linked to cofilin dephosphorylation and thereby activation, is a prerequisite for nuclear translocation of NFκB p65, underlining the interplay between TCR and costimulatory signaling (40). Within the nucleus, NFκB binds to its consensus DNA sequence within the promoter region of target genes, called response element (RE). Unlike p50, which is primarily necessary for DNA binding, the p65 subunit controls gene expression by initiating transcription (41,42). For optimal activation, NFκB subunits themselves can be phosphorylated. p50 phosphorylation at S337, for example, was associated with enhanced DNA binding (43). A number of regulatory phosphorylation sites, including S529 and S536, were also identified for p65 and found to result in enhanced transactivation potential (44,45). NFκB p65/p50 activation occurs quickly, but only transiently as it also controls expression of negative regulators like IκB (46). This negative feedback regulation is essential to prevent excess production of proinflammatory mediators.

Non-canonical activation of NFκB can be induced via tumor necrosis factor (TNF) superfamily receptors like lymphotoxin-ß receptor (LTßR), B-cell activating factor receptor (BAFFR) or receptor activator of NFκB (RANK), specifically (47–50). The non-canonical pathway does not rely on IκB degradation but rather on generation of functional NFκB p52 from the p100 precursor protein. Under resting conditions, TNF receptor-associated factor 3 (TRAF3) mediates NFκB-inducing kinase (NIK) ubiquitination and degradation. Upon stimulation, however, NIK can accumulate since TRAF3 is ubiquitinated and subsequently degraded (51). NIK activates IKKα, which is critically involved in the non-canonical NFκB pathway as it phosphorylates p100, which then undergoes proteasomal processing to p52 (52,53). Subsequently, the non-canonical NFκB heterodimer RelB/p52 can translocate to the nucleus, bind to NFκB REs and initiate target gene transcription. RelB/p52 regulates development of lymphoid organs, B and T cells as well as effector and memory T cell differentiation and maintenance (54).

1.3.2 Calcium/Calcineurin/NFAT signaling pathway

Calcium functions as a second messenger in controlling activation, proliferation and apoptosis of cells. Given a cytosolic Ca^{2+} concentration of about 50 – 100 nM in resting T cells and an extracellular concentration in millimolar range, a natural calcium gradient is formed across the plasma membrane. Calcium transport is controlled by Ca^{2+} channels, Ca^{2+}/H^{+} ATPase, and Na^{+}/ Ca^{2+} exchangers. While resting cells are characterized by low cytosolic Ca^{2+} levels, IP3 induces Ca^{2+}-release from the ER within seconds after TCR engagement. Calcium depletion from the ER results in opening of the so-called Ca^{2+} release-activated Ca^{2+} (CRAC) channels in the plasma membrane (55). Through uptake of extracellular Ca^{2+}, the cytosolic concentration is even further increased. The process of sustained calcium influx via CRAC channels is called store-operated Ca^{2+} entry (SOCE) and is necessary for full activation of calcium-dependent processes (56). Membrane-bound Ca^{2+}/H^{+} ATPase and Na^{+}/Ca^{2+} exchangers play an important role in promoting Ca^{2+} emission that is required to keep a balance between influx and efflux.

Calmodulin (CaM), a small adaptor protein and calcium sensor, changes its structure upon calcium binding and serves as a mediator to promote calcium-dependent processes (57). Numerous proteins, including the serine/threonine phosphatase calcineurin, contain CaM binding sites. Calcineurin forms an essential connection between calcium signaling and modification of protein phosphorylation. Following activation through Ca^{2+}/CaM binding, calcineurin dephosphorylates its substrates (reviewed by (58)). The nuclear factor of activated T cells (NFAT) transcription factor family constitutes the best studied calcineurin target.

In total, five proteins, namely NFAT1 (or NFATc2), NFAT2 (NFATc1), NFAT3 (NFATc4), NFAT4 (NFATc3) and NFAT5 make up the NFAT family. NFAT1 and NFAT2 play a major role in T cells and are the most-studied members. Unlike NFAT1, which is constitutively expressed in human T cells, NFAT2 is induced upon activation (59). Both proteins are regulated in a calcineurin-dependent manner. NFAT proteins reside in a phosphorylated form in the cytoplasm of resting cells. Calcineurin activates NFAT-dependent gene expression by dephosphorylation of various serine residues within the regulatory domain, which induces NFAT translocation to the nucleus (Figure 6) (60). NFAT can subsequently bind to REs in the promoter region of target genes and induce gene transcription. Different interactions between NFAT and other transcription factors such as AP-1 and forkhead box P3 have been described, representing another line of transcriptional control (61,62). It is well studied that NFAT forms complexes with AP-1 components (c-Fos/c-Jun) to induce transcription of cytokines like interleukin-2 (IL-2) and interferon-γ (IFN-γ) and other activation-related proteins in T cells. Therefore, target genes that require NFAT/AP-1 interaction will exclusively be expressed upon coordinate activation of both, calcium and the MAPK signaling pathway.

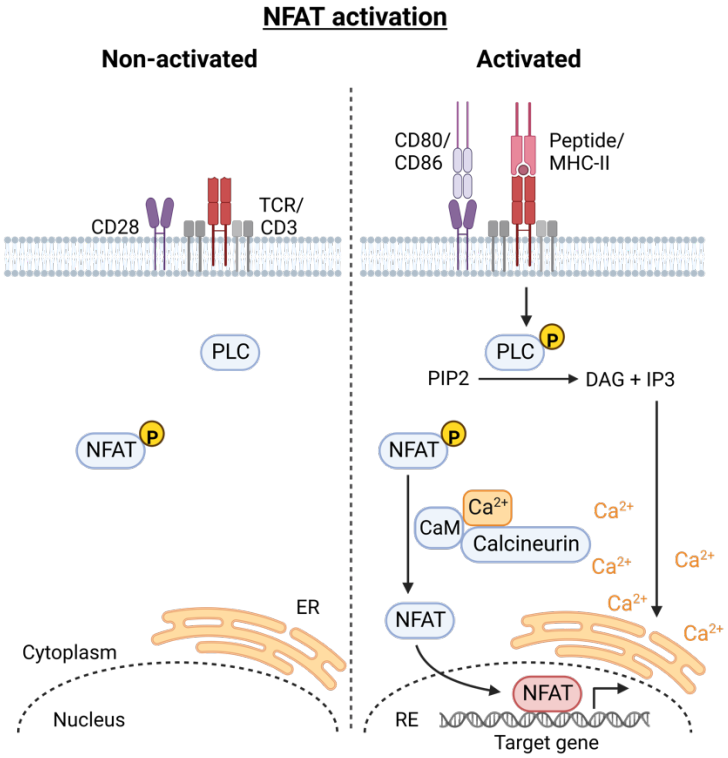

Figure 6: NFAT activation.

In a non-activated state, NFAT is phosphorylated and retained in the cytoplasm. Upon T cell stimulation, PLC generates IP3 that induces Ca^{2+} release from the ER. Ca^{2+}/CaM activates calcineurin, which dephosphorylates NFAT. Activated NFAT can subsequently translocate to the nucleus and initiate target gene transcription. This figure was created with BioRender.com.

T cell activation not only increases cytosolic calcium levels, but also the nuclear calcium concentration rises upon stimulation. Nuclear calcium is required for the induction of the activation markers CD25 and CD69 as well as cytokines like IL-2. As outlined above, cytosolic calcium is essential for NFAT activation. A lack of nuclear calcium signaling was found to have a negative impact on T cell activity and induces a hyporesponsive state. Therefore, nuclear calcium can be regarded as a key regulator of immune tolerance (63).

1.4 Involvement of reactive oxygen species in T cell receptor signaling

Reactive oxygen species (ROS) are a byproduct of cellular energy production and have long been associated solely with induction of cell death by reacting with proteins, lipids, and nucleic acids. However, it turned out that ROS at lower levels can function as important intracellular signaling molecules (64,65).

As activation and induction of effector functions is energy demanding, T cells have to adjust their metabolism in response to stimulation. This conversion from a catabolic to an anabolic state goes along with increased mitochondrial respiration, resulting in enhanced ROS generation. Apart from mitochondria, membrane-bound NADPH oxidases and other enzymes such as cyclooxygenases and lipoxygenases contribute to ROS production (66,67). To

maintain a balance and avoid oxidative stress, cells possess various antioxidant systems, including the ubiquitously expressed and most abundant glutathione (reviewed by (68)).

Low to moderate levels of ROS can positively contribute to signaling pathways mediating cell growth, death, and migration. One mechanism of action is the reversible post-translational modification of signaling molecules, by acting preferentially on cysteine residues, as it was described for H_2O_2 (69). Thereby, protein function can be altered and induce a different outcome of the respective signaling pathway. However, a clear statement on the involvement of ROS in a certain signaling pathway is made difficult by various targets within one and the same pathway and in some cases opposing ways of action are described.

In this context, the presence of ROS has been reported to be both, an activator and repressor of NFκB signaling. While a stimulating effect on NFκB activation is attributed to cytoplasmic ROS, nuclear ROS were described to rather inhibit NFκB activity (reviewed by (70)). Apart from the cellular compartment, the use of different methodologies and cell systems provides another explanation for the contradictory results. Multiple ways of ROS action on the NFκB pathway are described (reviewed by (71)). The NFκB p50 subunit, for example, contains a redox-active site (Cys62) and its oxidation is associated with impaired DNA binding capability (72–74). A more indirect way of negative regulation by ROS was found in human lens epithelial cells. Under sustained oxidative stress, proteasomal activity was inhibited, whereby IκB degradation and thus NFκB activation were impaired (75). Conversely, another study found that antioxidant treatment is able to block NFκB activation in the Jurkat T cell leukemia cell line in response to various stimuli (76).

Apart from NFκB, also the NFAT signaling pathway is sensitive to ROS regulation. *Sena et al.* found a direct link between activation-induced mitochondrial ROS production and NFAT activation with subsequent IL-2 production in primary murine $CD4^+$ T cells (77). This fits to the observation that mitochondria localize to the immunological synapse following TCR engagement (78). In contrast, also inhibitory effects of ROS on NFAT activation were described. NFAT DNA binding, for example, was found to be suppressed upon long-term exposure of human T cells to low-level H_2O_2, which resulted in diminished *IL2* transcription (79). As described in chapter 1.3.2, NFAT activation depends on dephosphorylation by the phosphatase calcineurin. Increased ROS levels interfere with calcineurin activity by oxidation of iron and zinc atoms in the active center (80) and thereby inhibit NFAT-dependent gene expression.

As introduced in chapter 1.3, the actin remodeling proteins LPL and cofilin, whose activation depends on T cell costimulation, are also sensitive to oxidation. ROS can reversibly oxidize LPL on Cys42 and Cys101, forming a disulfide bridge between the two residues. Thereby, the actin-bundling activity of LPL is decreased (36). Impaired T cell activation observed upon oxidative stress could be traced back to the oxidation and thereby inactivation of cofilin. The

identification of an oxidation-induced disulfide bridge formation between Cys39 and Cys80 can explain the observed inhibition of cofilin function (35). Excess ROS ultimately results in cell death and the translocation of oxidized cofilin into the mitochondria was found to induce programmed cell death independent of caspase activation in T cells upon long-term oxidative stress (81).

In conclusion, both, excess or insufficient ROS levels can negatively influence T cell function and signaling, wherefore ROS generation and elimination need to be tightly controlled in a spatiotemporal manner.

1.5 *Arnica montana* L.

Arnica montana L. (named Arnica in this thesis) is an herbaceous, perennial plant belonging to the plant family of Asteraceae. It is growing in Europe, northern Asia, Siberia as well as America at an altitude between 500 and 2500 meters. Arnica was first mentioned in Matthiolus's herb book in 1558 and has a long tradition of use as therapeutic plant for the treatment of various ailments. Due to intensive use, the plant was almost eradicated at the end of the 18th century. Nowadays, Arnica is classified as a strictly protected species in Germany (82).

1.5.1 *Arnica montana* as herbal remedy

Since centuries, Arnica is used in homeopathy and anthroposophy to treat inflammation and blunt injuries like contusions, bruises or hematoma. For medicinal purposes, the whole plant and especially the flower heads or the roots can be used. Arnica preparations are commonly applied topically in the form of creams and ointments. Due to their toxicity, Arnica products prepared from flower heads need to be highly diluted (≥ D4) for oral intake (drops or globules). For preparations of underground parts or the whole plant, undiluted mother tincture can be used.

In total about 150 therapeutically active substances were identified in Arnica (reviewed by (83)). Sesquiterpene lactones (SLs) like Helenalin (structure see Figure 7A), flavonoids and phenolic acids represent the main phytochemical compounds in aerial plant parts, especially the flower heads (84–86). The anti-inflammatory effect of Arnica preparations is particularly attributed to SLs (87), whereas flavonoids and phenolic acids mainly account for the antioxidant capacity (88). Underground plant parts contain essential oils rich in Thymol (structure see Figure 7B) and its derivatives (89,90). Different terpenes, oligosaccharides and numerous other phytoconstituents were also identified (89,91).

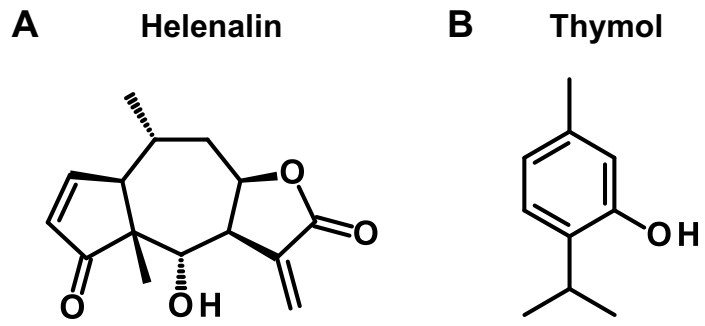

Figure 7: Chemical structure of Helenalin and Thymol.
Schematic representation of the chemical structure of Helenalin (**A**) and Thymol (**B**).

1.5.2 Anti-inflammatory activity of Arnica

The effect of Arnica extracts on immune cells was not intensively investigated yet, however two studies support their presumed anti-inflammatory mode of action. Treatment of the Jurkat T cell leukemia cell line with an Arnica flower tincture inhibited DNA binding of NFκB as well as NFAT, fitting to decreased IL-1ß and tumor necrosis factor-α (TNF-α) release by peripheral blood mononuclear cells (PBMCs) (87). Using a whole plant methanolic Arnica extract, *Verma et al.* showed diminished nuclear translocation of NFκB in a murine macrophage cell line. Also under these conditions, a reduced release of TNF-α was observed (92).

Among the SLs, especially Helenalin was investigated for its anti-inflammatory effects in different experimental systems. A diminished expression of proinflammatory cytokines (IL-2, IL-6, IFN-γ and TNF-α) upon Helenalin treatment was described in PBMCs (93). In 1997, *Lyss et al.* published that Helenalin mediates its effect via selective inhibition of the transcription factor NFκB (94). Using the Jurkat T cell leukemia cell line, Helenalin was found to specifically interfere with NFκB DNA binding by selective alkylation of the p65 subunit without affecting its nuclear translocation (95). *Berges et al.* studied the anti-inflammatory effect of Helenalin in primary human $CD4^+$ T cells and found a suppressive effect on NFAT1 nuclear translocation upon TCR engagement (96).

Although the anti-inflammatory effect of Arnica preparations is often related to SLs, an anti-inflammatory mode of action is also attributed to Thymol. Besides reducing the production of IL-2 and IFN-γ by Jurkat cells, Thymol significantly diminished nuclear NFAT2 and c-Fos levels (97). Using a murine macrophage cell line, Thymol inhibited IL-1ß production and decreased nuclear NFAT1, NFAT2 and c-Fos levels (98). Furthermore, Thymol was shown to diminish the release of elastase by primary human neutrophils in a concentration-dependent manner. This serine proteinase is associated with tissue destruction by degradation of various biomacromolecules and considered as a marker of inflammation (99).

1.5.3 Antioxidant activity of Arnica

Apart from anti-inflammatory properties, the antioxidant activity of Arnica preparations is jointly made responsible for their beneficial effects. The antioxidant potential of hydroalcoholic Arnica flower extract was confirmed by means of the DPPH (2,2'-diphenyl-1-picrylhydrazyl radical) free radical scavenging method, the TEAC (trolox equivalent antioxidant capacity) assay and the ORAC (oxygen radical absorbance capacity) assay (88). By comparison with other plants, a correlation between the total phenol and flavonoid content of an extract and its antioxidant activity was found (100).

No *in vitro* studies investigating the effect of non-toxic Helenalin concentrations on the cellular redox status are available. However, the cytotoxic effect of high Helenalin concentrations was linked to a reactive oxygen species (ROS)-inducing effect in primary human $CD4^+$ T cells (96). Similarly, Helenalin was shown to induce cell death of highly apoptosis-resistant Bcl2-overexpressing Jurkat cells by increasing intracellular ROS levels. Pretreatment with the antioxidant N-acetyl-L-cysteine (NAC) could prevent this effect (101). Also, in human renal carcinoma Caki cells, apoptosis induction by Helenalin was found to result from ROS induction, which could be inhibited by NAC (102). In contrast, the study published by *Li et al.* reports that Helenalin ameliorated hepatic injury in a mouse model of Lipopolysaccharide/D-Galactosamine-induced acute liver injury and inhibited ROS generation (103).

For Thymol, both, pro-oxidative and antioxidant effects are described. Using the cell-free TEAC assay, Thymol showed a concentration-dependent antioxidant activity similar to Trolox. Intracellular ROS levels in V79 Chinese hamster lung fibroblast cells were also found to be diminished upon Thymol treatment (104). In contrast, no effect on intracellular ROS levels in PBMCs was observed with the same Thymol concentration (105). Interestingly, an *in vivo* study by *Krishnan et al.* performed with zebra fish embryos describes Thymol as being prooxidative. Drug treatment showed a cytotoxic effect on the embryos which was linked to induction of ROS generation (106).

1.6 The role of immune cells in muscle healing

Muscle injuries, including contusions and bruises, result in destruction of body cells whereby so-called damage-associated molecular patterns (DAMPs) are released. These molecules are recognized by PRRs expressed on innate immune cells, which are thereby activated. The resulting inflammatory process represents the body's first reaction to a wound and is essential for proper wound healing. Persisting inflammation, however, has detrimental effects and induces tissue damage and delayed healing.

1.6.1 Normal muscle healing and regeneration

The normal muscle healing process in response to single trauma can be categorized into three overlapping phases: 1) the inflammatory phase, 2) the remodeling phase and 3) the regeneration and muscle growth phase (reviewed by (107)).

During the inflammatory phase (day 0 – 7), immune cells play a major role. After bleeding has been stopped by clot formation, different immune cell populations invade the injured tissue site in a temporally controlled manner (Figure 8A). Importantly, inflammation is induced to promote clearance of cell debris and activate various interactions between immune cells and muscle cells. Furthermore, tissue-resident muscle stem cells, the so-called satellite cells, are activated and start to proliferate, whereby muscle regeneration is initiated. In the remodeling phase (day 4 – 14), myofibers undergo proliferation, whereas in the regeneration and muscle growth phase (day 14 – 28) extracellular matrix (ECM) deposition and scar formation occur.

In the following, the role of different immune cells during normal muscle regeneration will be outlined. In response to injury, activated innate immune cells rapidly respond by releasing pro- as well as anti-inflammatory mediators like cytokines, chemokines and growth factors. Initially, an inflammatory response is generated, which by time is directed towards resolution in order to allow transition to the remodeling phase.

Activated tissue-resident myeloid cells, especially macrophages, promote the influx of neutrophils, which are among the first cells to arrive at the wound site and detectable as early as 1 hour post injury (hpi) (108). Their cell number peaks within 12 – 24 hpi, whereafter it rapidly declines again, demonstrating a transient role in initiating an inflammatory response and clearing cell debris. Chemoattractants secreted by neutrophils promote infiltration of other innate immune cells, such as macrophages, eosinophils, and mast cells that accumulate in the wound site between 1 h and 3 days post injury (dpi). These cells promote generation of an acute pro-inflammatory milieu.

In the further course of muscle healing, bone-marrow-derived monocytes are recruited, which can polarize either towards the pro-inflammatory M1-like macrophages or the M2-like wound macrophages depending on the cytokine environment. Pro-inflammatory cytokines such as IFN-γ and TNF-α promote M1-phenotype activation. M1-macrophages peak 2 dpi and are important for phagocytosis of cell debris (109) and production of pro-inflammatory cytokines like IFN-γ during early wound healing. Furthermore, they promote proliferation of satellite cells but inhibit their differentiation (110,111). When wound healing is progressing and cytokines like IL-4 and IL-13 are enriched, a switch towards the preferential polarization to pro-regenerative M2-like macrophages, peaking at 4 dpi, occurs (112). M2 macrophages help resolving the inflammation and promote muscle fiber repair by secretion of insulin-like growth factor 1 (IGF1) 3 – 7 dpi (113,114). Furthermore, they favor muscle regeneration by stimulating myoblast differentiation and fusion as well as myotubule formation (115). Although M1 and M2

macrophages can be clearly distinguished from each other, macrophage polarization should rather be considered as a broad spectrum of activation states with M1- and M2-phenotype at the hypothetical ends. *In vivo*, macrophages show a high degree of plasticity with highly complex regulatory networks.

Activation and recruitment of T cells to the injured site is mediated by antigen-presenting DCs and macrophages starting from 3 dpi (116). By influencing other cell types, including macrophages, stem cells, and myoblasts, T cells are critically involved in mediating tissue repair and promoting muscle fiber regeneration. Especially $CD4^+$ T cells play a major role in normal wound healing, but also $CD8^+$ cytotoxic T cells infiltrate the injured site (117). Different T helper cell subsets coordinate the muscle repair process by modifying the cytokine milieu. While Th1 cells induce M1-macrophage polarization, Th2 cells and Tregs promote the anti-inflammatory M2-type (118,119). Tregs, in addition, support tissue regeneration by secretion of growth factors like amphiregulin (120). By direct interaction with activated satellite cells, Tregs maintain their proliferation and survival prior to differentiation (121).

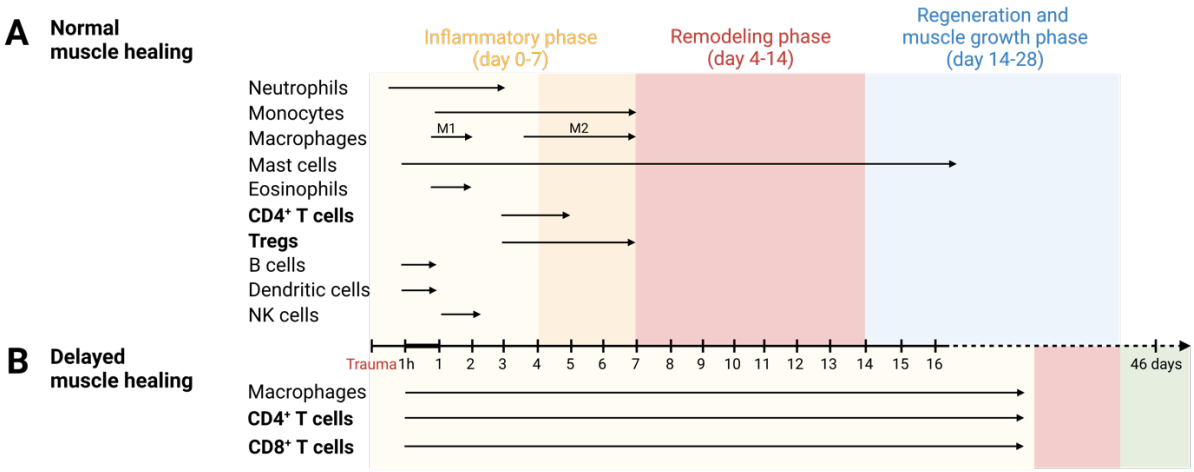

Figure 8: Normal versus delayed muscle healing and regeneration.

(**A**) Different immune cell types are critically involved in the process of normal muscle healing, which can be divided into three phases. As depicted, each cell population fulfils an important function during a certain period of time, whereafter it disappears again. $CD4^+$ T cells and Tregs contribute to muscle regeneration between day three and seven after injury. (**B**) Delayed muscle healing is associated with prolonged presence of macrophages and $CD4^+$ as well as $CD8^+$ T cells. This goes along with extension of the inflammatory phase and inhibited transition to the remodeling phase. This figure was created with BioRender.com and modified from (107).

1.6.2 Delayed muscle regeneration

While an isolated musculoskeletal wound in healthy individuals typically heals without complications and need for intensive care, patients with severe or polytraumatic injuries often suffer from delayed muscle regeneration. Another risk factor for impaired wound healing is the pre-existence of chronic inflammation, as observed in smoking or elderly people, as well as in patients with comorbidities such as rheumatoid arthritis or diabetes. These conditions are often

associated with prolonged or dysregulated inflammation, whereby the regenerative capacity of satellite cells is impaired. Chronic local inflammation results in enhanced ECM deposition, whereby myofiber formation at the injury site is inhibited, leading to replacement of muscle with fibrotic scar tissue (reviewed by (122)). A study by *Hurtgen et al.* associated delayed healing with elevated numbers of $CD4^+$ and $CD8^+$ T cells as well as macrophages (Figure 8B) (123). Therefore, interfering with long term presence of T cells represents one potential therapeutic target to resolve persisting inflammation and thereby promote muscle repair. However, the timing for interference has to be chosen carefully. As mentioned above, inflammation elicited immediately after injury is a prerequisite for proper healing and should not be dampened. This means that a detailed understanding of the spatiotemporal involvement of the different immune cell types and their interaction with muscle cells is indispensable.

1.7 Aim of the thesis

Herbal remedies have a long tradition of use for the treatment of various ailments. Although synthetic compounds commonly constitute the active ingredients in medicinal products used nowadays, plant-derived therapeutic products are more and more applied as complementary treatment option. Therefore, research increasingly focuses on investigating the mode of action of herbal drugs but there is still a huge lack of profound and scientifically validated knowledge. *Arnica montana*-based creams and ointments are used for centuries to treat inflammation and musculoskeletal injuries like contusions or bruises. Apart from protecting the host from infection and clearing invading pathogens as well as malignant cells, immune cells are critically involved in wound healing and tissue repair. As prolonged presence of $CD4^+$ and $CD8^+$ T cells was found to be a hallmark of deregulated inflammation and delayed wound healing, T cells represent an interesting immune cell type to be studied regarding a potential immunomodulatory effect of Arnica preparations.

Therefore, this thesis aimed at investigating the effect of differentially prepared Arnica extracts and corresponding lead substances on primary human peripheral blood T cells (PBTs) at a functional and molecular level. First, non-toxic extracts showing an effect on T cell activation marker expression and/or proliferation were selected for further investigation. In parallel, the lead substances Thymol and Helenalin were studied. In the further course of the study, the molecular mechanism underlying the observed functional effects was examined in terms of different signaling pathways. Based on a phytochemical characterization, the most prominent lead compounds contained in the tested Arnica extracts were selected and studied for their effect on T cells in a purified form. Eventually, the collected results will support a critical evaluation of Arnica-based complementary treatment options based on consolidated experimental data.

2 Materials and Methods

2.1 Materials

2.1.1 Buffers and solutions

Table 1: Composition of used buffers and solutions

Name	Ingredients / Vendor
Cytofix™ Fixation Buffer	BD Biosciences
FACS perm buffer	0.1 % Saponin in FACS wash buffer
FACS wash buffer	1 % Albumin Fraction V 0.07 % NaN_3 in PBS
Hypotonic Buffer	20 mM Tris-HCl (pH 7.5) 10 mM NaCl 3 mM $MgCl_2$ 1 mM NaF 0.1 mM EDTA 0.1 mM EGTA in Milli-Q® H_2O 0.5 mM PMSF were freshly added before use
Intercept® (TBS) Blocking Buffer	LI-COR
Nuclear Extraction Buffer	20 mM HEPES-NaOH (pH 7.9) 400 mM NaCl 1 mM EDTA 1 mM EGTA in Milli-Q® H_2O 1 mM DTT, 1 mM PMSF and Protease Inhibitor Cocktail (1:100) were freshly added before use
Phosflow™ Perm Buffer III	BD Biosciences
Reporter Assay Lysis Buffer	25 mM Tris 4 mM EGTA 1 % Triton™ X-100 10 % Glycerol 2 mM DTT in Milli-Q® H_2O adjust pH to 7.8

Name	Ingredients / Vendor
SDS-PAGE Running Buffer	25 mM Tris-HCl (pH 8.8) 190 mM Glycine 0.1 % SDS in Milli-Q® H_2O
3X SDS-PAGE Sample Buffer	190 mM Tris (pH 6.8) 150 mM DTT 3 % SDS 30 % Glycerol Bromphenol blue in Milli-Q® H_2O
SDS polyacrylamide stacking gel	125 mM Tris (pH 6.8) 5 % Acrylamide 0.1 % APS 0.08 % TEMED in Milli-Q® H_2O
SDS polyacrylamide resolving gel (14 %)	375 mM Tris (pH 8.8) 14 % Acrylamide 0.1 % APS 0.08 % TEMED in Milli-Q® H_2O
10X TBS	1.5 M NaCl 0.5 M Tris in Milli-Q® H_2O adjust pH to 7.3
TBS-T	Tween® 20 (1:1,000) in 1X TBS
Western Blot Transfer Buffer	48 mM Tris 39 mM Glycine 20 % Methanol 0.037 % SDS in Milli-Q® H_2O

2.1.2 Chemicals and reagents

Table 2: Summary of used chemicals and reagents

Name	Vendor
Acrylamide	Carl Roth
Albumin Fraction V (BSA)	Carl Roth
APS	Carl Roth
Beetle-Juice	PJK
Bromphenol blue	Merck
Dimethyl sulfoxide (DMSO)	Sigma-Aldrich
DTT	Gerbu Biotechnik
EGTA	AppliChem
Ethanol absolute	Sigma-Aldrich
Ethylenediaminetetraacetic Acid (EDTA)	AppliChem
FicoLite-H	Linaris
Foetal Bovine Serum (FBS)	PAN-Biotech
Glycerol	AppliChem
Glycine	Sigma-Aldrich
GolgiStop™	BD Biosciences
HEPES	Carl Roth
Ionomycin	Sigma-Aldrich
L-glutamine	Gibco
Magnesium chloride ($MgCl_2$)	AppliChem
Methanol	VWR
N-Acetyl-L-cysteine (NAC)	Sigma-Aldrich
Nonidet P-40 Assay Reagent	Cayman Chemical
Paraformaldehyde (PFA)	Sigma-Aldrich
Phosphate-buffered saline (PBS)	Sigma-Aldrich
Phytohaemagglutinin (PHA)	Merck
PMSF	Sigma-Aldrich

Name	Vendor
Precision Plus Protein™ All Blue Prestained Protein Standards	Bio-Rad
Protease Inhibitor Cocktail	Sigma-Aldrich
Recombinant human IL-2	PeproTech
RPMI 1640 Medium	Gibco
Saponin	Sigma-Aldrich
SDF-1α	R&D Systems
SDS	Serva
Sodium azide (NaN_3)	Carl Roth
Sodium chloride (NaCl)	Sigma-Aldrich
Sodium fluoride (NaF)	Merck
TEMED	Carl Roth
Tert-Butyl hydroperoxide (TBHP)	Alfa Aesar
TPCA-1	Abcam
Tris	Carl Roth
Tris-HCl	Sigma-Aldrich
Triton™ X-100	Carl Roth
Tween® 20	Carl Roth

2.1.3 Cell culture media

Table 3: Composition of cell culture media

Name	Ingredients
RPMI complete medium	10 % FBS 2 mM L-glutamine in RPMI 1640 Medium
RPMI reporter assay medium	5 % FBS 2 mM L-glutamine in RPMI 1640 Medium

2.1.4 Consumables

Consumables for general use in the laboratory were purchased from Thermo Scientific, Sarstedt, Corning and Greiner Bio-One.

2.1.5 Primary cells and cell lines

Table 4: List of used primary cells and cell lines

Name	Source
Peripheral blood T cells (PBTs)	Venous blood of healthy donors
Jurkat E6.1 cells	ATCC®

2.1.6 *Arnica montana* extracts

Table 5: Specification of tested *Arnica montana* extracts

Extract	Abbr.	Plant material	Extraction procedure	Solvent	Manufacturer
Planta tota Rh ∅ V.21	-	Press juice of entire flowering plant (fresh)	Aqueous Rh mother tincture (GHP 21)	H_2O	Weleda
Rh ∅ V.21 (Radix)	-	Press juice of rootstock (fresh)	Aqueous Rh mother tincture (GHP 21)	H_2O	Weleda
E floribus LA 20%	-	Flower heads (fresh)	Aqueous alcoholic essence (GHP 12c)	20 % EtOH	WALA
E planta tota ferm 33c	Ferm	Entire flowering plant (fresh)	Aqueous fermented mother tincture (GHP 33c)	H_2O	WALA
Planta tota ∅ V.2b	Tota	Entire flowering plant (fresh)	Aqueous alcoholic mother tincture (Ph.Eur. 1.1.4, GHP 2b)	30 % EtOH	Weleda
Mother tincture	Radix	Underground parts (dried)	Ph.Eur. 1.1.8 (GHP 4a)	86 % EtOH	DHU

2.1.7 Plant-derived substances

Table 6: Summary of tested plant-derived substances

Name	Abbreviation	Stock concentration	Vendor
Thymol	Th	1 M	Sigma-Aldrich
Helenalin	Hel	10 mM	Focus Biomolecules
3-*O*-Caffeoylquinic acid	3-CQA	100 mM	Extrasynthese
3,5-Di-*O*-caffeoylquinic acid	3,5-diCQA	100 mM	Extrasynthese
3,4,5-Tri-*O*-caffeoylquinic acid	3,4,5-triCQA	10 mM	MedChemExpress

2.1.8 Antibodies

2.1.8.1 Fluorescently-labeled antibodies

Table 7: List of used fluorescently-labeled antibodies

Antigen	Species	Conjugate	Clone	Vendor
CD3	mouse	Pacific Blue	SK7	BioLegend
CD25	mouse	APC	M-A251	BioLegend
CD69	mouse	FITC	FN50	BioLegend
IL-2	rat	APC	MQ1-17H12	BioLegend
Phospho-NFκB p65 (S529)	mouse	AF488	K10-895.12.50	BD Biosciences
Rabbit IgG	donkey	IRDye® 800CW	-	LI-COR
Mouse IgG	donkey	IRDye® 680RD	-	LI-COR

2.1.8.2 Unlabeled antibodies

Table 8: Summary of unlabeled antibodies

Antigen	Species	Clone	Vendor	Concentration / Dilution
CD3	mouse	OKT3	Self-made	20 ng/ml
CD28	mouse	CD28.2	BD Biosciences	75 – 5,000 ng/ml
Cofilin	rabbit	polyclonal	Self-made	1:10,000
Phospho-Cofilin (S3)	rabbit	polyclonal	Cell Signaling	1:1,000
GAPDH	rabbit	polyclonal	Thermo Fisher Scientific	1:5,000
L-plastin	mouse	LPL4A.1	Thermo Fisher Scientific	1:1,000
Phospho-L-plastin (S5)	rabbit	monoclonal	Self-made	1:1,000
Mouse IgG + IgM (H+L)	goat	-	Jackson ImmunoResearch	7 μg/ml

2.1.9 Fluorescent dyes used for flow cytometry

Table 9: Overview of fluorescent dyes used for flow cytometry

Name	Target	Vendor	Concentration
7-AAD	DNA of dead cells	BioLegend	2.5 μg/ml
CellROX™ Green Reagent	Detection of oxidative stress	Thermo Fisher Scientific	5 μM
CFSE	Free amins of intracellular proteins	Thermo Fisher Scientific	1 μM
Indo-1 AM	Detection of intracellular calcium	Thermo Fisher Scientific	2 μg/ml

2.1.10 Commercial Kits

Table 10: List of used commercial kits

Name	Vendor
Amnis® NFκB Translocation Kit	Luminex
Direct-zol™ RNA Microprep Kit	Zymo Research
Human T cell Nucleofector™ Kit	Lonza
LEGENDplex™ Human Th panel (12-plex)	BioLegend
nCounter® Human Immunology V2 Panel	nanoString Technologies
NFκB (p65) Transcription Factor Assay Kit	Cayman Chemical
Pan T cell Isolation Kit, human	Miltenyi Biotec
Pierce™ Coomassie Plus (Bradford) Assay Kit	Thermo Scientific
Pierce™ 660 nm Protein Assay Kit	Thermo Scientific

2.1.11 Instruments

Table 11: Summary of used devices

Device	Vendor
Amaxa® Nucleofector® II Device	Lonza
Amnis® ImageStream® Mk II	Luminex Corporation
BD™ LSRII	BD Biosciences
BD LSRFortessa™	BD Biosciences
Fisherbrand™ Isotemp™ CO_2 Incubator	Thermo Fisher Scientific
GFL 1092 water bath	Gesellschaft für Labortechnik
Heraeus Megafuge 40R	Thermo Scientific
ID 03 Inverted Microscope	Zeiss
Microcentrifuge 5415C	Eppendorf
Milli-Q® ultrapure water system	Merck
Mini-PROTEAN® Electrophoresis System	Bio-Rad
Minishaker MS3 basic	IKA

Device	Vendor
NanoDrop2000c Spectrophotometer	Thermo Scientific
Odyssey® Imaging System	LI-COR
PerfectBlue™ Semi-Dry Electro Blotter	Peqlab
SterilGARD Hood SG-600 (laminar flow hood)	Baker
Tecan Sunrise Microplate Reader	Tecan
Tecan Ultra Microplate Reader	Tecan
Thermomixer 5436	Eppendorf

2.1.12 Software

Table 12: Software used for data analysis and thesis writing

Name	Vendor
FlowJo 10.7.1	FlowJo, LLC
IDEAS® Analysis Software 6.2	Luminex Corporation
Image Studio™ Lite Software 5.2.5	LI-COR
LEGENDplex™ Data Analysis Software Suite	BioLegend
Microsoft Office 2019	Microsoft
NormFinder Excel Add-In v0.953	Department of Molecular Medicine, Aarhus University Hospital
nSolver™ Analysis Software 4.0	nanoString Technologies
Prism 9	GraphPad
Zotero 6.0.9	Roy Rosenzweig Center for History and New Media

2.2 Methods

2.2.1 Plant extracts and lead substances

Arnica montana extracts (specified in Table 5) were kindly provided by WALA Heilmittel GmbH (E planta tota ferm 33c, E floribus LA 20%), Weleda AG (Planta tota ∅ V.2b, Planta tota Rh ∅ V.21, Rh ∅ V.21 (Radix)) and DHU-Arzneimittel GmbH & Co. KG (Mother tincture).

Arnica E planta tota ferm 33c (Ferm), Planta tota ∅ V.2b (Tota) and Mother tincture (Radix) were selected to be studied in more detail.

For the aqueous fermented extract (Ferm; manufactured according to GHP 33c) fresh flowering plant material was mixed with honey, water and lactose monohydrate at a ratio of 100: 0.75: 125: 0.75 parts by mass (corresponds to 44.15 % plant material). The one-week fermentation process was followed by six-month maturation at 15 °C.

The hydroethanolic liquid extract (Tota; manufactured according to Ph.Eur. 1.1.4 (GHP 2b)) was prepared from fresh flowering plant material mixed with ethanol 62 % (*m/m*). The ratio depends on the water content of the plant material which was determined as described in Ph.Eur. 1.1.4. After incubation at room temperature with repeated stirring for 10 – 30 days, the mixture was pressed and filtered. The final tincture contains 30 % ethanol (*m/m*).

For the Arnica mother tincture (Radix; manufactured according to Ph.Eur. 1.1.8 (GHP 4a)), 1 part of freshly powdered plant material was extracted with 10 parts of ethanol 86 % (*m/m*). The plant powder was mixed with part of the ethanol and incubated for approximately 24 h to allow pre-swelling of the drug. This step was followed by slow percolation at room temperature with the remaining ethanol. The residue was pressed out, the liquid was combined with the percolate and filtered.

Plant-derived substances (see Table 6) were dissolved in DMSO and aliquots were stored at -80 °C.

2.2.2 Isolation of primary human T cells

Primary human T cells (PBTs) were freshly isolated from heparinized venous whole blood of healthy donors. Therefore, peripheral blood mononuclear cells (PBMCs) were obtained by density gradient centrifugation as described earlier (124). Pan T cell isolation Kit (Miltenyi Biotec) was used for the negative magnetic bead selection of untouched total $CD3^+$ T cells from PBMCs based on the manufacturer's protocol. The isolated cells were resuspended in RPMI complete medium and kept at 37 °C with 5 % CO_2.

2.2.3 Cultivation of Jurkat E6.1 cells

Jurkat E6.1 cells were cultivated at 37 °C, 5 % CO_2 in T75 cell culture flasks (Thermo Fisher Scientific) containing 20 ml RPMI complete medium. Three times a week, cells were centrifuged (5 min, 300 g) and subcultured with a concentration of $2*10^5$ cells/ml.

2.2.4 Drug treatment and *in vitro* stimulation of cells

PBTs as well as Jurkat E6.1 cells were stimulated using plate-bound anti-CD3 and anti-CD28 antibodies. Cell culture plates were coated with goat anti-mouse antibodies (7 μg/ml) diluted in PBS overnight at 4 °C. After washing twice with PBS, unspecific binding sites were blocked for 30 min at room temperature with RPMI complete medium. Next, anti-CD3 (20 ng/ml) and anti-CD28 (75 ng/ml; for titration experiments 10 – 5,000 ng/ml) antibodies diluted in RPMI complete medium were added and incubated for 1 h at room temperature. Unbound antibodies were removed by washing twice with PBS.

The test drugs were prediluted in PBS (plant extracts) or culture medium (substances) before being added to the cells. For comparability, a final ethanol or DMSO concentration of maximum 0.1 % was maintained in the final culture of vehicle control as well as drug treated samples. PBTs and Jurkat cells were preincubated for 1 h at 37 °C, 5 % CO_2 with drug or vehicle control at a final concentration of $1*10^6$ cells/ml in RPMI complete medium. Pretreated or untreated cells were then transferred to coated wells and brought in contact with the antibodies by centrifugation (1 min, 300 g). Depending on the readout, cultures were incubated for 30 min to 72 h, as indicated.

2.2.5 Assessment of cell viability

PBTs or Jurkat E6.1 cells were washed once with FACS wash buffer and incubated with 7-AAD viability staining solution (2.5 μg/ml) diluted in FACS wash buffer for 15 min at room temperature in the dark. After washing twice with FACS wash buffer, samples were resuspended in PBS and immediately analyzed by flow cytometry (BD™ LSRII).

2.2.6 T cell proliferation assay

To analyze the proliferation capacity of PBTs, cells were washed twice with PBS and subsequently labeled with 1 μM CFSE (Thermo Fisher Scientific) diluted in PBS for 15 min at 37 °C, 5 % CO_2. Per $1*10^6$ cells 100 μl staining solution were used. The staining process was stopped by adding RPMI complete medium. Following centrifugation (5 min, 300 g) and another washing step with RPMI complete medium, cells were resuspended in RPMI complete medium, preincubated with test drugs and stimulated as described in section 2.2.4. After 72 h of stimulation, T cell proliferation was analyzed by CFSE dilution measured on a flow cytometer (BD™ LSRII).

2.2.7 T cell migration assay

T cell migration was assessed using Transwell™ 96-Well inserts (Corning) with 5 μm pore size. The lower compartment was filled with RPMI complete medium containing 100 ng/ml SDF-1α as a chemoattractant. $5*10^4$ PBTs preincubated with drug or vehicle (see section 2.2.4) were

transferred to the upper compartment. Cells were allowed to migrate for 90 min at 37 °C, 5 % CO_2. The liquid in the lower compartment containing migrated cells was transferred to round bottom test tubes (Corning) and Negative Control CompBeads (BD Biosciences) diluted in PBS (one drop in 500 µl) were added. To determine the number of migrated cells, a defined number of 10,000 bead events was acquired from each sample using flow cytometry (BD™ LSRII). The percentage of migrated cells was calculated based on a control sample with 100 % migrated cells, for which the cell suspension was added to the lower compartment. Measurements were performed in triplicates.

2.2.8 Analysis of intracellular ROS levels

PBTs were preincubated with test drugs as described in section 2.2.4. To check for antioxidative effects, cells were treated with 200 µM tert-Butyl hydroperoxide (TBHP) for 30 min at 37 °C, 5 % CO_2 to induce oxidative stress. Subsequently, 5 µM CellROX™ Green Reagent (Thermo Fisher Scientific) was added and cells were incubated for 30 min at 37 °C, 5 % CO_2. After washing three times with PBS, intracellular ROS levels were immediately analyzed by flow cytometry (BD™ LSRII). To analyze prooxidative effects, CellROX™ Green Reagent was directly added following preincubation with test drugs, omitting TBHP treatment.

2.2.9 Flow cytometry

2.2.9.1 Staining of surface proteins

PBTs were preincubated and stimulated for 24 h as described in section 2.2.4. The samples were transferred to a round bottom 96-well plate (Thermo Fisher Scientific) and washed once with FACS wash buffer. Surface proteins were stained for 20 min on ice with fluorescently-labeled antibodies diluted in FACS wash buffer. After washing three times with FACS wash buffer, cells were resuspended in PBS. The expression of surface proteins was analyzed by flow cytometry (BD™ LSRII).

2.2.9.2 Staining of intracellular IL-2

As described in section 2.2.4, PBTs were preincubated with test drugs or vehicle and stimulated. After 20 h, GolgiStop™ (1:1,000) was added for the final 4 h to stop the protein export from the cells and enrich IL-2 and other proteins intracellularly. For intracellular staining, cells were first fixed with 1.5 % PFA for 7 min at room temperature. After washing once with FACS wash buffer, cell membranes were permeabilized for 10 min at room temperature in saponin-containing FACS perm buffer. Fluorescently-labeled anti-IL-2 antibodies were diluted in FACS perm buffer and added to the cells for 20 min at room temperature. Cells were washed three times with FACS perm buffer, resuspended in PBS and IL-2 staining was analyzed by flow cytometry (BD™ LSRII).

2.2.9.3 Staining of phospho-NFκB p65 (S529)

For staining of phospho-NFκB, PBTs were preincubated for 1 h and stimulated for 30 min as described in section 2.2.4. Thereafter, cells were fixed for 10 min at 37 °C, 5 % CO_2 with prewarmed Cytofix™ Fixation Buffer (BD Biosciences). After washing once with FACS wash buffer, cell membranes were permeabilized with Phosflow™ Perm Buffer III (BD Biosciences) for 30 min on ice. Fluorescently-labeled anti-phospho-NFκB p65 (S529) antibodies were diluted in FACS wash buffer and cells were incubated with staining solution for 30 min at room temperature in the dark. Unbound antibodies were removed by washing three times with FACS wash buffer before the samples were analyzed by flow cytometry (BD™ LSRII).

2.2.9.4 Cytokine quantification in cell culture supernatant by LEGENDplex™

PBTs were preincubated and stimulated for 24 h as described in section 2.2.4. After centrifugation (2 min, 300 g), supernatants were transferred to a round bottom 96-well plate (Thermo Fisher Scientific) and stored at -20 °C until analysis. The concentration of twelve different cytokines (IL-2, IL-4, IL-5, IL-6, IL-9, IL-10, IL-13, IL-17A, IL-17F, IL-22, IFN-γ, and TNF-α) was simultaneously detected in the supernatants using LEGENDplex™ Human Th Cytokine Panel Kit (BioLegend) according to the manufacturer's instructions.

In short, 25 µl sample or standard dilution were mixed with 25 µl Assay Buffer and 25 µl Capture Bead mixture in the provided V-bottom 96-well plate. Following two-hour incubation on a shaker at room temperature, the plate was centrifuged (5 min, 200 g) and cells were washed twice with Wash Buffer. 25 µl biotinylated Detection Antibodies were added to each sample. The plate was incubated on a shaker at room temperature for 1 h, whereafter 25 µl of Streptavidin-PE was pipetted into each well. After shaking for 30 min at room temperature, beads were washed twice with Wash Buffer. The samples were read on a flow cytometer (BD™ LSRII) and the cytokine concentrations in each sample were determined based on the standard samples using the LEGENDplex™ Data Analysis Software Suite (BioLegend).

2.2.10 Detection of phospho-L-plastin and phospho-cofilin

2.2.10.1 SDS polyacrylamide gel electrophoresis (SDS-PAGE)

For the detection of total L-plastin, phospho-L-plastin, total cofilin and phospho-cofilin, PBTs were preincubated and stimulated for 30 min as described in section 2.2.4. The cells were washed twice with PBS and whole cell lysates were prepared by resuspending in 1X SDS-PAGE Sample Buffer and shaking for 5 min at 95 °C. The lysates were loaded on 14 % SDS polyacrylamide gels (prepared according to Table 1) which were run in SDS-PAGE Running Buffer using the Mini-PROTEAN® Electrophoresis System (Bio-Rad). Proteins were separated by size by applying an electric current of 25 mA per gel for about 1.5 h until the dye

front leaked from the bottom of the gel. Precision Plus Protein™ All Blue Prestained Protein Standards (Bio-Rad) were used as a reference for molecular weight estimation.

2.2.10.2 Western Blotting and immunostaining

Semi-dry Western Blotting was performed as described earlier (125). Proteins were blotted for 1 h at 10 V on an Immobilon-FL PVDF membrane with 0.45 μm pore size (Merck Millipore) using the PerfectBlue™ Semi-Dry Electro Blotter (Peqlab). The membrane was washed for 15 min in 1X TBS and blocked for 1 h in Intercept® (TBS) Blocking Buffer (LI-COR) at room temperature. Antibodies were diluted in Intercept® (TBS) Blocking Buffer (LI-COR) as indicated in Table 8. Primary antibodies against non-phosphorylated proteins were incubated for 1 h at room temperature. p-L-plastin (S5) was stained for 2 h at room temperature, p-cofilin (S3) overnight at 4 °C. After washing three times with TBS-T Buffer, membranes were incubated with appropriate fluorescently-labeled secondary antibodies for 1 h at room temperature and the signal was detected using the Odyssey® Imaging System (LI-COR). Signal intensity was evaluated using the Image Studio™ Lite Software (LI-COR) and normalized to the housekeeping protein GAPDH.

2.2.11 Analysis of NFκB nuclear translocation by imaging flow cytometry

$1*10^6$ PBTs per sample were preincubated with test drug or vehicle for 1 h and stimulated for 30 min as described in section 2.2.4. To assess the nuclear translocation of NFκB, the Amnis® NFκB Translocation Kit was used according to the manufacturer's protocol. Therefore, cells were transferred to a round bottom 96-well plate (Thermo Fisher Scientific) and washed once with PBS. Next, 100 μl 1X Fixation Buffer were added and cells were fixed for 10 min at room temperature. After washing twice with 1X Assay Buffer, cells were stained for 30 min at room temperature with anti-NFκB p50 AF488 antibody diluted in Permeabilization Buffer. Unbound antibodies were removed by washing twice with 1X Assay Buffer and cells were resuspended in 50 μl 0.25X Fixation Buffer. The cell nuclei were stained by adding 5 μl 7-AAD reagent and incubating for 5 min at room temperature. Fluorescent signals were detected on the Amnis® ImageStream® Mk II (Luminex Corporation) imaging flow cytometer and data were analyzed using the IDEAS® Analysis Software (Luminex Corporation). The gating strategy is depicted in Figure 9.

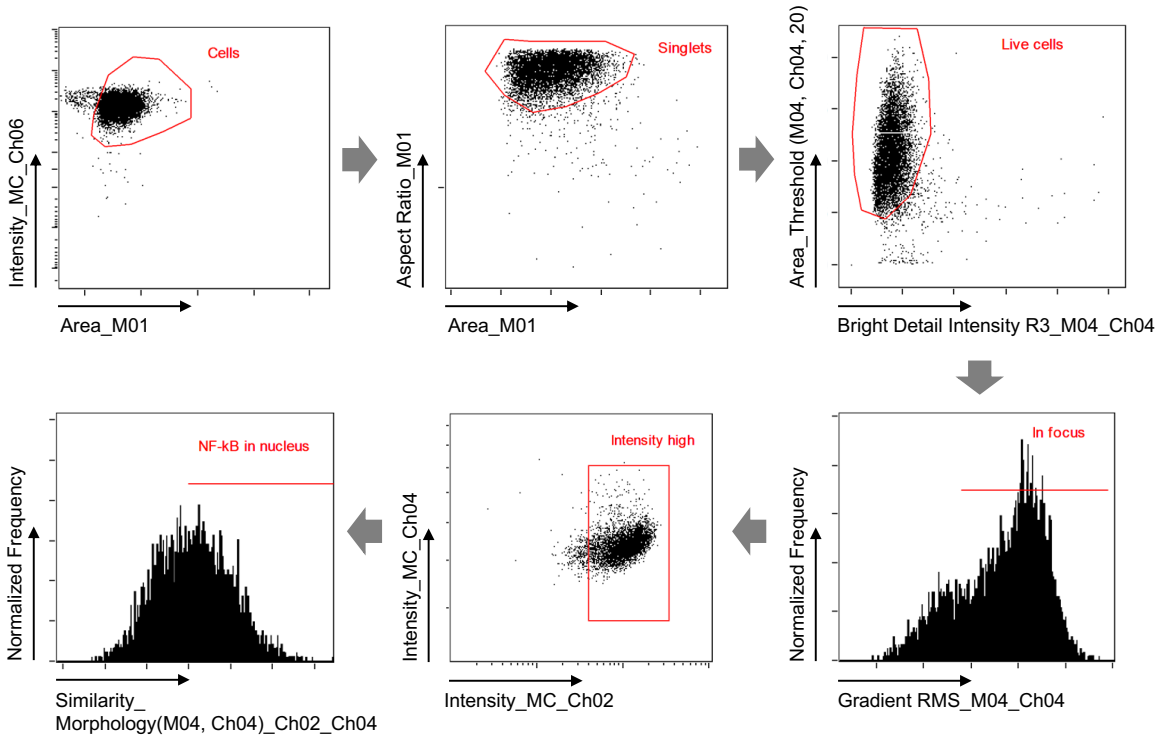

Figure 9: Gating strategy for the analysis of NFκB nuclear translocation by imaging flow cytometry. Sequential gating was performed to exclude cell doublets, apoptotic cells and cells out of focus from the analysis. For the remaining cells, a mask defining the cell nucleus was created based on the 7-AAD signal (Ch04). Nuclear translocation of NFκB p50, expressed as the percentage of cells with nuclear NFκB, was quantified by calculating the similarity between the cell nucleus mask and the NFκB p50 AF488 signal (Ch02).

2.2.12 NFκB DNA binding assay

Nuclear lysates were prepared from PBTs that were pretreated for 1 h and activated for 30 min as described in section 2.2.4. The cells were washed twice with cold PBS + 1 mM NaF and resuspended in ice-cold Hypotonic Buffer. After incubation on ice for 15 min to allow cell swelling, Nonidet P-40 Assay Reagent (Cayman Chemical) was added to disrupt the cell membranes. Cell nuclei were pelleted by centrifugation (1 min, 14,000 g, 4 °C) and the cytoplasmic fraction in the supernatant was removed. To obtain pure nuclear lysates, the pellet was washed once with Hypotonic Buffer. The nuclei were then resuspended in Nuclear Extraction Buffer and rocked on a shaking platform with maximum speed at 4 °C for 30 min. The samples were centrifuged (10 min, 14000 g, 4 °C) and the nuclear lysate in the supernatant was transferred to a new microcentrifuge tube. Aliquots were stored at -80 °C until the samples were analyzed.

The DNA binding activity of NFκB in nuclear lysates was assessed using the ELISA-based NFκB (p65) Transcription Factor Assay Kit (Cayman Chemical) according to the manufacturer's protocol. In brief, 10 µl of sample or Positive Control lysate (provided with the Kit) and 90 µl Complete Transcription Factor Binding Assay Buffer (CTFB) were added in duplicates to each well of the 96-well plate precoated with a consensus dsDNA sequence.

100 µl CTFB were used for blank wells. DNA binding was allowed overnight at 4 °C without shaking. The next day, wells were emptied and washed five times with 1X Wash Buffer. 100 µl of diluted anti-NFκB p65 antibody was pipetted in each well (except from blank) and the plate was shaken for 1 h at room temperature. After washing five times with 1X Wash Buffer, 100 µl of diluted HRP-conjugated secondary antibody was added to each well (except from blank). The plate was shaken for 1 h at room temperature, followed by washing five times with 1X Wash Buffer. 100 µl Transcription Factor Developing Solution was added into each well and was incubated for 30 min at room temperature on a shaker before the reaction was stopped by adding 100 µl Transcription Factor Stop Solution. The absorbance at 450 nm was immediately measured on a Tecan Sunrise Microplate Reader. Mean absorbance values obtained after blank subtraction were normalized to the protein concentration of nuclear lysates which was determined using the Pierce™ Coomassie Plus (Bradford) Assay Kit (Thermo Scientific) according to the manufacturer's protocol. In short, 75 µl of nuclear lysate dilution (1:20 in H_2O) or BSA standard dilution (in 1:20 diluted Nuclear Extraction Buffer) was mixed with 75 µl room temperature Coomassie Plus Reagent. After shaking for 30 s and incubating at room temperature for 10 min, the absorbance at 595 nm was measured using a Tecan Sunrise Microplate Reader. Measurements were performed in duplicates and the protein concentration for each sample was determined based on a BSA standard curve generated by the four-parameter logistic model.

2.2.13 NFAT luciferase reporter assay

Jurkat E6.1 cells were transfected with NFAT luciferase reporter plasmid based on the pGL2-Promoter Vector (NFAT-pGL2-Promoter Vector; plasmid map see section 5.4) using Human T cell Nucleofector™ Kit (Lonza). Therefore, $1*10^6$ cells per sample were resuspended in 100 µl Nucleofector™ Solution for Human T cells. 2 µg plasmid DNA per sample were transferred to each aluminum cuvette and the cell suspension was added. The cells were transfected with program X-001 (for high viability) using a Amaxa® Nucleofector® II Device (Lonza). The samples were incubated for 5 min at room temperature before they were transferred to 1 ml of prewarmed RPMI reporter assay medium each. After 24-hour incubation at 37 °C, 5 % CO_2, cells were resuspended in fresh RPMI reporter assay medium and preincubated as well as stimulated for 6 h as described in section 2.2.4. Cells were washed once with PBS and lysates were prepared by adding 100 µl Reporter Assay Lysis Buffer and incubating 15 min at 37 °C. The samples were centrifuged (10 min, 22,000 g, 4 °C) and the protein lysate in the supernatant was transferred to fresh microcentrifuge tubes. Aliquots were stored at -80 °C until further analysis.

To quantify NFAT-dependent gene expression, luminescence was measured in duplicates after mixing 20 µl of lysate with 100 µl D-Luciferine-containing Beetle-Juice (PJK) and

incubating for 5 min at room temperature using a Tecan Ultra Microplate Reader. After blank subtraction, luminescence values were normalized to the protein concentration in the lysates which was determined using Pierce™ 660 nm Protein Assay Kit (Thermo Scientific) according to the manufacturer's instructions. Therefore, 10 µl of undiluted sample or BSA standard dilution (in Reporter Assay Lysis Buffer) was mixed with 150 µl room temperature Protein Assay Reagent. After shaking for 1 min and incubating at room temperature for 5 min, the absorbance at 660 nm was measured using a Tecan Sunrise Microplate Reader. Samples were analyzed in duplicates and the protein concentration for each sample was determined based on a BSA standard curve generated by the four-parameter logistic model.

2.2.14 Measurement of intracellular calcium levels

PBTs were labeled for 45 min at 37 °C, 5 % CO_2 with 2 µg/ml Indo-1 AM (Thermo Fisher Scientific) diluted in RPMI complete medium. To remove excess dye, the cells were washed three times with RPMI complete medium.

For calcium analysis without stimulation, cells were transferred to a round bottom test tube (Falcon) and analyzed on a BD LSR Fortessa™ flow cytometer. Since the emission wavelength of the dye changes depending if calcium is bound to it (~400 nm) or not (~475 nm), the fluorescent signal was measured in two different channels (Indo-1 AM calcium bound; Indo-1 AM no calcium bound). The cells were measured without treatment for 2 min to assess baseline calcium levels. After 2 min, the prediluted test drugs or vehicle were added and measurement was continued for 10 min before maximum calcium influx was induced by the addition of 4 µg/ml Ionomycin. The fluorescent signal was analyzed for further 2 min, whereafter the acquisition was stopped. To completely remove Ionomycin from the flow cytometer, it was washed for 5 min before proceeding with the next sample.

To analyze stimulation-induced calcium influx, cells were pretreated with test drugs or vehicle as described in section 2.2.4. Baseline Indo-1 AM signal was analyzed for 1 min as indicated above. Thereafter, 20 ng/ml anti-CD3 antibody was added and the measurement was continued for 4 min. T cell activation was induced by pipetting 8 µg/ml goat anti-mouse antibody to the cell suspension for crosslinking of CD3. Calcium influx was continuously acquired for 14 min, before 4 µg/ml Ionomycin was added to induce maximum intracellular calcium levels. After another 2 min, the analysis was stopped. As described above, the flow cytometer was rinsed for 5 min after each sample. Data were analyzed in FlowJo by calculating the ratio of Indo-1 AM calcium bound to Indo-1 AM no calcium bound signal and are presented as Area Under the Curve (AUC).

2.2.15 Gene expression analysis

2.2.15.1 Real-Time PCR (qPCR)

The optimal stimulation period for nCounter gene expression analysis was determined based on a kinetics by which *IL2*, *IL2RA* and *CD69* expression was assessed at different time points based on qPCR. Therefore, $1*10^6$ PBTs per sample were stimulated for different time periods as described in section 2.2.4. The cells were then transferred to microcentrifuge tubes, centrifuged (1 min, 300 g) and resuspended in 700 µl MagNA Pure LC mRNA Isolation Kit I - lysis buffer (Roche LifeScience). All subsequent steps were performed by Simone Fomuki (Heidelberg University Hospital, Institute of Immunology, AG Giese). Using the MagNA Pure LC mRNA HS Kit I (Roche LifeScience) according to the manufacturer's protocol, total mRNA was isolated and used for cDNA-synthesis, which was carried out using the First Strand cDNA Synthesis Kit (Sigma Aldrich) according to the manufacturer's instructions. The synthesized cDNA was used for qPCR analysis by LightCycler® (Roche LifeScience).

2.2.15.2 RNA isolation for nCounter

$1*10^6$ PBTs per sample were pretreated with drug or vehicle for 1 h and stimulated for 4 h as outlined in section 2.2.4. Total RNA was isolated using the Direct-zol™ RNA Microprep Kit (Zymo Research) according to the manufacturer's protocol. Therefore, the cells were transferred to RNase-free microcentrifuge tubes (Sarstedt), resuspended in 300 µl TRI Reagent® and mixed thoroughly. After adding 300 µl absolute ethanol (Sigma-Aldrich) and mixing thoroughly, samples were transferred to Zymo-Spin™ IC Columns, which were centrifuged for 30 s at 13,000 g to bind the RNA to the column matrix. The RNA was washed with 400 µl RNA Wash Buffer followed by treatment with 30 U DNase I diluted in DNA Digestion Buffer for 15 min at room temperature. The columns were washed twice with 400 µl Direct-zol™ RNA PreWash and once more with 700 µl RNA Wash Buffer. 15 µl DNase/RNase-Free Water were used to elute the RNA into an RNase-free tube. Aliquots were stored at -80 °C until further processing.

2.2.15.3 Quality control and quantitation of nCounter RNA samples

The quality and quantity of isolated RNA (see section 2.2.15.2) was assessed using a NanoDrop2000c Spectrophotometer (Thermo Scientific). As recommended by nanoString Technologies, samples for nCounter analysis required a 260/280 ratio of at least 1.9 and a 260/230 ratio of 1.8 or greater. Furthermore, Ralph Röth from the nCounter Core Facility of the Heidelberg University Hospital (AG Niesler) quantified the RNA samples using the Qubit Fluorometer (Thermo Fisher Scientific) and assessed the RNA integrity on the Agilent 2100 Bioanalyzer (Agilent Technologies). The RNA Integrity Number (RIN) values of all samples were between 7.2 and 9.5 (0 = completely degraded RNA; 10 = perfectly intact RNA).

2.2.15.4 nCounter run

Total RNA for nCounter analysis was isolated as described in section 2.2.15.2 and quantified as well as quality controlled (see section 2.2.15.3). The expression of 579 immune-related genes including cytokines, interferons and the corresponding receptors as well as many others plus 15 housekeeping genes as internal reference was analyzed using the nCounter® Human Immunology V2 Panel (nanoString Technologies).

The nCounter run was performed in collaboration with the nCounter Core Facility (Heidelberg University Hospital, AG Niesler). All following steps were executed by Ralph Röth (Heidelberg University Hospital, Institute of Human Genetics, AG Niesler). nCounter® Reporter CodeSet (3 µl) and nCounter® Capture ProbeSet (2 µl) were hybridized to their specific RNA targets (5 µl total RNA per sample) in 5 µl Hybridization Buffer overnight at 65 °C. After cooling the samples down to 4 °C, excess probes were removed and the target-probe complexes were immobilized on the cartridge via the biotinylated capture probe. Gene expression was assessed by barcode counting on the nCounter® SPRINT Profiler (nanoString Technologies). The generated data were provided as RCC files and analyzed as described in the following section.

2.2.15.5 nCounter data analysis

The obtained RCC files were imported to the nSolver™ Analysis Software (version 4.0) provided by nanoString Technologies. NormFinder algorithm was used to identify the most stable housekeeping genes among the 15 included internal reference genes based on the raw data. Genes showing a stability value below 0.5 were used for data normalization in nSolver. The normalized data were exported to Excel (Microsoft) and analyzed further. Genes were considered as ‘expressed’ if the counts in at least 50 % on the tested donors were above the threshold (here 25 counts) defined based on the negative control samples. Outliers among expressed genes were identified using GraphPad Prism 9 and excluded from the analysis. Based on the geometric mean of the codeset counts from five different donors, expression fold changes of drug treated samples versus the respective solvent control sample were calculated. Using GraphPad Prism 9, a multiple t test analysis was performed to identify the significantly up- or downregulated genes with a p-value ≤ 0.05. The data are presented as volcano plots showing log2 fold change plotted versus -log10 p-value for each gene.

nCounter data normalized to the housekeeping genes were used as input material for the KEGG (Kyoto Encyclopedia of Genes and Genomes) pathway gene set enrichment analysis (GSEA) that was performed by Dr. Carsten Sticht (Heidelberg University, Medical Faculty Mannheim, NGS Core Facility). In brief, GSEA was used to identify statistically significant changes in the distribution of defined gene sets within a ranked gene list using software packages in R. The pathway analysis was performed with fgsea package (126) and the

enrichmentbrowser package (127). Pathways linked to various cellular functions like cell cycle or intracellular signaling were obtained from the publicly available external database KEGG (https://www.genome.jp/kegg).

2.2.16 HPLC-MS/MS analysis of plant extracts

In collaboration with Dr. Bernhard Wetterauer (Heidelberg University, Institute of Pharmacy and Molecular Biotechnology, Pharmaceutical Biology) an HPLC-MS/MS analysis was performed for phytochemical characterization of the plant extracts. Dr. Wetterauer conducted the following steps. Before analysis, each sample was ultrasonicated for 2 min and diluted to an approximate concentration of 5 mg/ml in the respective plant extract solvent. All used solvents were of analytical grade. After centrifugation (10 min, 13,000 rpm), samples were transferred to GC-vials.

A Finnigan LCQ-Duo ion trap mass spectrometer with an ESI source (ThermoQuest) coupled to a Thermo Scientific Accela™ HPLC-system with an EC 150/3 Nucleodur 100-3 C18ec column (Macherey-Nagel) was used for HPLC-MS/MS analysis. A gradient of water and acetonitrile (VWR) with 0.1 % formic acid (Merck) was applied from 5 % to 30 % acetonitrile in 60 min and to 95 % acetonitrile in another 60 min at 30 °C. The injection volume was 20 µl and a flow rate of 0.5 ml/min was applied. For each sample, measurement was performed in ESI+ and ESI- mode. The mass spectrometer was operated with a capillary voltage of 10 V (ESI+) or -10 V (ESI-), respectively. A source temperature of 240 °C and high purity nitrogen as a sheath and auxiliary gas at a flow rate of 80 and 40 (arbitrary units), respectively, was used. The ions were detected in a mass range of 50 – 2,000 m/z. For fragmentation, a collision energy of 35 % was used. Data were acquired and analyzed using the Xcalibur™ 2.0.7 software (Thermo Scientific). Phytochemical compounds were determined by tentative identification based on literature.

2.2.17 Statistical analysis

Statistical analyses were performed using the GraphPad Prism 9 software. The data are presented as mean ± SEM. Significant numerical differences compared to the respective solvent control sample were determined based on a one-way Analysis of Variance (ANOVA) or a Mixed-effects analysis in case of missing values. Differences with a p-value ≤ 0.05 were considered as being statistically significant (*$p \leq 0.05$; **$p \leq 0.01$; ***$p \leq 0.001$; ****$p \leq 0.0001$).

3 Results

3.1 Titration of anti-CD28 antibody for T cell costimulation

pAPCs such as DCs activate T cells *in vivo* by binding of peptide-loaded MHC to the TCR-CD3 complex and ligation of CD80 or CD86 to the costimulatory receptor CD28. These two signals can be mimicked in experimental *in vitro* settings using a combination of plate-bound antibodies against CD3 and CD28 (CD3x28 stimulation).

In order to identify the optimal concentration for the stimulation of primary human PBTs, a titration of the anti-CD28 antibody was performed. A constant concentration of anti-CD3 antibody (20 ng/ml) which was previously defined in the lab to not induce T cell activation by itself, was combined with increasing concentrations of anti-CD28 antibody ranging from 10 ng/ml to 5,000 ng/ml.

Activation of T cells, inter alia, induces changes in the expression of surface proteins. CD25 (IL-2Rα) as well as CD69 are two such molecules being upregulated upon stimulation. By measuring the expression of these surface markers, T cell activation can be quantified. After 24 h of stimulation, a dose-dependent increase in surface expression of the T cell activation markers, CD25 (Figure 10A) and CD69 (Figure 10B) was observed when compared to the unstimulated control. Using a combination of 20 ng/ml anti-CD3 and 75 ng/ml anti-CD28 antibodies, a robust activation could be reached but not hundred percent of PBTs were activated (Figure 10A-C). This setting was considered ideal for investigating the effects of different drugs on T cell activation, since the test substances might have either an inhibitory or promoting effect. Both ways of influence can be identified with the above-mentioned concentrations of the stimulating antibodies.

Apart from upregulating CD25 and CD69 expression, activation of T cells triggers cell proliferation which represents a central effector function to ensure an efficient immune response. To study their cell division rate, PBTs were labeled with CFSE, a fluorescent dye that passively diffuses into the cells and gets trapped. Upon cell division, the dye is equally distributed to the daughter cells, whereby the fluorescent signal decreases by around half (128). Measuring the CFSE dilution by flow cytometry thus allows to track the proliferative capacity of cells. As depicted in Figure 10D, the percentage of proliferating cells assessed after 72 h of stimulation was significantly elevated when using 75 ng/ml anti-CD28 antibody compared to the unstimulated control. Based on these results, the combination of 20 ng/ml anti-CD3 and 75 ng/ml anti-CD28 antibodies was selected to be used for all further experiments (Figure 10C, E).

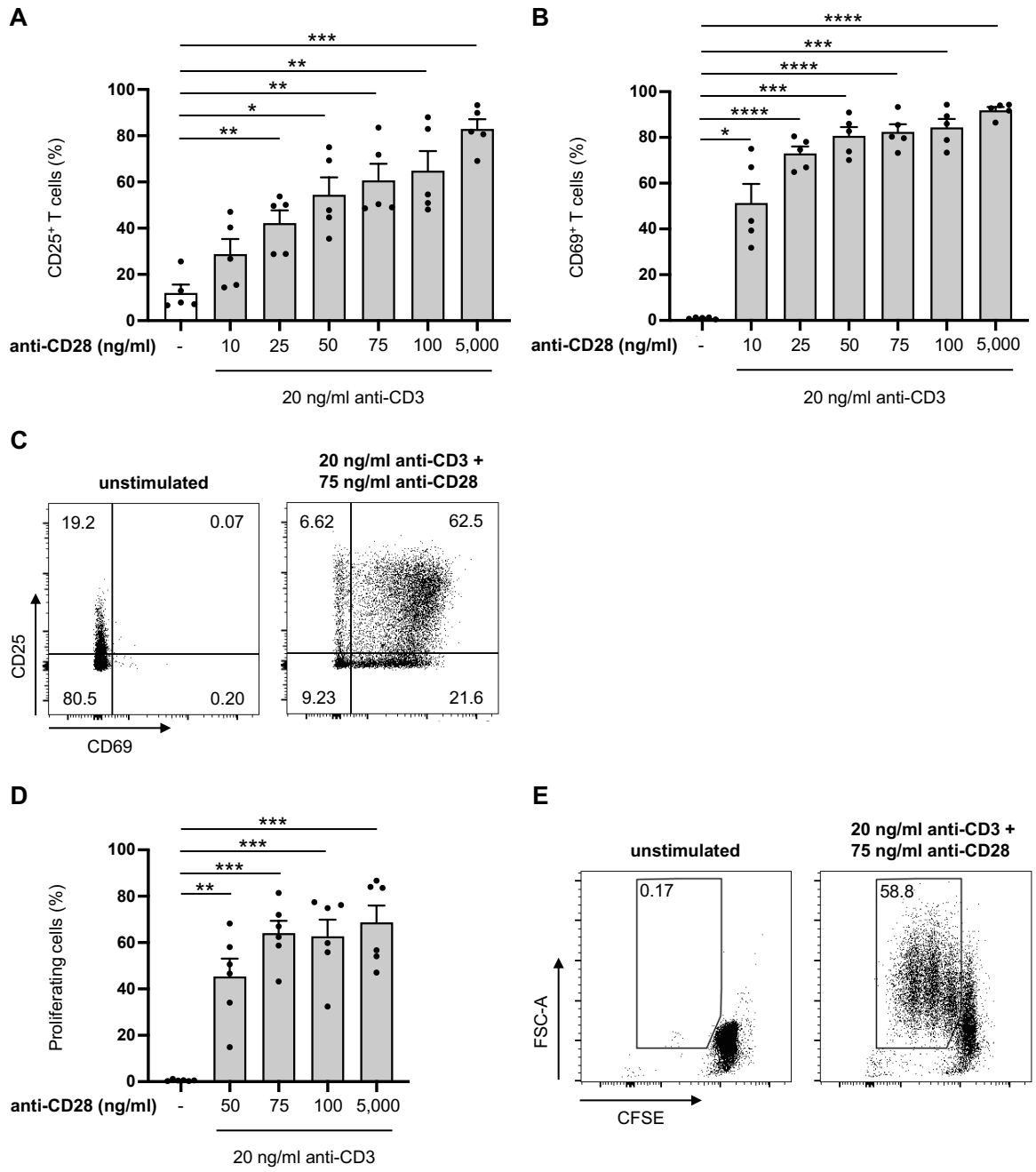

Figure 10: 20 ng/ml anti-CD3 combined with 75 ng/ml anti-CD28 induces robust T cell activation and proliferation.

(**A**-**C**) PBTs were left unstimulated (white bar) or activated with 20 ng/ml anti-CD3 antibody combined with 10 – 5,000 ng/ml anti-CD28 antibody (grey bars) for 24 h. Surface expression of CD25 and CD69 was analyzed by flow cytometry. Statistical evaluation of $CD25^+$ (**A**) and $CD69^+$ (**B**) T cells from five independent experiments. Each data point represents an individual T cell donor. (**C**) Representative dot plots of unstimulated PBTs (left) and PBTs stimulated with 20 ng/ml anti-CD3 plus 75 ng/ml anti-CD28 (right) including percent values. (**D**, **E**) PBTs were labeled with CFSE and left unstimulated (white bar) or activated with 20 ng/ml anti-CD3 antibody combined with 50 – 5,000 ng/ml anti-CD28 antibody (grey bars) for 72 h. T cell proliferation was assessed by CFSE dilution. (**D**) Statistical evaluation of proliferating cells from six independent experiments. Each data point represents an individual T cell donor. (**E**) Representative dot plots of unstimulated PBTs (left) and PBTs stimulated with 20 ng/ml anti-CD3 plus 75 ng/ml anti-CD28 (right). Data are expressed as mean ± SEM. *$p \leq 0.05$; **$p \leq 0.01$; ***$p \leq 0.001$; ****$p \leq 0.0001$

3.2 Selection of promising Arnica extracts and optimal test concentrations of extracts and lead substances

The immunomodulatory potential of *Arnica montana* L. (Arnica) preparations was investigated using the experimental workflow depicted in Figure 11. In short, primary human PBTs were freshly isolated by negative selection from venous whole blood of healthy donors. Next, the cells were preincubated with drug or vehicle for 1 h and subsequently activated by CD3x28 stimulation. Depending on the final readout, PBTs were stimulated for 30 min to 72 h.

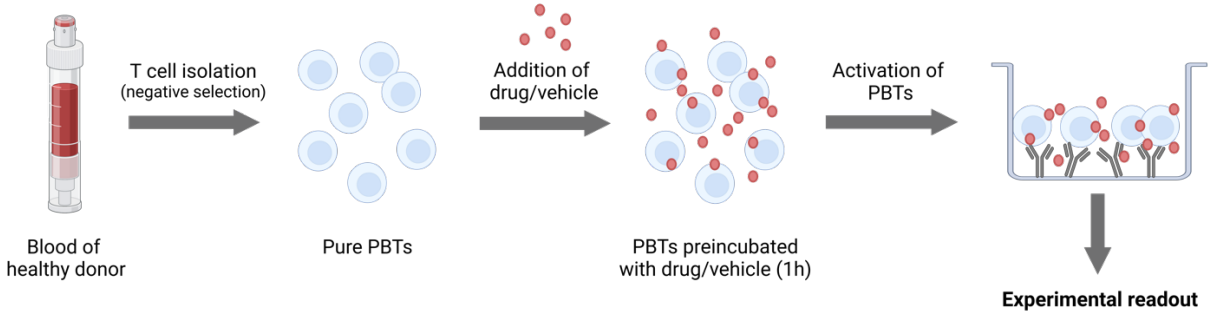

Figure 11: Scheme of the experimental workflow.

PBTs were obtained by negative selection from peripheral blood of healthy donors. Following 1-hour preincubation with drug or vehicle, PBTs were activated by CD3x28 stimulation. Depending on the readout, PBTs were stimulated for 30 min to 72 h. This figure was created with BioRender.com.

Six differentially prepared Arnica extracts, summarized in Table 13, were kindly provided by WALA Heilmittel GmbH (Bad Boll), Weleda AG (Schwäbisch Gmünd), and DHU-Arzneimittel GmbH & Co. KG (Karlsruhe). For information on the manufacturing processes please refer to the methods section 2.2.1 and Table 5.

Based on the companies' experiences, it was suggested to test serial 1:10 dilutions of the extracts ranging from 1:10 to 1:10,000. However, the maximum extract concentration to be tested in our system (see Figure 11) was limited by ethanol (EtOH) contained in hydroalcoholic extracts and by the pH value of aqueous extracts, respectively. 1:10 dilutions of aqueous extracts induced a color change of phenol red contained in the cell culture medium towards orange / yellow, indicating an acidic milieu. To circumvent this, aqueous extracts were finally diluted at least 1:100. Regarding the final EtOH concentration in culture, a maximum of 0.1 % EtOH was set to avoid effects being induced by the solvent itself. Furthermore, a sample treated with EtOH only was included in each assay as a direct solvent control.

To select the most promising candidates, all six extracts were tested for their effect on T cell viability, activation and proliferation during an initial screening. Some extracts proved to be cytotoxic for PBTs even at higher dilutions, others had no effect on T cell function (data not shown). This provided the basis for selecting the three most promising candidates (screening data will be shown in the following) for further investigation (Table 13). While Ferm and Tota extract were prepared from the whole fresh flowering plant, the dried underground parts were

used as raw material for preparation of the Radix extract. Ferm (aqueous) and Tota (hydroalcoholic) extracts differ in their solvent and the fermentation process, which only Ferm underwent.

Table 13. Summary of tested *Arnica montana* extracts

Arnica extract	Abbreviation	Used plant parts	Solvent	Manufacturer	Selected
Planta tota Rh ∅ V.21	-	Press juice of entire flowering plant (fresh)	H_2O	Weleda	No
Rh ∅ V.21 (Radix)	-	Press juice of rootstock (fresh)	H_2O	Weleda	No
E floribus LA 20%	-	Flower heads (fresh)	20 % EtOH	WALA	No
E planta tota ferm 33c	Ferm	Entire flowering plant (fresh)	H_2O	WALA	Yes
Planta tota ∅ V.2b	Tota	Entire flowering plant (fresh)	30 % EtOH	Weleda	Yes
Mother tincture	Radix	Underground parts (dried)	86 % EtOH	DHU	Yes

Given the final maximum concentration of 0.1 % EtOH, the highest possible test concentration of Tota extract (30 % EtOH) was a 1:300 dilution. The Radix extract (86 % EtOH) had to be diluted at least 1:860. Thus, both extracts were tested in a 1:1,000 dilution. For comparability, the aqueous Ferm extract was also diluted 1:1,000.

Before studying the effects of Arnica preparations on T cell functions, it was excluded that the test substances affect cell viability. Therefore, PBTs were preincubated with a 1:1,000 dilution of the respective extract or vehicle control. The final EtOH concentration in the control and drug treated samples was kept at a maximum of 0.1 % to ensure direct comparability. Next, PBTs were activated for 24 h or 72 h, respectively, using CD3x28 stimulation. Cell viability was assessed using 7-AAD viability dye, which is excluded from live cells and specifically stains dead cells because of their disrupted membrane. The fluorescent signal will be located in the cell nucleus since the dye intercalates into double-stranded DNA (129). None of the three Arnica extracts decreased cell viability below the defined threshold of 90 % live cells after 24 h and 72 h, respectively (Figure 12A, B).

Helenalin and Thymol are among the 150 therapeutically active substances identified in Arnica. The sesquiterpene lactone Helenalin is mainly found in aerial plant parts, especially in Arnica flowers. Thymol, in contrast, is a monoterpene phenol that is contained in the essential oil and therefore mainly present in Arnica roots (reviewed by (83)). These two lead compounds were selected to be studied in parallel to the Arnica extracts.

In order to identify the highest usable, non-toxic concentration of both substances, a titration experiment was performed and cell viability was assessed by 7-AAD exclusion. The substances were dissolved in DMSO and a limit of 0.1 % DMSO in the final culture was defined. Consequently, the drug treated as well as the solvent control sample were prepared to contain 0.1 % DMSO for direct comparability. Based on the concentrations used in literature (97,130,131), Thymol was tested in a range from 100 μM to 500 μM. No toxic effect could be observed after 24-hour and 72-hour incubation with any of the used concentrations (Figure 12C, D). Therefore, 500 μM Thymol were used in all further experiments. Similarly, for Helenalin, which is commonly used in a range of 0.1 μM to 1 μM (96,132), a cytotoxic effect was also excluded. After 24-hour incubation, the highest non-toxic concentration was 0.5 μM Helenalin (Figure 12E, F). A dose-dependent cytotoxic effect on PBTs was observed after 72 h for concentrations greater than 0.25 μM. Based on these data, 0.25 μM Helenalin was selected to be used for all subsequent assays.

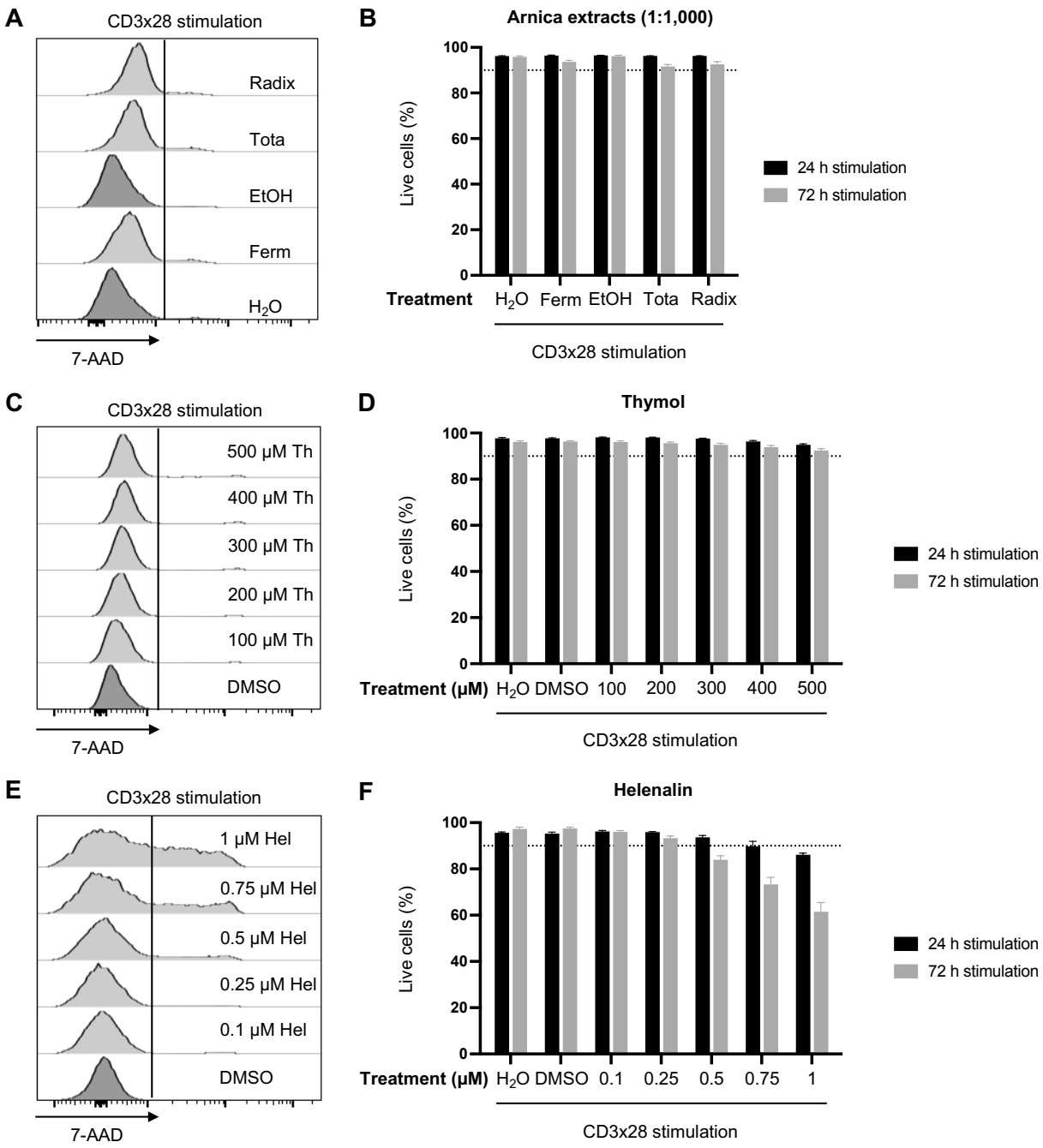

Figure 12: Selected extract and drug concentrations are not cytotoxic to PBTs.

PBTs were pretreated with drug or vehicle for 1 h and subsequently activated with anti-CD3/CD28 antibodies. Cell viability after treatment with Arnica extracts (**A**, **B**), Thymol (**C**, **D**) or Helenalin (**E**, **F**) was assessed by 7-AAD exclusion. (**A**, **C**, **E**) Representative histograms of solvent control (dark grey) and drug treated samples (light grey) after 72-hour stimulation. (**B**, **D**, **F**) Data summary from 3 – 6 independent experiments after 24-hour (black) and 72-hour stimulation (grey). Data are expressed as mean ± SEM.

3.3 Arnica preparations inhibit CD25 (IL-2Rα) expression and T cell proliferation

To study the influence of the test drugs on surface expression of the T cell activation markers CD25 (IL-2Rα) and CD69, PBTs were preincubated with drug or vehicle and stimulated with anti-CD3/CD28 antibodies. After 24 h, cells were stained for CD25 and CD69 and analyzed by flow cytometry. Since there are different ways of data analysis and representation, the procedure used in this thesis will be shortly summarized in the following using CD25 as an example. In general, flow cytometry provides information on two parameters. First, the percentage of cells expressing the protein of interest (Figure 13A, B) and second the mean fluorescent intensity (MFI) represented by the geometric mean (Geo mean) in this work (Figure 13C, D). Based on the MFI, the average expression of the protein of interest per cell can be assessed. Eventually, there are two options of displaying MFI data. Either the percentage of $CD25^+$ cells (Figure 13B) is shown in combination with the Geo mean of CD25 for the $CD25^+$ cells (Figure 13C) or only the Geo mean for all T cells (Figure 13D) is presented, which combines both information. For this thesis, the second option was chosen and the Geo mean will always be calculated for total T cells.

Statistical analyses were always performed compared to the respective solvent control (dark grey bars). Only experiments showing a significant difference between the unstimulated sample and the stimulated H_2O control were evaluated. Therefore, significances for this comparison are not indicated in the graphs.

Concerning the effect of Arnica preparations on T cell activation marker expression, it was found that all three extracts significantly diminished CD25 expression compared to the H_2O or EtOH control, respectively (Figure 13A, D). The Radix extract was most efficient, followed by Tota and Ferm. CD69 expression was only reduced by Radix extract, while Tota and Ferm had no significant effect on this marker (Figure 13A, E). These data already indicate differences in the mode of action of the three extracts which were manufactured by completely different procedures.

In parallel, the effect of Thymol and Helenalin was studied. Compared to the DMSO control sample, both substances significantly inhibited CD25 expression and Thymol had a stronger effect than Helenalin (Figure 14A, B). No significant influence was observed on the Geo mean of CD69 (Figure 14A, C).

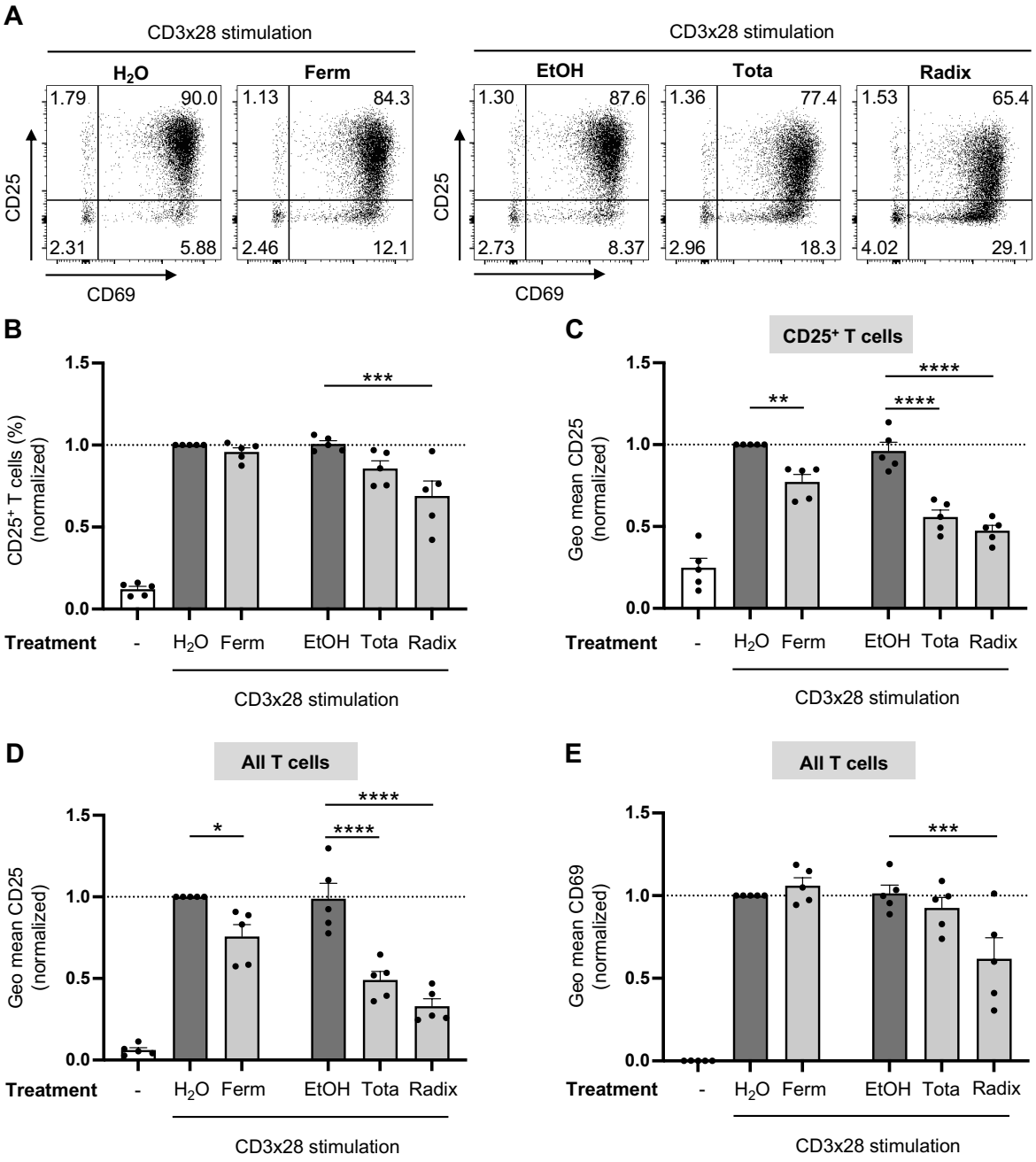

Figure 13: All Arnica extracts downregulate CD25, while Radix extract also reduces CD69 expression.
PBTs were left unstimulated (white bar) or pretreated with Arnica extract (light grey bars) or vehicle (dark grey bars) for 1 h and subsequently activated with anti-CD3/CD28 antibodies for 24 h. Surface expression of CD25 and CD69 was analyzed by flow cytometry. Representative dot plots including percent values (**A**) and statistical evaluation of CD25 (**B**-**D**) and CD69 (**E**) MFI from five independent experiments. Each data point represents an individual T cell donor. Data were normalized to the H_2O control sample and are expressed as mean ± SEM. *$p \leq 0.05$; **$p \leq 0.01$; ***$p \leq 0.001$; ****$p \leq 0.0001$

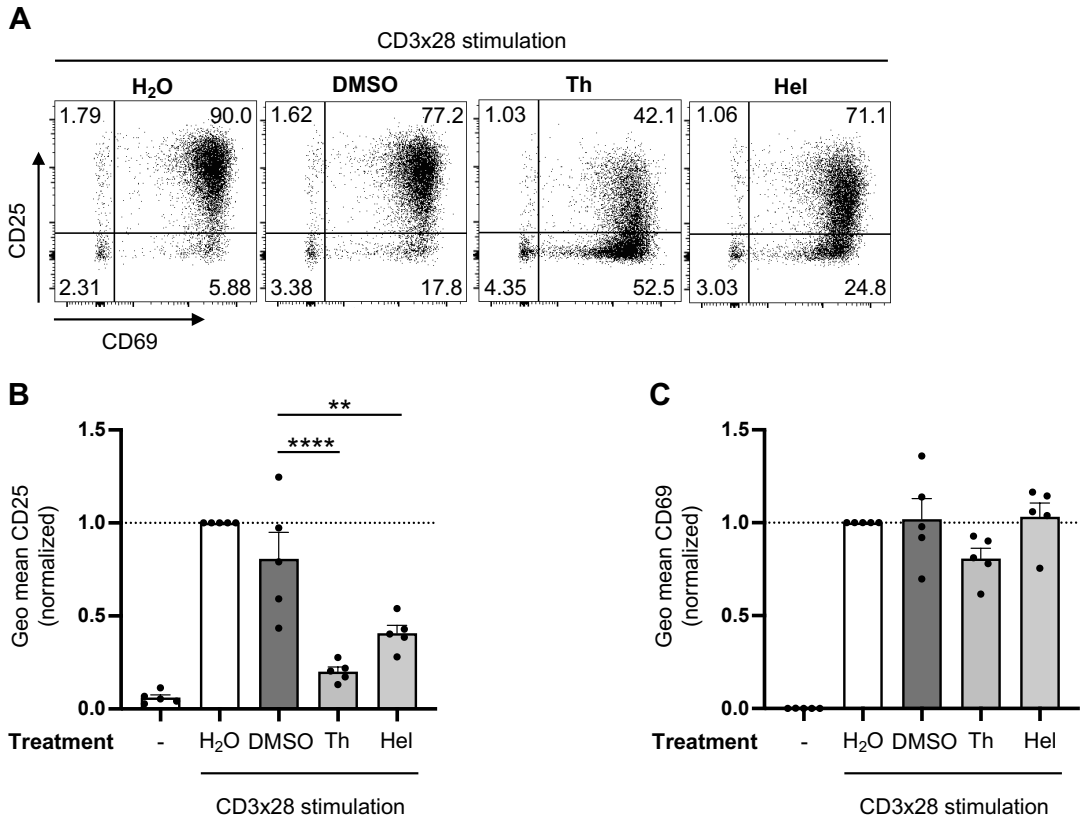

Figure 14: Thymol and Helenalin diminish CD25 but not CD69 expression.

PBTs were left unstimulated (left white bar) or pretreated with substance (light grey bars) or vehicle (dark grey bar) for 1 h and subsequently activated with anti-CD3/CD28 antibodies for 24 h. Surface expression of CD25 and CD69 was analyzed by flow cytometry. Representative dot plots including percent values (**A**) and statistical evaluation of CD25 (**B**) and CD69 (**C**) MFI from five independent experiments. Each data point represents an individual T cell donor. Data were normalized to the H_2O control sample and are expressed as mean ± SEM. $^{**}p \leq 0.01$; $^{****}p \leq 0.0001$

Within 72 h of CD3x28 stimulation, T cells undergo proliferation (clonal expansion) to increase their number. Thus, as a next step, the influence of Arnica extracts and lead substances on this essential effector function was analyzed. Briefly, PBTs were labeled with CFSE dye and CFSE dilution was analyzed by flow cytometry. The proliferative capacity of cells can be expressed by means of the Division Index. This Index is an average for the number of cell divisions each cell, including non-dividers, has undergone.

As depicted in Figure 15A and B, Arnica extracts diminished T cell proliferation. Again, the Radix extract had the most prominent effect, followed by Tota and Ferm. Similarly, treatment with Thymol and Helenalin resulted in decreased T cell proliferation (Figure 15C, D).

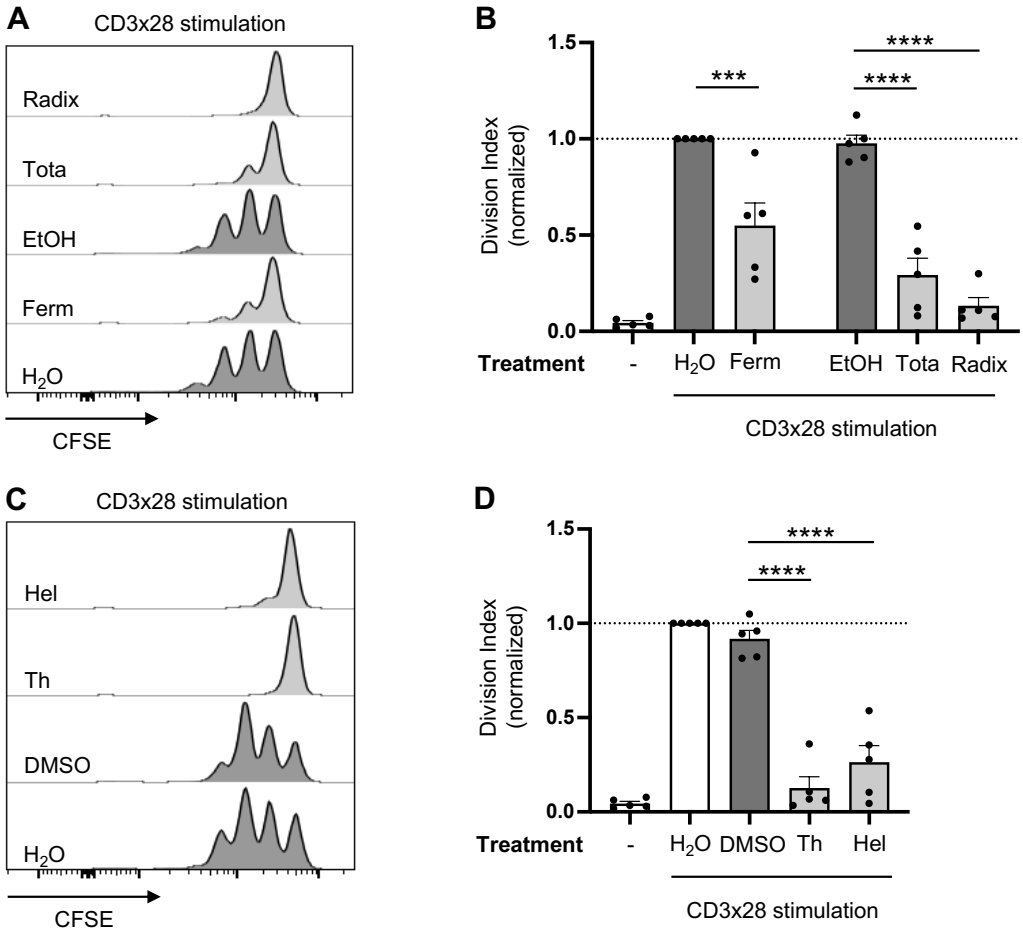

Figure 15: Arnica preparations diminish T cell proliferation.

PBTs were labeled with CFSE, left unstimulated (left white bar) or pretreated with drug (light grey) or vehicle (dark grey) for 1 h and subsequently activated with anti-CD3/CD28 antibodies for 72 h. T cell proliferation after treatment with Arnica extracts (**A**, **B**) or lead substances (**C**, **D**) was assessed by CFSE dilution. Representative histograms (**A**, **C**) and statistical evaluation (**B**, **D**) from five independent experiments. Each data point represents an individual T cell donor. Data were normalized to the H_2O control sample and are expressed as mean ± SEM. ***$p \leq 0.001$; ****$p \leq 0.0001$

3.4 Arnica preparations diminish IL-2 production but T cell proliferation cannot be rescued by IL-2 supplementation

T cell proliferation greatly depends on the presence of IL-2, a growth factor that is produced by activated T cells. IL-2 acts in an autocrine as well as paracrine manner and stimulates cell division upon binding to the IL-2R. IL-2-dependent signaling is connected to the activation-induced increase in CD25 expression, since this protein represents the IL-2Rα chain that is essential for creating a high-affinity IL-2R. Therefore, a reduction of CD25 expression and/or a lack of IL-2 production can give a potential explanation for diminished proliferation.

IL-2 released by PBTs was quantified based on a cytometric bead array (LEGENDplex^{TM}) after 24 h of stimulation and the effects of the different treatments were analyzed. As shown in Figure 16A, the Arnica extracts diminished the IL-2 content in the cell culture medium with similar efficiency. The inhibitory effect of Thymol and Helenalin on the IL-2 content was found to be even greater (Figure 16B).

The observed decrease of IL-2 in the supernatant can result from different scenarios. Either IL-2 production by transcription and translation or the cellular export is disturbed by drug treatment or the consumption of IL-2 is increased. An intracellular staining of IL-2 was performed to investigate which of the options occurs upon treatment with Arnica preparations. All Arnica extracts significantly diminished the percentage of IL-2$^+$ cells after 24 h of CD3x28 stimulation (Figure 16C, E). The same effect was observed upon Thymol or Helenalin treatment (Figure 16D, F). Taking these results together, it was shown that Arnica preparations diminish IL-2 production, which is the cause for the observed diminished IL-2 concentration in the supernatant.

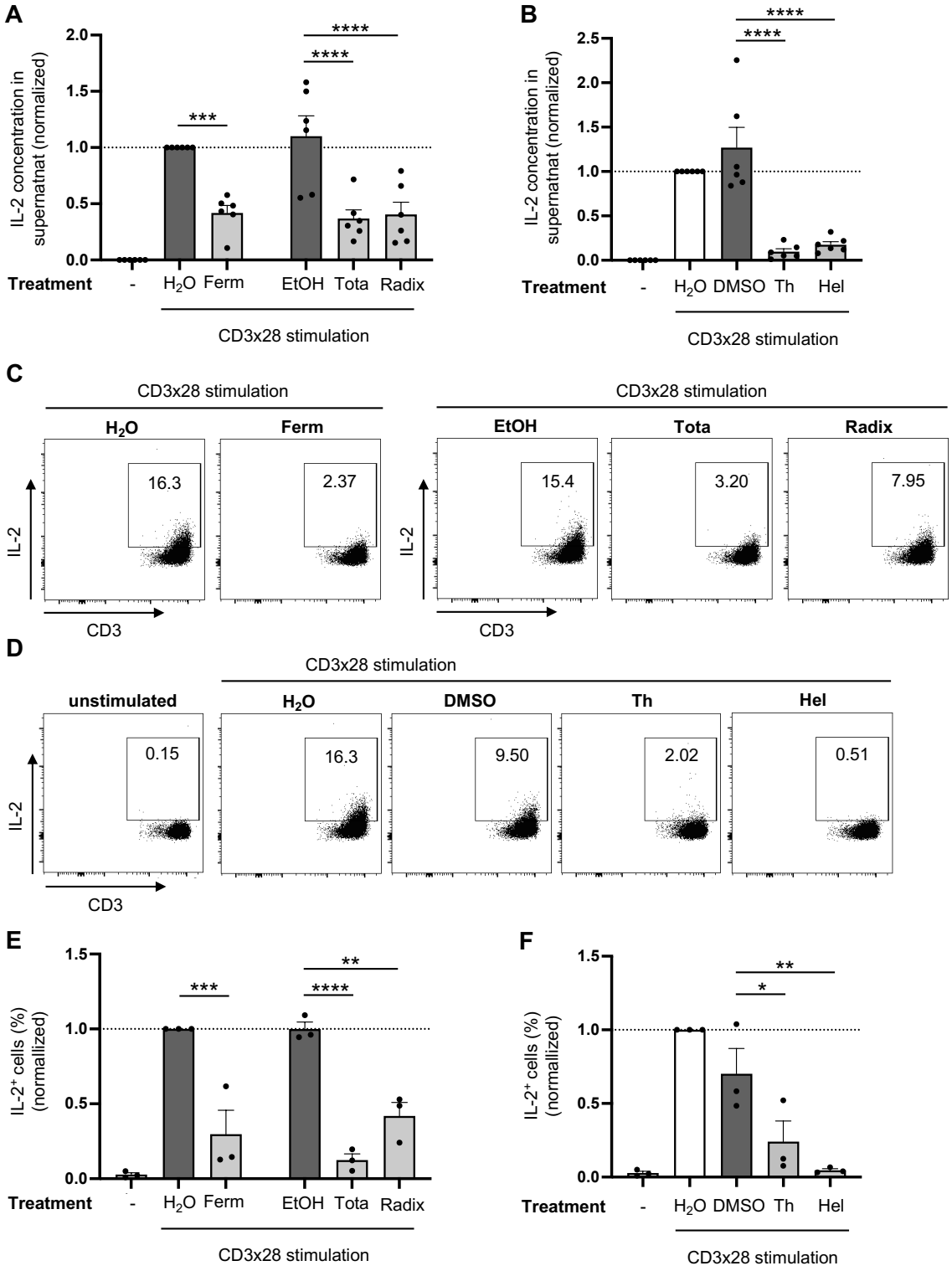

Figure 16: Arnica preparations inhibit IL-2 production in human PBTs.

PBTs were left unstimulated (left white bar) or pretreated with drug (light grey bars) or vehicle (dark grey bars) for 1 h and subsequently activated with anti-CD3/CD28 antibodies for 24 h. (**A**, **B**) IL-2 released to the supernatant after treatment with Arnica extracts (**A**) or lead substances (**B**) was quantified by cytometric bead array (LEGENDplex™) in six independent experiments. Each data point represents an individual T cell donor. (**C**-**F**) Intracellular IL-2 staining after treatment with Arnica extracts (**C**, **E**) or lead substances (**D**, **F**) analyzed by flow cytometry. Representative dot plots (**C**, **D**) and statistical evaluation (**E**, **F**) from three independent experiments. Each data point represents an individual T cell donor. Data were normalized to the H_2O control sample and are expressed as mean ± SEM. *$p \leq 0.05$; **$p \leq 0.01$; ***$p \leq 0.001$; ****$p \leq 0.0001$

Considering that IL-2 is essential for stimulating T cell division, a rescue experiment was performed in order to find out if supplementation of IL-2 can restore normal T cell proliferation upon drug treatment. Therefore, CFSE-labeled PBTs were stimulated in the presence of drug or vehicle control in medium with or without 40 U/ml recombinant human IL-2. After 72 h, the samples were analyzed by flow cytometry and the Division Indices of samples with and without IL-2 supplementation were compared. For none of the Arnica extracts, T cell proliferation could be restored in the presence of IL-2 (Figure 17A). The same findings were noticed for Thymol or Helenalin treatment (Figure 17B).

A control experiment was performed to verify IL-2 functionality. CFSE-labeled PBTs were stimulated overnight with 2 μg/ml Phytohaemagglutinin (PHA). However, this stimulation alone does not induce T cell proliferation (Figure 17C). Instead, functional recombinant human IL-2 (40 U/ml) is needed to stimulate cell division. Since after 72 h the percentage of proliferating PBTs increased significantly in the presence of PHA and IL-2, cytokine functionality was proven (Figure 17C).

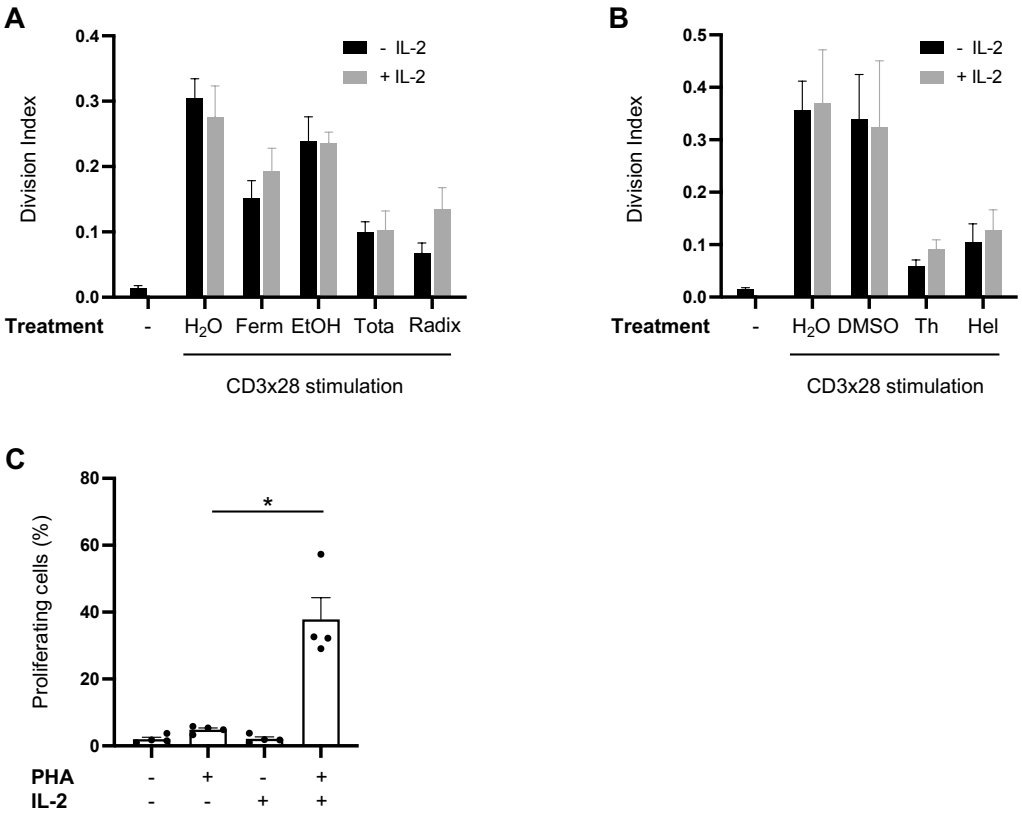

Figure 17: Inhibited T cell proliferation cannot be rescued by IL-2 supplementation.

(**A**, **B**) PBTs were labeled with CFSE, left unstimulated or pretreated with drug or vehicle for 1 h and subsequently activated with anti-CD3/CD28 antibodies for 72 h in the presence (grey bars) or absence (black bars) of 40 U/ml recombinant human IL-2. T cell proliferation after treatment with Arnica extracts (**A**) or lead substances (**B**) was assessed by CFSE dilution in five independent experiments. (**C**) PBTs were labeled with CFSE and left untreated or pretreated with PHA overnight. After PHA removal, PBTs were incubated for 72 h with or without 40 U/ml recombinant human IL-2. T cell proliferation way assessed by CFSE dilution in four independent experiments. Each data point represents an individual T cell donor. Data are expressed as mean ± SEM. *$p \leq 0.05$

Based on these findings it can be concluded that drug-induced inhibition of IL-2 production is not the only reason for diminished T cell proliferation but other factors such as the observed reduction in IL-2Rα (CD25) expression (Figure 13D, Figure 14B) contribute to this effect.

3.5 Thymol and Helenalin inhibit T cell migration, while Arnica extracts have no effect

Apart from increasing their number by proliferation, migration is another hallmark of T cell function. It allows naïve T cells to scan the body for their cognate antigen and effector T cells to arrive at sites of infection or inflammation. Immune cell migration in general is controlled by secreted molecules, the so-called chemokines, which specifically attract certain cell types. Stromal Cell-Derived Factor-1α (SDF-1α) is a chemokine produced by bone marrow stromal cells and well described to serve as a potent chemoattractant for peripheral blood lymphocytes (PBLs) that include T cells (133,134).

Using Transwell™ inserts with 5 μm pore size, the effect of Arnica preparations on the migratory capacity of PBTs towards SDF-1α (100 ng/ml) was assessed. Therefore, PBTs pretreated with drug or vehicle were placed in the upper compartment that is separated from the lower, chemoattractant-containing compartment by a permeable membrane. During 90 min of incubation, the PBTs actively have to squeeze through the pores in the membrane to end up in the lower compartment. Finally, PBTs in the lower compartment are counted using flow cytometry and the results are expressed as percentage of migrated cells. The calculations are based on a comparison to the positive control with hundred percent of cells in the lower compartment. As summarized in Figure 18A, treatment with any of the Arnica extracts did not affect T cell migration towards SDF-1α. In contrast, both, Thymol as well as Helenalin, significantly diminished the migratory capacity of PBTs (Figure 18B).

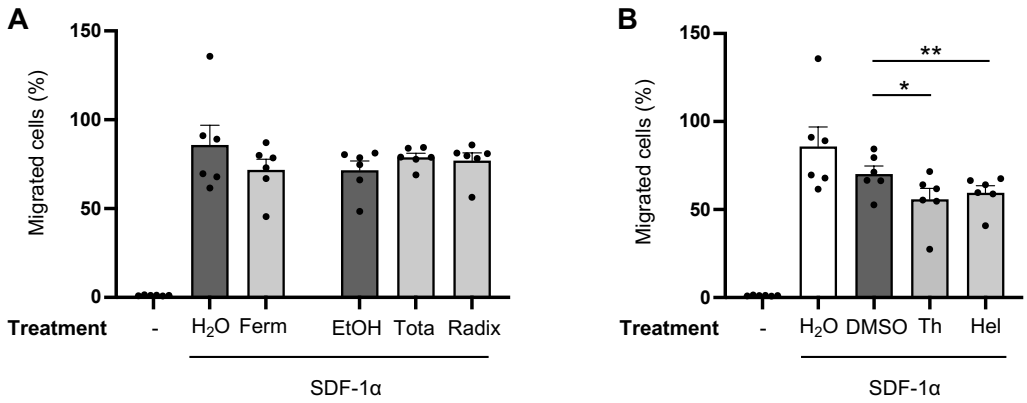

Figure 18: T cell migration is inhibited by Thymol and Helenalin but not by Arnica extracts.

PBTs were left unstimulated (left white bar) or pretreated with drug (light grey bars) or vehicle (dark grey bars) for 1 h and transferred to the upper compartment of a 5 μm pore size Transwell™ insert. SDF-1α was used as a chemoattractant in the lower compartment. T cell migration after treatment with Arnica extracts (**A**) or lead substances (**B**) was quantified by flow cytometry in six independent experiments. Each data point represents an individual T cell donor. Data are expressed as mean ± SEM. *$p \leq 0.05$; **$p \leq 0.01$

Dynamic reorganization of the actin cytoskeleton is a prerequisite for the ability of cells to change their shape which is not only closely linked to cellular migration but also to other functions such as proliferation or immune synapse formation. In T cells, L-plastin (LPL) and cofilin are two important proteins that are involved in actin bundling and depolymerization, respectively (reviewed by (135)). Upon T cell costimulation, LPL is activated by phosphorylation (28) whereas cofilin activity is induced by dephosphorylation (29,30).

The influence of different Arnica preparations on LPL and cofilin activation was assessed after 30 min of CD3x28 stimulation. Representative Western Blots of phosphorylated and total proteins are shown in Figure 19A-D. For the three Arnica extracts no significant effect could be observed on LPL phosphorylation (Figure 19A, E) and cofilin dephosphorylation (Figure 19A, G). Interestingly, treatment with Thymol or Helenalin also had no significant influence on both parameters (Figure 19C, F, H). Therefore, diminished T cell migration observed upon Thymol or Helenalin treatment did not result from impaired actin-remodeling through LPL and/or cofilin.

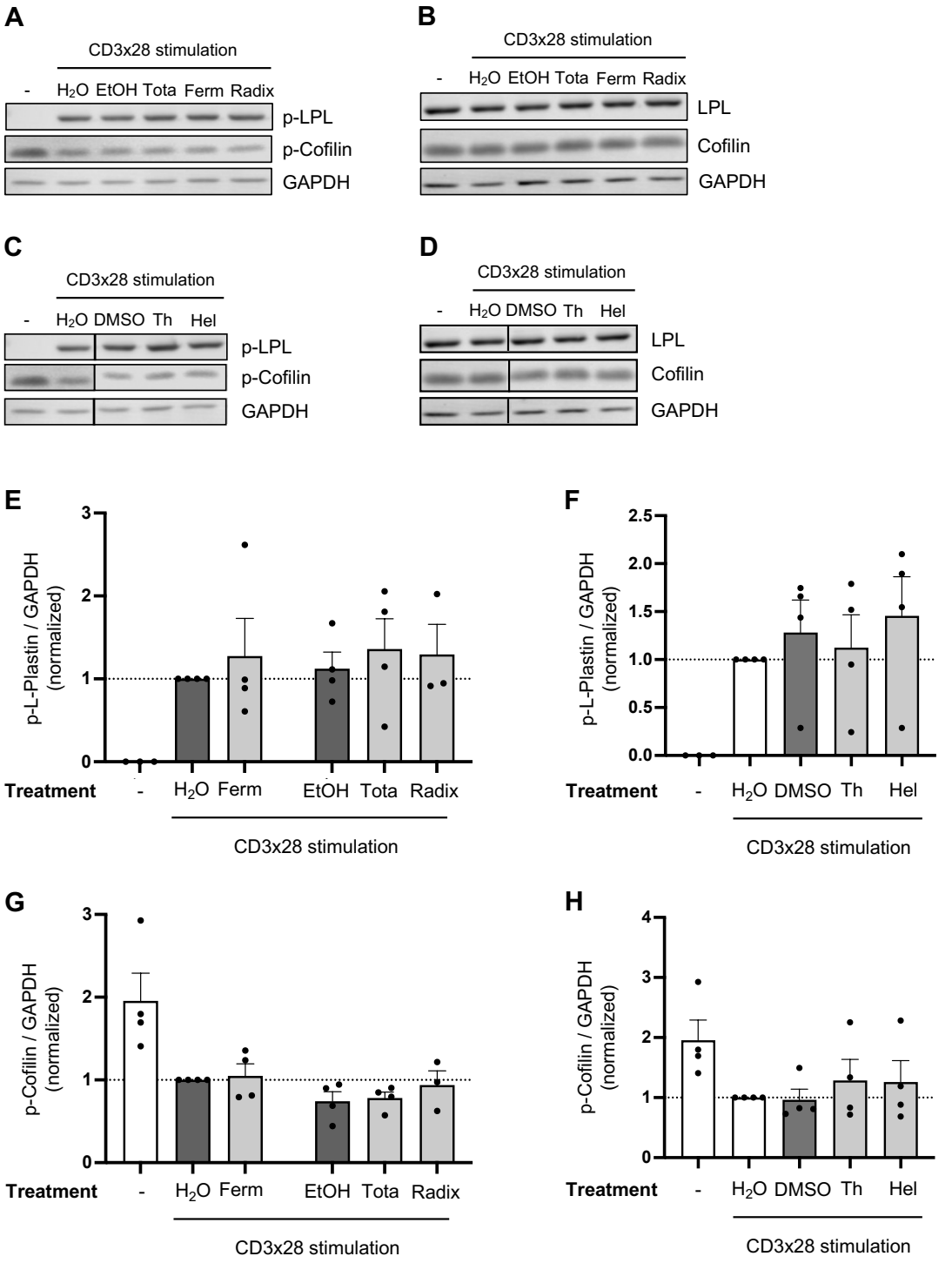

Figure 19: Arnica preparations do not affect LPL phosphorylation and cofilin dephosphorylation.
PBTs were left unstimulated (left white bar) or pretreated with drug (light grey bars) or vehicle (dark grey bars) for 1 h and subsequently activated with anti-CD3/CD28 antibodies for 30 min. Phosphorylated and total LPL or cofilin was quantified by western blot after treatment with Arnica extracts (**A**, **B**, **E**, **G**) or lead substances (**C**, **D**, **F**, **H**). Representative blots (**A**-**D**) and statistical evaluation of p-LPL and p-cofilin bands (**E**-**H**) from four independent experiments. Each data point represents an individual T cell donor. Data were normalized to the H_2O control sample and are expressed as mean ± SEM.

3.6 Arnica preparations intervene in the TCR signaling pathway

In order to get a first impression of the molecular mechanism underlying the functional effects of Arnica preparations on human PBTs, a gene expression analysis using the nCounter® technology by nanoString was performed.

In a preliminary experiment, the optimal timepoint for isolation of total RNA from CD3x28-stimulated PBTs was determined. Therefore, a kinetics was performed for up to six hours and *IL2*, *IL2RA* (encoding CD25), and *CD69* transcription was quantified by real-time PCR. The qPCR analysis after RNA isolation was conducted by Simone Fomuki (Heidelberg University Hospital, Institute of Immunology, AG Giese) and the results are depicted in Figure 20A. After 4-hour stimulation, the number of *IL2* and *IL2RA* transcripts reached a maximum. *CD69* expression was found to be highest after 1 h of stimulation, however, after 4 h, the number of transcripts was still clearly elevated. Based on these data 4-hour stimulation was regarded as optimal for subsequent gene expression analysis.

Total RNA was isolated from drug or vehicle treated PBTs after 4-hour CD3x28 stimulation and provided to the nCounter Core Facility (Heidelberg University Hospital, AG Niesler). Ralph Röth (Heidelberg University Hospital, Institute of Human Genetics, AG Niesler) conducted the gene expression analysis using the nCounter® Human Immunology V2 Panel. This panel allows to simultaneously detect the expression of 579 immune-related genes including cytokines, interferons and the corresponding receptors as well as many others in addition to 15 housekeeping genes as internal reference.

After normalization to the housekeeping genes, significantly up- or downregulated genes were identified for each treatment. The effects of treatment with Arnica extracts compared to the respective solvent control are depicted in Figure 20B-D. Significantly downregulated genes are colored in blue while significantly upregulated genes are shown in red. When comparing the three extracts, it becomes apparent that Arnica Tota (Figure 20C) had the strongest effect on gene expression, followed by Radix (Figure 20D) and finally by Ferm (Figure 20B). The lead substances Thymol (Figure 20E) and Helenalin (Figure 20F) had an even more pronounced influence on gene expression. A summary of significantly regulated genes is provided in Table 14. As indicated in Figure 20B-F, numerous cytokine genes were among the significantly downregulated candidates with all tested treatments.

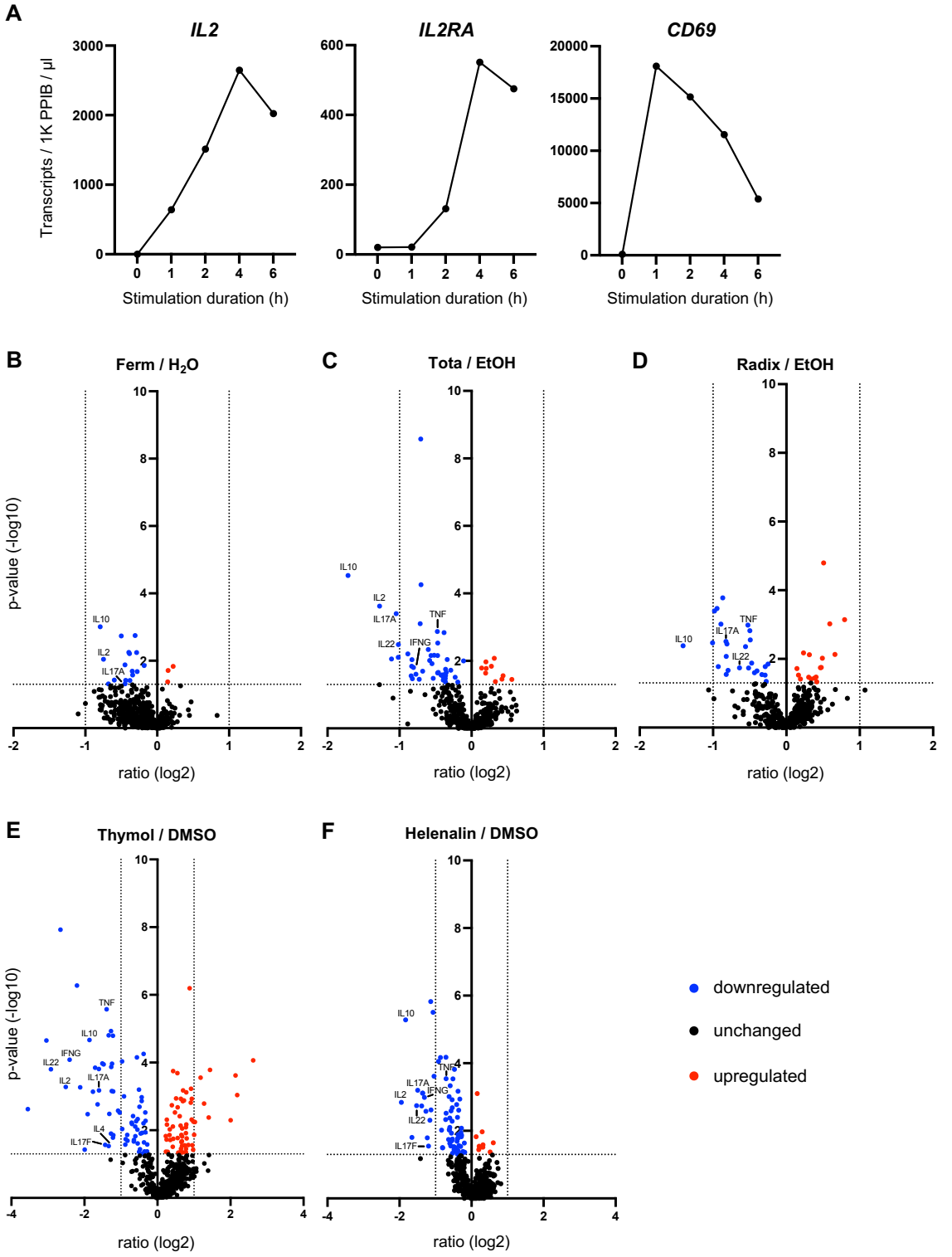

Figure 20: Arnica extracts and lead substances differentially affect gene expression in human T cells.
(**A**) PBTs were left unstimulated or activated with anti-CD3/CD28 antibodies for 1 h to 6 h. *IL2*, *IL2RA* and *CD69* transcripts were quantified by qPCR. (**B**-**F**) PBTs were pretreated with drug or vehicle for 1 h and subsequently activated with anti-CD3/CD28 antibodies for 4 h. Total RNA was isolated and mRNA transcripts of 579 immune-related genes (Human Immunology V2 Panel) were counted using the nCounter® technology by nanoString. Pairwise comparisons of gene expression from drug treated samples and the respective solvent control are shown as volcano plots. Significantly downregulated (blue) and upregulated genes (red) are indicated. Some interesting candidates are labeled. A summary of significantly up-or downregulated genes upon treatment with the different test drugs compared to their solvent control is provided in Table 14.

Table 14: Summary of significantly up- or downregulated genes upon treatment with Arnica preparations

For each significantly regulated gene ($p \leq 0.05$), the ratio (log2) of differential expression upon treatment with the different test drugs compared to their respective solvent control is indicated in numbers. Significantly downregulated genes are shaded in blue, significantly upregulated genes in red.

Gene	ratio (log2)				
	Ferm	Tota	Radix	Thymol	Helenalin
ABCB1		0,42			0,60
AHR			0,48	-0,42	
ARG2				1,02	
ARHGDIB				0,91	
ATG16L1				0,26	
BATF		-0,73		-1,64	-1,27
BATF3		-0,36	-0,50	-1,71	-0,64
BAX	0,22	0,20	0,17	0,25	0,21
BCAP31		0,33			
BCL10	0,15	0,28	0,51	0,55	0,30
BCL2				0,92	
BCL2L11		-0,47	-0,51	-1,27	-0,71
BCL6			0,59	0,79	-0,39
BTK	-0,68			0,65	
BTLA					-0,80
C8A				0,63	
CASP2				0,61	
CASP8				0,67	
CCL20		-0,36		-0,92	-1,04
CCND3				0,95	
CCR7				2,18	
CD27				0,94	
CD274			-0,81	-1,24	-0,41
CD28	0,15			1,44	
CD3D				0,51	
CD3E				0,42	
CD3EAP				-0,54	-0,39
CD40LG				-1,32	
CD45RA				0,98	
CD45RB				0,78	
CD48		-0,23		0,26	-0,32
CD5				2,14	
CD59		0,44	0,38		0,32
CD6				1,28	
CD7				0,64	-0,58
CD82		-0,42		-0,67	-0,72
CD96			0,30	0,70	
CD97					-0,49
CEBPB		0,31	0,79	0,72	0,31
CHUK				-0,33	
CISH	-0,29	-0,70	-0,87	-2,20	-0,86
CRADD				0,78	
CSF1				-0,65	
CSF2		-0,83	-0,82	-3,04	-1,36
CTLA4_all		-0,58		0,69	-0,49
CTLA4-TM		-0,55		0,55	-0,62
CTNNB1		0,14	0,14		0,16
CUL9				0,57	
CXCR4				2,01	
DUSP4		-0,83			-1,12
EGR2					-0,37
FKBP5			-0,29		
FOXP3	-0,44			0,61	
FYN				0,34	-0,24
GBP1				-1,34	-0,28
GFI1	-0,39	-0,60		-0,49	-0,92
GZMB				-1,99	
ICAM1				-1,27	
ICAM2				0,39	
ICAM3					0,23
ICOS		-0,46			-0,56
IFI16					-0,19
IFITM1		-0,52	-0,95	-0,65	
IFNAR1				0,78	
IFNAR2			0,41	1,18	
IFNG		-0,81		-2,41	-1,31
IFNGR1		0,19			
IL10	-0,79	-1,72	-1,41	-1,86	-1,83
IL16				2,62	
IL17A	-0,45	-1,05	-0,82	-1,60	-1,49
IL17F				-1,43	-1,19
IL18R1				-0,83	
IL18RAP		-0,68		-0,88	-0,81
IL1R1			0,49		-0,59
IL1RL1		-0,77			
IL2	-0,75	-1,28		-2,51	-1,95
IL21		-1,11	-0,93	-2,12	-1,39
IL21R					-0,53
IL22		-1,02	-0,64	-2,92	-1,53
IL23A				-0,71	
IL23R			0,31		
IL2RA				-1,25	-0,59
IL3				-3,55	-1,66
IL4				-1,34	
IL4R					-0,62
IL7R			0,66	0,65	
ILF3		-0,35			-0,38
IRAK1					-0,30

Gene	ratio (log2)				
	Ferm	Tota	Radix	Thymol	Helenalin
IRF1				-0,46	
IRF4		-0,39			-0,61
IRF8	-0,60	-0,88	-1,01	-1,77	-1,16
ITGA5				1,41	
ITGA6		0,56		-0,55	
ITGAE				0,67	
JAK1			0,34		
JAK2	-0,50	-0,36		-1,27	-0,54
JAK3		-0,56			-0,53
KIR_Activating_Subgroup_1				0,80	
KIR_Inhibiting_Subgroup_2				0,61	
KLRB1				0,69	
KLRC1				0,79	
KLRC2				0,67	
KLRC4			0,46		
KLRK1				1,00	
LAMP3	-0,28		-0,47	-1,47	-0,54
LCK			0,19	0,88	
LCP2		-0,47	-0,29	-0,35	-0,57
LEF1				0,94	
LIF		-0,82	-0,82	-1,60	-0,83
LILRA4				0,75	0,52
LTA	-0,34	-0,71	-0,98	-2,66	-1,13
LTB4R2	-0,35				
MAF		-0,40			
MALT1				-0,61	
MAP4K2				0,98	
MAPK14				0,64	
MAPKAPK2		-0,34			
MCL1				0,42	
MIF					-0,54
MYD88		-0,11	-0,49		
NFATC3				0,43	
NFIL3				-0,97	
NFKB1					-0,38
NFKBIA				-0,61	
NOTCH1	-0,38	-0,53		-0,70	-0,55
NOTCH2				-0,54	
PDCD1				0,33	
PLAU				-0,87	
POU2F2					-0,60
PRKCD				-0,43	
PSMB7				-0,28	
PSMB8			-0,34	-0,40	-0,35
PSMB10					-0,37
PSMC2		0,20		0,23	0,13
PSMD7			0,23		
PTGER4				-0,28	-0,40
PTPN2				-0,33	-0,28
PTPN22				0,67	
PTPN6		-0,39	-0,43	-0,48	-0,45
PTPRC_all				0,78	
RELB				-0,37	-0,30
RORC		-0,38		0,70	-0,35
SELL				-0,50	
SKI			-0,25	-0,33	0,20
SLAMF6				0,85	
SLC2A1			0,41		
SOCS1			-0,56	-1,22	
SOCS3			-0,89	-1,51	
STAT5A	-0,31	-0,47		-0,43	-0,71
STAT5B		-0,29		0,64	-0,40
STAT6					-0,60
TAGAP		-0,38		0,43	-0,47
TAP1			-0,40	-0,97	
TAP2				-0,38	-0,24
TAPBP	-0,18			-0,51	-0,52
TBX21				-1,08	
TCF7				0,78	
TFRC				-1,21	
TGFB1		-0,19	-0,28	-0,58	-0,28
TNF		-0,48	-0,53	-1,39	-0,71
TNFAIP3	-0,45	-0,37			-0,61
TNFRSF13C					-0,45
TNFRSF14				0,55	
TNFRSF4		-1,02		-1,04	-1,36
TNFRSF9	-0,40	-0,71		-0,56	-1,07
TNFSF10				-1,21	
TNFSF11				-0,82	
TNFSF8		-0,84		-1,91	-1,23
TOLLIP				0,23	
TP53				0,48	
TRAF2					-0,20
TRAF4				-0,38	-0,39
TRAF5		-0,36		0,28	-0,38
TYK2				0,35	
XCL1				-1,22	

downregulated genes upregulated genes

The normalized gene expression data were used for a KEGG (Kyoto Encyclopedia of Genes and Genomes) pathway gene set enrichment analysis, performed by Dr. Carsten Sticht (Heidelberg University, Medical Faculty Mannheim, NGS Core Facility). All tested treatments were found to significantly intervene in the TCR signaling pathway (hsa04660) (Figure 21A). Interestingly, Arnica Ferm extract upregulated the TCR signaling pathway, whereas all other test candidates showed a negative normalized enrichment score (NES). A schematic representation of the KEGG TCR signaling pathway is depicted in Figure 21B.

Besides other functional outcomes such as proliferation and differentiation, TCR signaling induces the production of various cytokines including IL-2, IL-10, IFN-γ, and TNF-α. Although the Arnica preparations targeted different genes within this complex pathway, they all reduced the expression of cytokines. To validate these changes at the protein level, the concentration of 12 different Th cell-related cytokines was simultaneously quantified in cell culture supernatant using LEGENDplex™. After 24h stimulation, the levels of IL-4, IL-6, IL-9 and IL-17F were below the limit of quantification. For the eight remaining cytokines (IL-2, IL-5, IL-10, IL-13, IL-17A, IL-22, IFN-γ, and TNF-α), it was evaluated if Arnica preparations affect their production and secretion. As summarized in Figure 22A, the three tested extracts significantly diminished IL-2, IL-10, IL-22 and IFN-γ to a similar extent. For IL-5, IL-13, IL17A, and TNF-α, differential effects were observed. The same analysis was performed for the lead compounds. Thymol as well as Helenalin significantly reduced the concentration of all analyzed cytokines in the cell culture supernatant without specificity for certain analytes (Figure 22B). By means of the inhibitory effect on IL-2, IL-10, and IFN-γ expression and/or production, an interference of Arnica preparations with the TCR signaling pathway could be reinforced. That the treatment with Ferm extract reduces cytokine expression and production and at the same time promotes activation of the TCR signaling pathway might be explained by the use of a pre-designed panel covering a defined and limited set of genes, which does not consider all the players involved. Therefore, Ferm extract might negatively act on additional genes that were not analyzed. The TCR signaling pathway comprises a complex network of signaling cascades including NFκB and Calcium/Calcineurin/NFAT signaling, which were investigated in more detail to generate a clearer picture of the molecular mechanism of action.

A

hsa04660_T cell receptor signaling pathway

	NES	p-value
Ferm / H_2O	1,76	0,0029
Tota / EtOH	-1,47	0,0408
Radix / EtOH	-1,51	0,0321
Thymol / DMSO	-1,56	0,0267
Helenalin / DMSO	-1,74	0,0037

negative NES positive NES

B

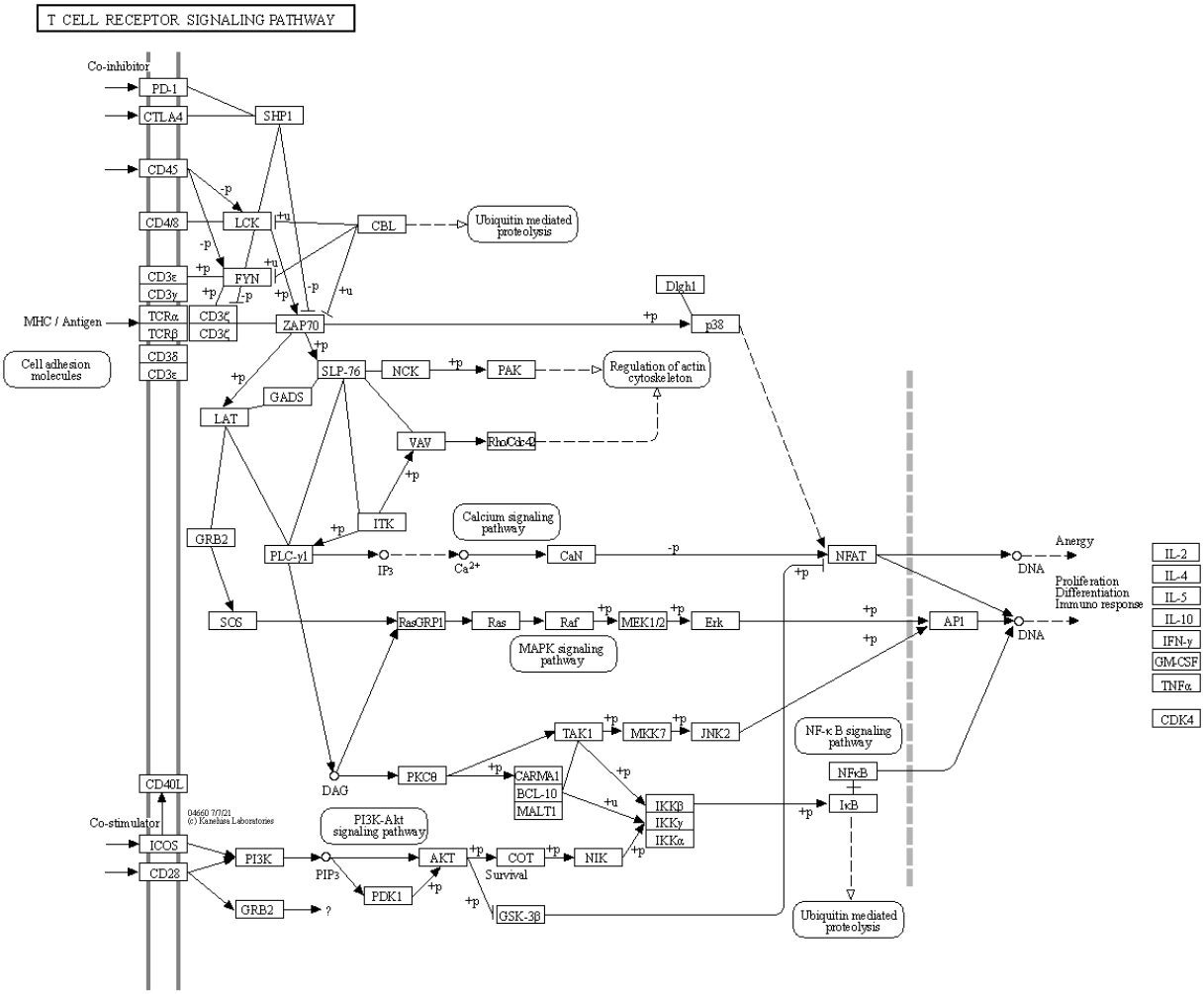

Figure 21: Arnica preparations differentially intervene in the TCR signaling pathway.

Gene expression data generated using the nCounter® technology and the Human Immunology V2 Panel from nanoString were used to perform a KEGG pathway gene set enrichment analysis. (**A**) Normalized enrichment scores (NESs) and p-values of the different test substances compared to the respective solvent control for the T cell receptor signaling pathway (hsa04660). (**B**) Schematic representation of the KEGG T cell receptor signaling pathway (https://www.genome.jp/pathway/hsa04660) (136).

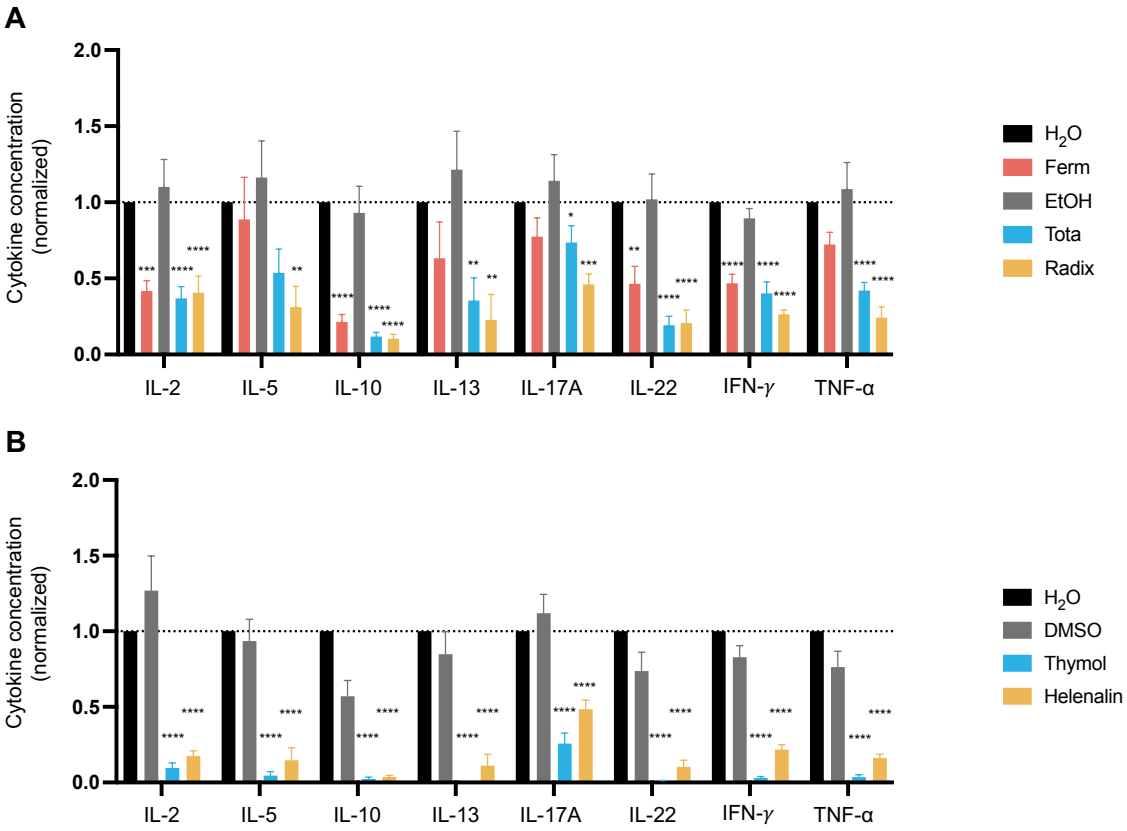

Figure 22: Arnica preparations decrease cytokine production in T cells.

PBTs were left untreated (black bar) or pretreated with drug (red, blue, and yellow bars) or vehicle (grey bars) for 1 h and subsequently activated with anti-CD3/CD28 antibodies for 24 h. (**A**, **B**) Different Th cell-related cytokines (IL-2, IL-5, IL-10, IL-13, IL-17A, IL-22, IFN-γ, and TNF-α) released to the supernatant after treatment with Arnica extracts (**A**) or lead substances (**B**) were quantified by cytometric bead array (LEGENDplex™) in six independent experiments. Data were normalized to the H_2O control sample and are expressed as mean ± SEM. *$p \leq 0.05$; **$p \leq 0.01$; ***$p \leq 0.001$; ****$p \leq 0.0001$

3.7 Arnica preparations differentially affect the NFκB signaling pathway

The transcription factor NFκB is known to regulate the expression of a variety of inflammation-related genes such as the proinflammatory cytokine IL-2. Given the observed diminished IL-2 production in PBTs upon treatment with Arnica preparations (Figure 16 and Figure 22), the NFκB signaling pathway constitutes one interesting target to be studied regarding the molecular mechanism of Arnica extracts and lead substances. A detailed description of the NFκB signaling pathway can be found in section 1.3.1.

In brief, NFκB will be released from its inhibitor IκB and translocate from the cytoplasm to the nucleus upon T cell stimulation. Nuclear translocation of proteins can be reliably studied using imaging flow cytometry, a combination of common flow cytometry and fluorescence microscopy. This technique offers the possibility to analyze the subcellular localization of fluorescent signals within each single cell. By labeling the nucleus with 7-AAD and staining the NFκB p50 subunit with a fluorophore-conjugated antibody, the overlap of both fluorescent

signals provides the basis for calculating the percentage of cells with nuclear NFκB (Figure 23A).

Whether the treatment of PBTs with Arnica preparations influences nuclear translocation of NFκB in PBTs was investigated after 30 min of CD3x28 stimulation. While costimulation clearly induced nuclear translocation (Figure 23B), Arnica extracts had no significant effect on the percentage of PBTs with nuclear NFκB compared to solvent controls (Figure 23D). Thymol, however, significantly diminished the translocation (Figure 23C, E) and a similar result was obtained upon Helenalin treatment (Figure 23E). As positive control, cells were treated with 10 μM TPCA-1, an IκB kinase inhibitor (137). Expectedly, the inhibitor significantly diminished NFκB nuclear translocation compared to the DMSO solvent control sample (Figure 23E).

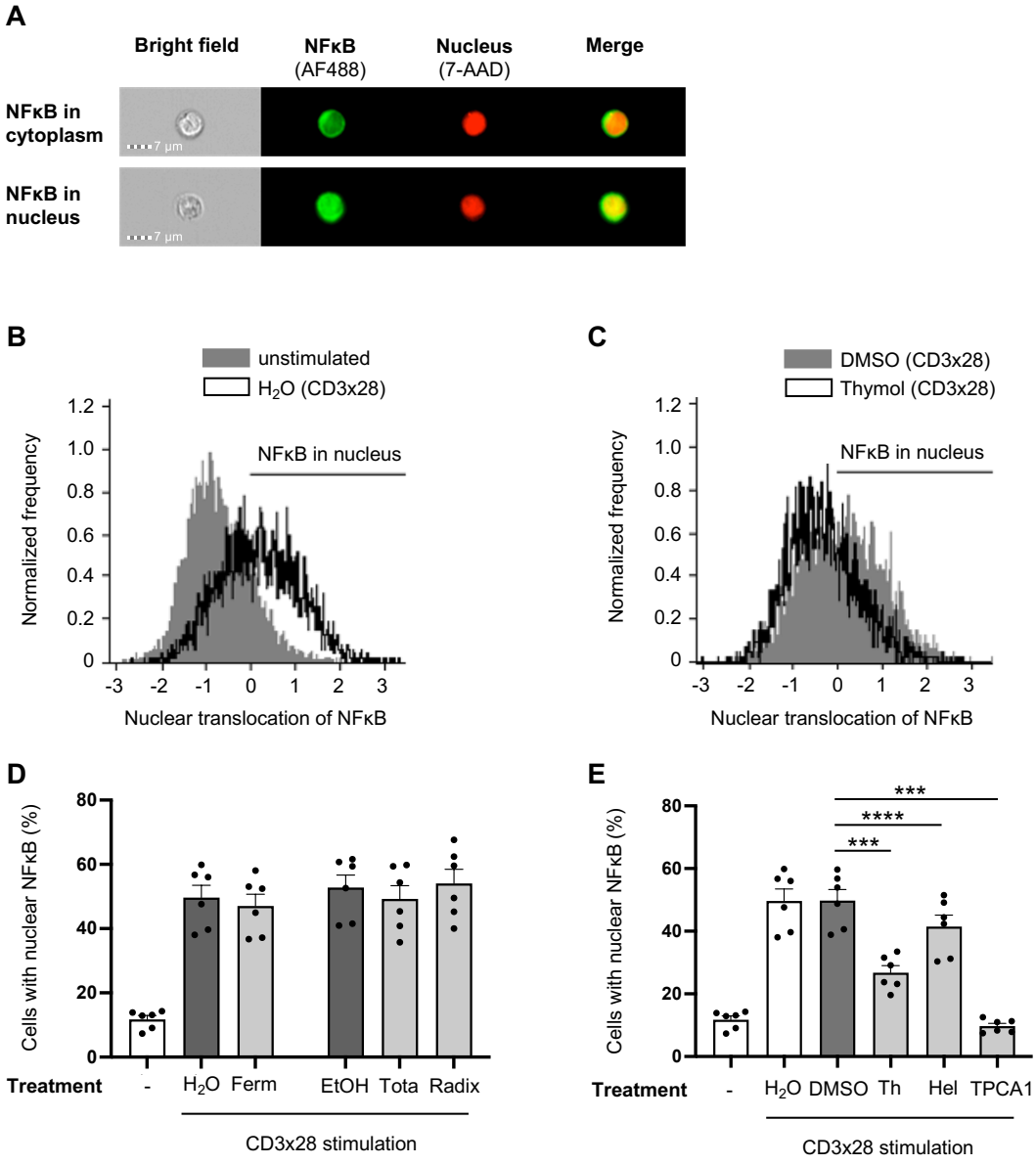

Figure 23: NFκB nuclear translocation is diminished by Thymol and Helenalin, whereas Arnica extracts have no effect.

PBTs were left unstimulated (left white bar) or pretreated with drug (light grey bars) or vehicle (dark grey bars) for 1 h and subsequently activated with anti-CD3/CD28 antibodies for 30 min. Nuclear translocation of NFκB was quantified by imaging flow cytometry (**A**). Representative histograms of unstimulated versus costimulated H_2O control sample (**B**) and costimulated DMSO control versus Thymol treatment (**C**). Statistical evaluation of NFκB nuclear translocation after treatment with Arnica extracts (**D**) or lead substances (**E**) from six independent experiments. Each data point represents an individual T cell donor. Data are expressed as mean ± SEM. ***$p \leq 0.001$; ****$p \leq 0.0001$

Following nuclear translocation, NFκB binds to its consensus DNA sequence to initiate transcription of target genes. Since Arnica extracts did not affect NFκB nuclear translocation (Figure 23D), their influence on NFκB DNA binding was studied. Therefore, PBTs preincubated with drug or vehicle were stimulated for 30 min and nuclear lysates were prepared. The lysates were incubated with plate-bound NFκB consensus DNA sequence and binding of NFκB to the DNA was quantified by means of an ELISA-based detection method as summarized in Figure 24A.

Arnica Radix extract significantly diminished NFκB DNA binding (Figure 24B). Ferm and Tota extracts showed a similar tendency, but did not reach statistical significance probably because of the donor-to-donor variability. In parallel, the effect of Thymol and Helenalin on NFκB DNA binding was assessed. Both drugs significantly diminished DNA binding (Figure 24C). However, it could not be validated if this effect is indeed derived from specific interference with NFκB DNA binding activity or rather related to the inhibition of NFκB nuclear translocation by Thymol and Helenalin since equal lysate volumes were used for each sample. Adjusting the lysate volume for these two samples was not deemed as an adequate modification of the assay, as also other components of the nuclear extract would thereby be enriched and might trigger unpredictable effects.

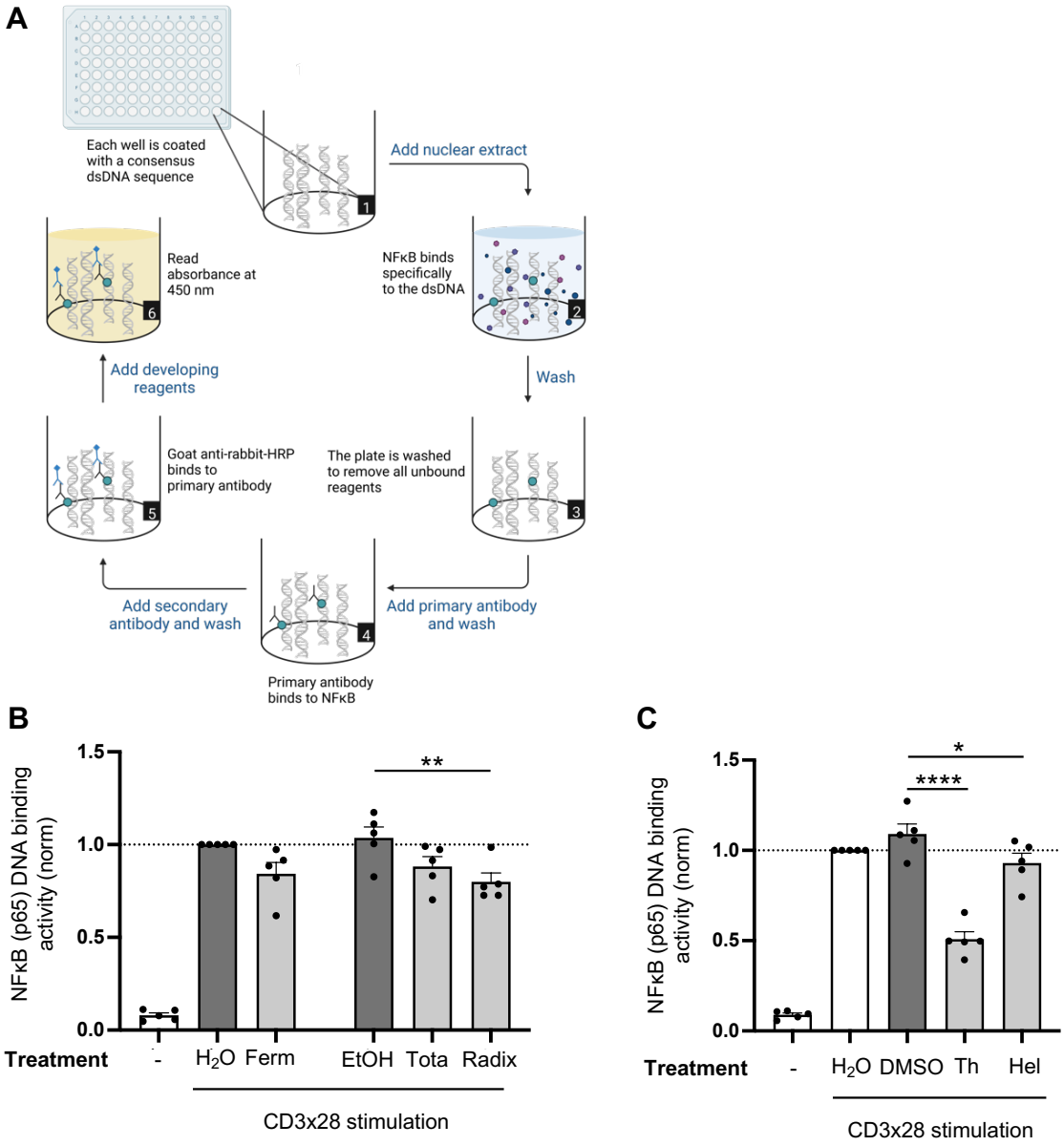

Figure 24: NFκB DNA binding is significantly reduced by Arnica Radix extract.

PBTs were left unstimulated (left white bar) or pretreated with drug (light grey bars) or vehicle (dark grey bars) for 1 h and subsequently activated with anti-CD3/CD28 antibodies for 30 min. NFκB DNA binding was assessed by means of an ELISA-based detection method (**A**). Statistical evaluation of NFκB DNA binding after treatment with Arnica extracts (**B**) or lead substances (**C**) from five independent experiments. Each data point represents an individual T cell donor. Data were normalized to the H_2O control sample and are expressed as mean ± SEM. *p ≤ 0.05; **p ≤ 0.01; ****p ≤ 0.0001. (**A**) was created with BioRender.com based on the schematic from Cayman.

Phosphorylation of the p65 subunit on serine 529 (S529) positively regulates NFκB transcriptional activity (45), which constitutes another level of control for NFκB-dependent gene expression. As outlined above, none of the tested Arnica extracts affected NFκB nuclear translocation (Figure 23D) and only the Radix extract significantly diminished NFκB DNA binding (Figure 24B). Especially for the Ferm and Tota extracts, it was therefore interesting to study if they influence NFκB phosphorylation and thus transcriptional activity.

After 30 min of CD3x28 stimulation, PBTs were stained for phospho-NFκB p65 (S529) and analyzed by flow cytometry. No significant effect of Arnica extracts was found on the percentage of phospho-NFκB p65 (S529)-positive cells (Figure 25A, C). For the lead substances, only Thymol was found to significantly inhibit NFκB p65 phosphorylation at S529, while Helenalin had no influence (Figure 25B, D).

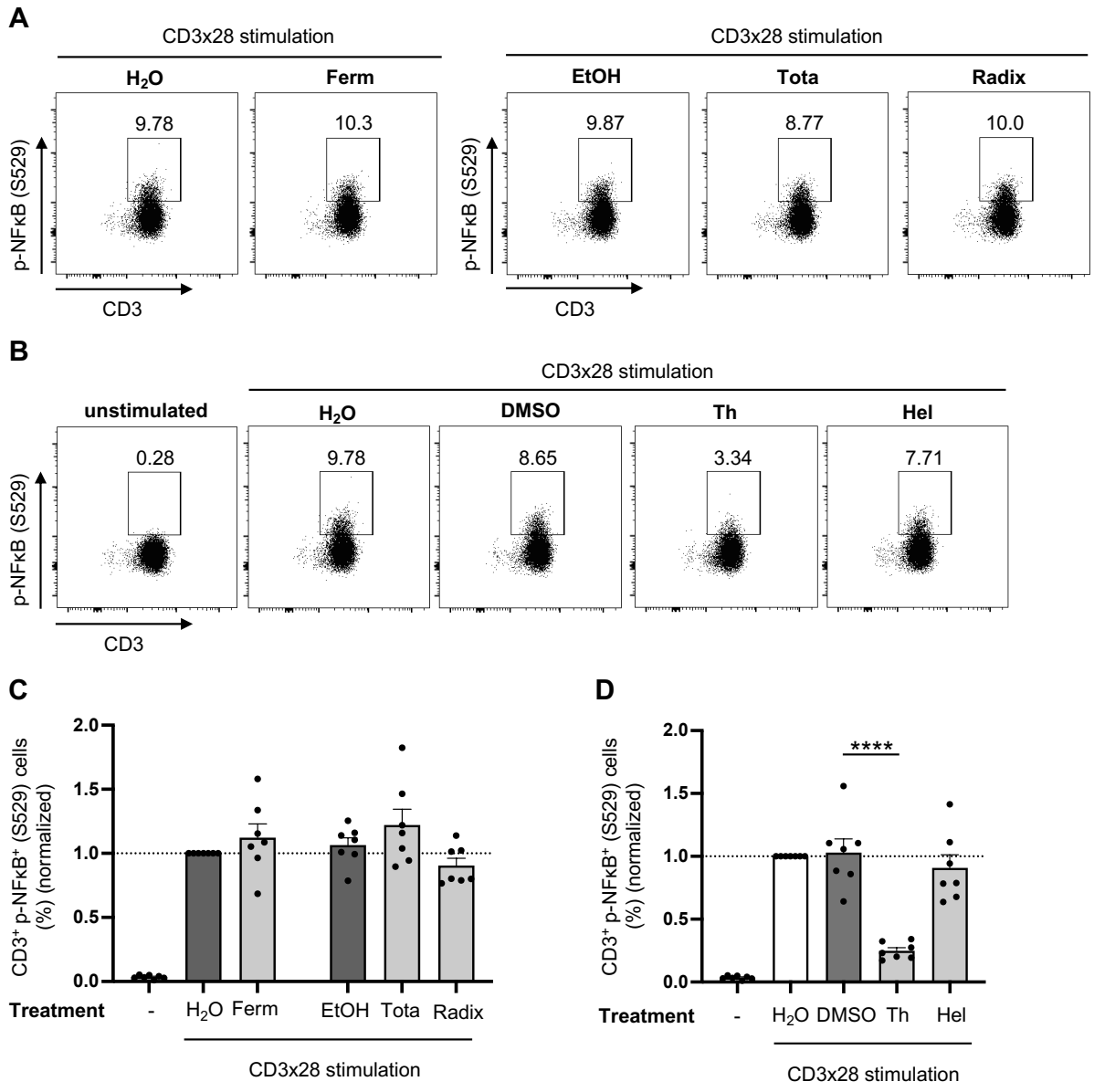

Figure 25: NFκB phosphorylation (S529) is inhibited by Thymol but not by Arnica extracts and Helenalin. PBTs were left unstimulated (left white bar) or pretreated with drug (light grey bars) or vehicle (dark grey bars) for 1 h and subsequently activated with anti-CD3/CD28 antibodies for 30 min. Phosphorylation of NFκB p65 on S529 after treatment with Arnica extracts (**A**, **C**) or lead substances (**B**, **D**) was quantified by flow cytometry. Representative dot plots (**A**, **B**) and statistical evaluation (**C**, **D**) from seven independent experiments. Each data point represents an individual T cell donor. Data were normalized to the H_2O control sample and are expressed as mean ± SEM. ****$p \leq 0.0001$

Taken together, it can be concluded that Arnica Radix extract specifically inhibits NFκB DNA binding. Ferm and Tota extract showed a similar trend, which was however not significant. Helenalin inhibited NFκB nuclear translocation, but an effect on DNA binding could not be verified. The same applies to Thymol, which furthermore inhibited NFκB transcriptional activity by reducing S529 phosphorylation of the p65 subunit.

3.8 Arnica Ferm extract and Thymol inhibit the Calcium/Calcineurin/NFAT signaling pathway

Apart from NFκB, NFAT is critically involved in regulating the expression of *IL2* and other genes. Thus, the NFAT signaling pathway constitutes another potential molecular target for Arnica preparations to reduce IL-2 production in PBTs as it was observed in Figure 16 and Figure 22.

NFAT-dependent gene expression was analyzed by a luciferase reporter assay. A six-hour CD3x28 stimulation of Jurkat E6.1 cells transfected with a NFAT-pGL2-Promoter vector resulted in significantly increased luminescence compared to the unstimulated control. As summarized in Figure 26A, treatment with Arnica Ferm extract significantly decreased luminescence, which corresponds to an inhibition of NFAT-dependent gene expression. Arnica Tota extract showed a similar trend, which did not reach statistical significance, presumably due to donor variations. The Radix extract did not affect NFAT-dependent gene expression. None of the extracts was toxic to the Jurkat E6.1 cell line as confirmed by 7-AAD exclusion (Figure 26B). The same assay was performed after pretreating PBTs with lead substances. Significantly less NFAT-dependent gene expression was observed upon Thymol treatment, whereas Helenalin had no effect (Figure 26C). Again, none of the drugs was cytotoxic to Jurkat E6.1 cells (Figure 26D).

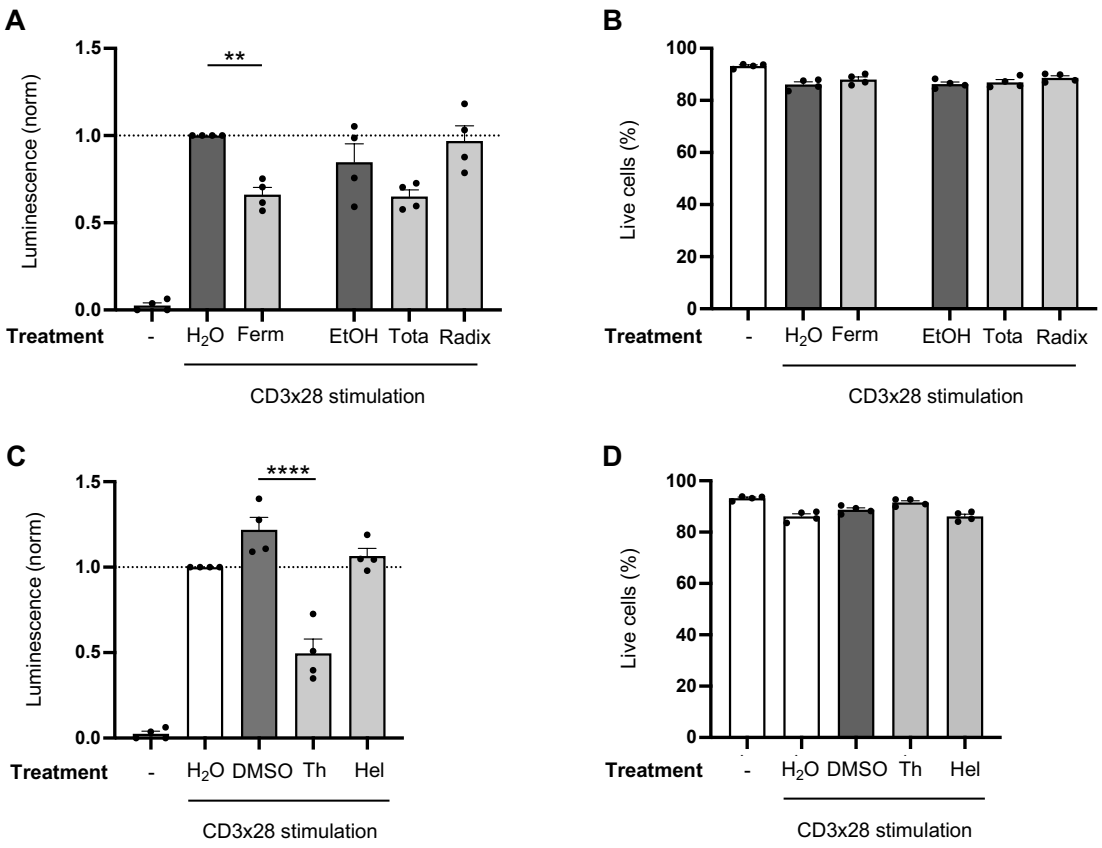

Figure 26: NFAT-dependent gene expression is significantly diminished by Arnica Ferm extract and Thymol.

(**A**, **C**) Jurkat E6.1 cells were transfected with NFAT-pGL2-Promoter vector reporter plasmid and either left unstimulated (left white bar) or pretreated with drug (light grey bars) or vehicle (dark grey bars) for 1 h and subsequently activated with anti-CD3/CD28 antibodies for 6 h. NFAT-dependent gene expression after treatment with Arnica extracts (**A**) or lead substances (**C**) was quantified by measuring luciferase activity in four independent experiments. Each data point represents an individual T cell donor. Data were normalized to the H_2O control sample. (**B**, **D**) Jurkat E6.1 cells were left unstimulated (left white bar) or pretreated with drug (light grey bars) or vehicle (dark grey bars) for 1 h and subsequently activated with anti-CD3/CD28 antibodies for 6 h. Cell viability after treatment with Arnica extracts (**B**) or lead substances (**D**) was quantified by 7-AAD exclusion in four independent experiments. Each data point represents an individual T cell donor. Data are expressed as mean ± SEM. **$p \leq 0.01$ ****$p \leq 0.0001$

NFAT activation is directly linked to the stimulation-induced increase in intracellular calcium levels as explained in section 1.3.2. According to the literature, Thymol itself is able to induce calcium influx without stimulation of cells. This effect was observed with different cell types including for example PC3 human prostate Cancer cells (138), pituitary GH_3 cells (139), human glioblastoma cells (140), and bone marrow-derived mast cells (141).

To study if Thymol and other Arnica preparations affect intracellular Ca^{2+} levels in unstimulated PBTs, cells were labeled with the calcium indicator Indo-1. Baseline intracellular calcium was measured before the test drugs were added to the cells. Finally, maximum calcium influx was induced by the addition of the Ca^{2+} ionophore Ionomycin. No difference compared to baseline Ca^{2+} levels was observed upon treatment with Arnica extracts (Figure 27A).

Fitting to the published data generated with other cell types, Thymol significantly increased intracellular calcium levels in unstimulated PBTs (Figure 27B, C). Helenalin treatment induced a marginal, though significant, Ca^{2+} rise (Figure 27B).

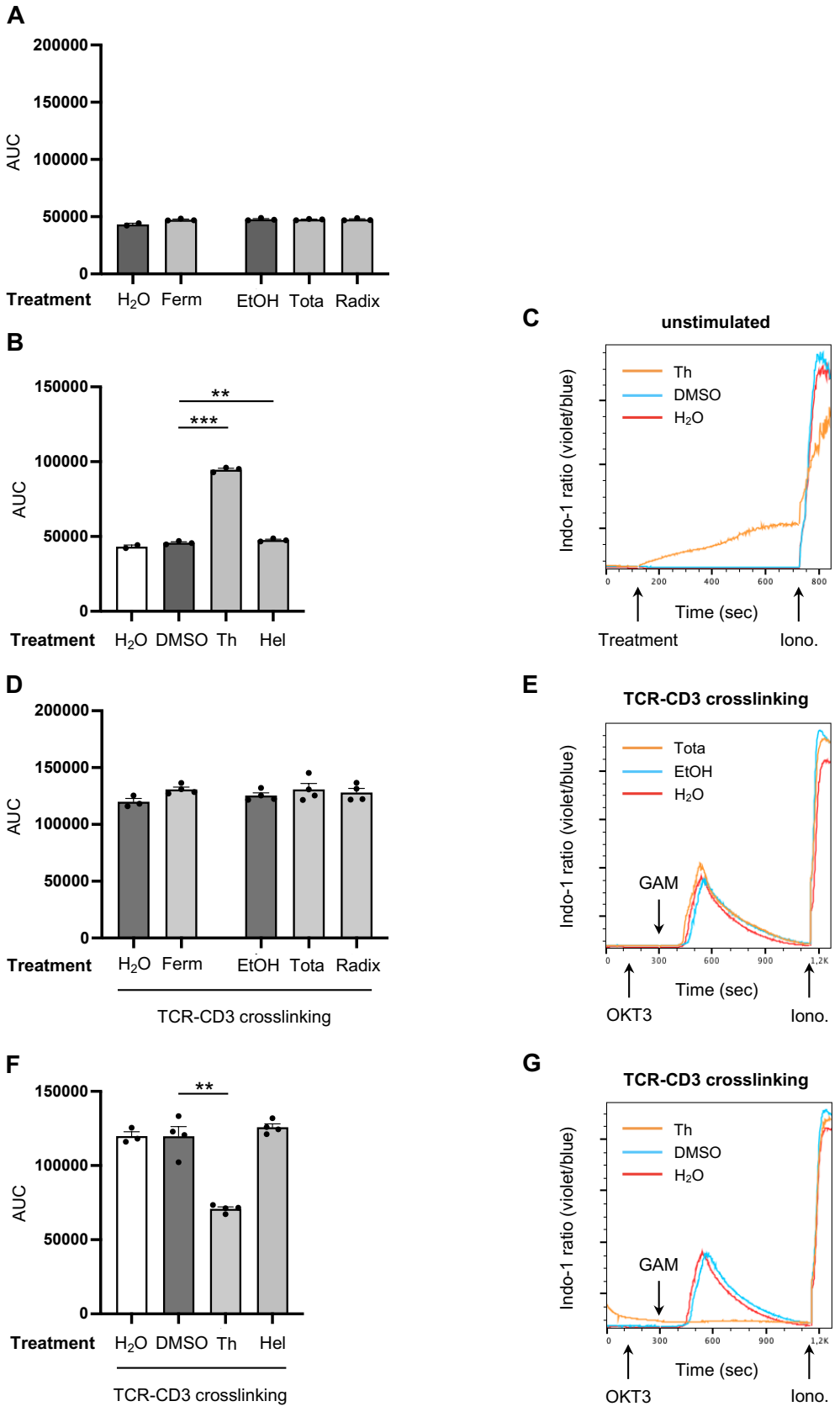

Figure 27: Thymol induces Ca^{2+} influx without stimulation and inhibits activation-induced Ca^{2+} influx, Arnica extracts and Helenalin have no effect on intracellular calcium levels.

(**A**-**C**) PBTs were labeled with Indo-1 and changes in intracellular calcium levels upon addition of drug (light grey bars) or vehicle (dark grey bars) were assessed by flow cytometry. Statistical evaluation after treatment of unstimulated PBTs with Arnica extracts (**A**) or lead substances (**B**) from three independent experiments. (**C**) Representative kinetics of intracellular calcium levels upon Thymol treatment of unstimulated PBTs compared to solvent control sample. (**D**-**G**) PBTs were labeled with Indo-1, pretreated with drug (light grey bars) or vehicle (dark grey bars) for 1 h and subsequently activated by TCR-CD3 crosslinking. The effect of Arnica extracts (**D**, **E**) or lead substances (**F**, **G**) on stimulation-induced calcium influx was analyzed by flow cytometry. Statistical evaluation of four independent experiments (**D**, **F**) and representative kinetics of intracellular calcium levels after treatment with Arnica Tota extract (**E**) or Thymol (**G**) compared to the respective solvent control. Each data point represents an individual T cell donor. Data are expressed as mean ± SEM. $^{**}p \leq 0.01$; $^{***}p \leq 0.001$

Since stimulation-induced Ca^{2+} influx regulates essential signaling pathways, including NFAT activation, the effects of Arnica preparations on TCR-CD3-induced Ca^{2+} levels in Indo-1-labeled PBTs was analyzed next. Baseline Ca^{2+} of drug treated cells was measured before an antibody to CD3 was added. T cell activation was induced by the addition of goat anti-mouse antibody that leads to TCR-CD3 crosslinking. Eventually, Ionomycin treatment was used to reach maximum calcium influx. None of the Arnica extracts affected the stimulation-induced Ca^{2+} influx (Figure 27D, E). Thus, Arnica Ferm extract exerts its inhibitory effect on NFAT-dependent gene expression (Figure 26A) via another mechanism that is not related to intracellular calcium levels. For Helenalin, no significant influence on calcium levels was observed (Figure 27F), fitting to normal NFAT activity (Figure 26C). Thymol treatment, however, resulted in significantly diminished stimulation-induced Ca^{2+} influx (Figure 27F, G), which gives one possible explanation for reduced NFAT-dependent gene expression (Figure 26C).

3.9 Arnica preparations differentially affect the intracellular redox status

ROS play an important role as signaling molecules. Since increased concentrations induce oxidative stress and are cytotoxic, intracellular ROS levels need to be tightly regulated. Plants in general are a rich source for natural antioxidants and according to the literature, also Arnica has antioxidative properties (88).

Various fluorogenic probes are available to quantify intracellular ROS levels. The cell-permeant ROS sensor CellROX™ Green Reagent is only weakly fluorescent in a reduced state. Upon oxidation, the probe becomes highly fluorescent and will bind to DNA. Therefore, the fluorescent signal is localized in cell nuclei and mitochondria. Using CellROX™ Green Reagent, the effect of Arnica extracts and lead substances on the intracellular redox status of human T cells was studied. To this end, an assay in which oxidative stress is induced by treating the cells with tert-Butyl hydroperoxide (TBHP) was established. With this experimental setup, the antioxidative capacity of test substances can be analyzed.

After preincubation with drug or vehicle, 200 μM TBHP were added to the cells. Finally, intracellular ROS levels were detected by incubation with CellROX™ Green Reagent. Changes in the fluorescent intensity of the ROS sensor were analyzed by flow cytometry. For all Arnica extracts, an antioxidative effect was observed in PBTs (Figure 28A). The potent antioxidant NAC (reviewed by (142)) was used as a positive control and was also found to significantly diminish intracellular ROS levels induced by TBHP compared to the H_2O solvent control (Figure 28B). Helenalin treatment had no influence on the intracellular redox status, while Thymol was found to further increase oxidative stress (Figure 28B).

To screen for prooxidative effects, the experimental protocol was slightly modified and measurements were repeated without TBHP treatment. Even without induction of oxidative stress, the Radix extract still showed a significant reduction of intracellular ROS levels. This effect was, however, not, or only by trend, observed for Arnica Ferm and Tota (Figure 28C). Using this setup, the prooxidative effect of Thymol could be confirmed and was even more prominent (Figure 28D). For Helenalin, a prooxidative effect could be excluded.

Taken together, the three tested Arnica extracts were found to have antioxidant properties in human PBTs. In contrast, Thymol turned out to have a prooxidative effect. No influence on the intracellular redox status was observable after Helenalin treatment.

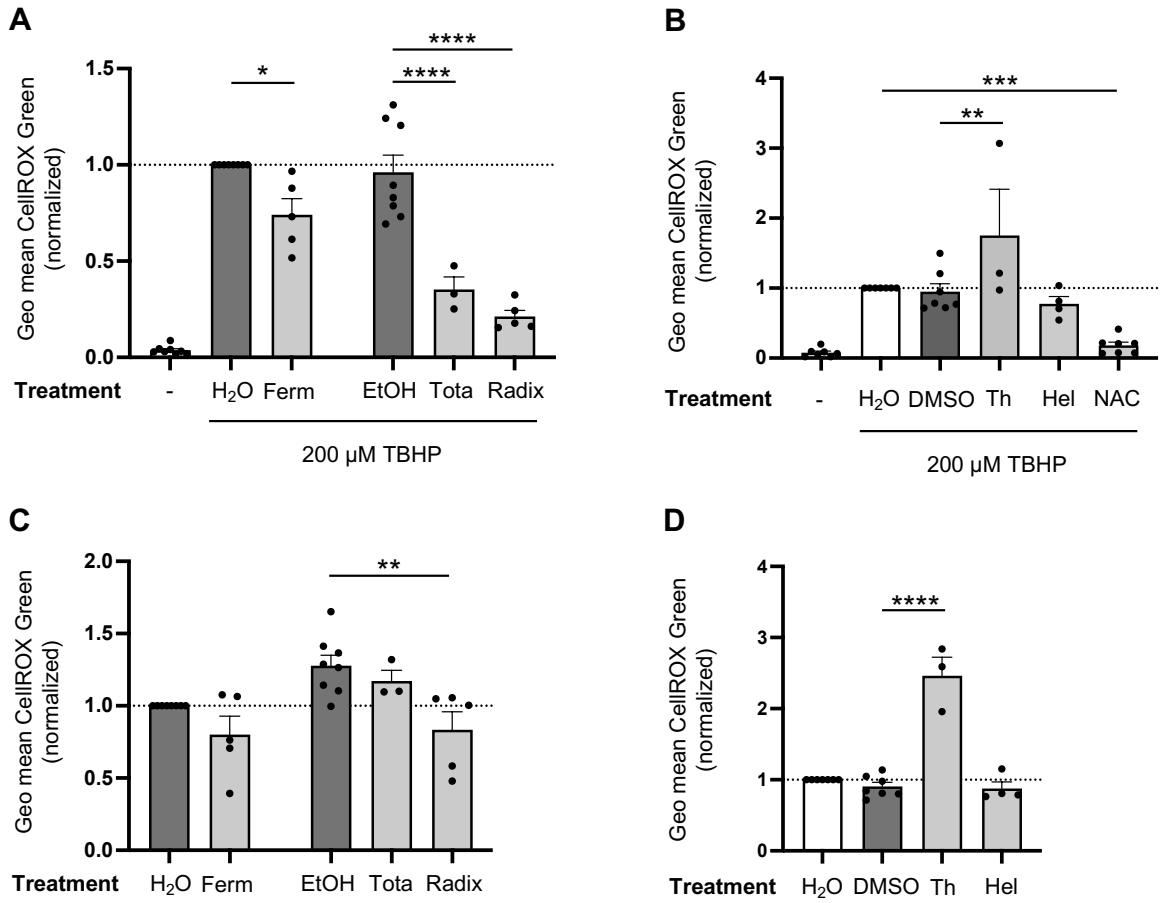

Figure 28: Arnica extracts have antioxidant properties, whereas Thymol is prooxidative.

(**A**, **B**) PBTs were pretreated with drug (light grey bars) or vehicle (dark grey bars) for 1 h and oxidative stress was induced by addition of TBHP. Intracellular ROS levels were quantified by flow cytometry using CellROX™ Green Reagent. Statistical evaluation after treatment with Arnica extracts (**A**) or lead substances (**B**) from 3 – 5 independent experiments. (**C**, **D**) PBTs were pretreated with drug (light grey bars) or vehicle (dark grey bars) for 1 h and intracellular ROS levels were quantified by flow cytometry using CellROX™ Green Reagent. Statistical evaluation after treatment with Arnica extracts (**C**) or lead substances (**D**) from 3 – 5 independent experiments. Each data point represents an individual T cell donor. Data were normalized to the H_2O control sample and are expressed as mean ± SEM. *$p \leq 0.05$; **$p \leq 0.01$; ***$p \leq 0.001$; ****$p \leq 0.0001$

3.10 Phytochemical composition of differentially manufactured Arnica extracts

Depending on several factors such as the manufacturing procedure, the plant part used as well as the solvent system, the final extract will differ in its phytochemical composition. To allow conclusions about the most prevalent extract components, which might play a major role in mediating the extract's effect, an HPLC-MS/MS analysis was performed by Dr. Bernhard Wetterauer (Heidelberg University, Institute of Pharmacy and Molecular Biotechnology, Pharmaceutical Biology).

The photodiode array (PDA) chromatogram (top) and total ion chromatogram (TIC, bottom) obtained for the Arnica Radix extract are depicted in Figure 29A. Expectedly, many extract components were not optically active and therefore only appear in the TIC but not in the PDA chromatogram. Three peaks (numbered in red) occur exclusively in the PDA chromatogram and refer to compounds that were optically active but not detectable by mass spectrometry (MS).

For direct comparison of the three Arnica extracts, the TICs are displayed below one another in Figure 29B. Starting with the aqueous Ferm extract (top), the EtOH concentration in the extraction solvent gradually increases from 30 % in the Tota (middle) to 86 % in the Radix extract (bottom). While the aqueous extract mainly contains water-soluble plant components, more and more non-polar compounds are expected with increasing EtOH concentration in the extraction solvent. Non-polar compounds will elute later during reversed-phase LC.

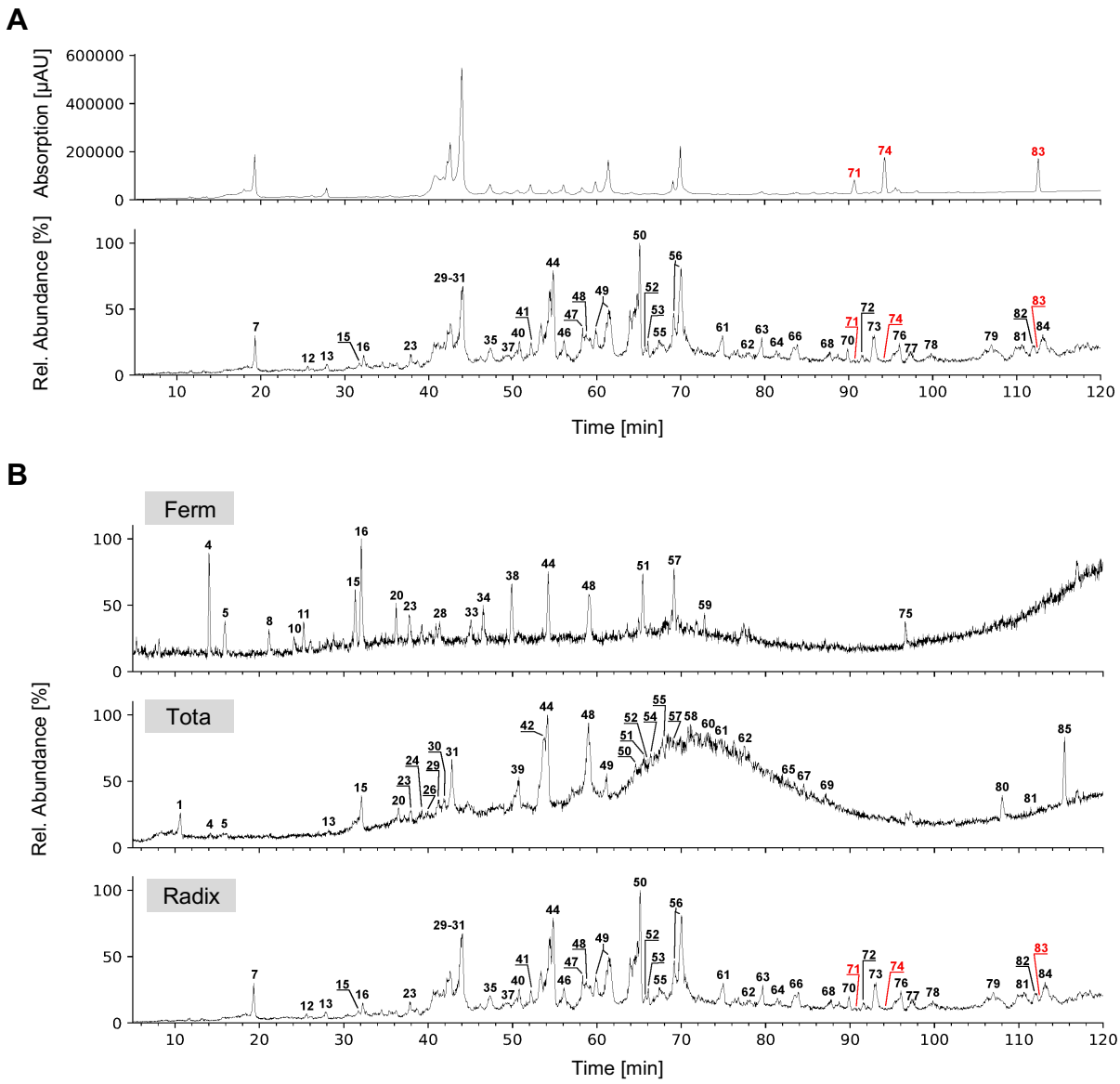

Figure 29: Different phytochemical composition of Arnica extracts depending on the extraction procedure and the plant parts used.

HPLC-MS/MS chromatograms of *Arnica montana* extracts with peak annotations. (**A**) Photodiode array (PDA) chromatogram (λ = 200 – 600 nm) and total ion chromatogram (TIC) in negative ionization mode (*m/z* = 50 – 2000) of Radix extract. (**B**) Comparison of TICs in negative ionization mode (*m/z* = 50 – 2000) of Ferm, Tota and Radix extract. For peak annotations please see Table 15.

Based on the retention time and the MS fragmentation pattern in negative ionization mode, a tentative identification of phytochemical components was performed by Dr. Bernhard Wetterauer (Table 15). However, this proved to be difficult for all Arnica extracts, since the compounds did not match well with published literature and despite intensive efforts, only very few substances could be identified. As summarized in Table 15, each of the three extracts had a completely different phytochemical composition. Interestingly, Helenalin was not found at a detectable concentration in any of the analyzed Arnica extracts.

Nevertheless, (Mono-, di-, and tri-) Caffeoylquinic acids were found to be the most prominent constituents and thus represented interesting targets to be studied for their effects on T cells in a pure form.

Table 15: Analysis of *Arnica montana* extracts by HPLC-MS/MS and tentative identification of phytochemical components

Peak No.	t_R [min][a]	*m/z*[b]		Tentative Identification	Occurrence in Arnica extracts		
		Precursor	Product		Ferm	Tota	Radix
1	7.9 - 10.8	353.0	191.2	Caffeoylquinic acid derivative (143,144)		x	
2	10.1	353.1	191.2	Caffeoylquinic acid derivative (143,144)			
3	12.1	439.2	241.1	N/A			
4	14.0 - 14.2	443.2	381.1	N/A	x	x	
5	15.9	197.1	161.1	N/A	x	x	
6	17.8	194.9	165.1	N/A			
7	19.3	353.1	191.2	Caffeoylquinic acid derivative (143,144)			x
8	21.1	489.1	425.1	N/A	x		
9	21.6	489.2	425.1	N/A			
10	24.1 - 24.4	165.1	147.0	N/A	x		
11	25.2 - 25.6	473.2	427.1	N/A	x		
12	25.6 - 26.4	463.3	331.1	N/A			x
13	27.9 - 28.2	515.2	353.1	Dicaffeoylquinic acid derivative (144)		x	x
14	28.3	421.2	241.1	N/A			
15	29.9 - 31.7	471.1	425.1	N/A	x	x	
16	32.0 - 32.2	525.1	481.3	N/A	x		x
17	32.3	509.0	463.2	N/A			
18	34.0	389.1	345.2	N/A			
19	34.8	417.1	425.2	N/A			
20	36.0 - 36.5	449.3	269.1	N/A	x	x	
21	36.7	471.1	425.1	N/A			
22	37.1	528.2	496.2	N/A			
23	37.6 - 37.9	373.1	329.1	N/A	x	x	x
24	39.2	477.1	301.1	Quercetin-glucuronide / Quercitin-O-rhamnoside isomer (145,146)		x	
25	39.9	187.2	125.1	N/A			
26	40.0	515.2	352.9	Dicaffeoylquinic acid derivative (144)		x	
27	40.3	241.2	197.1	N/A			
28	41.2 - 41.4	363.1	319.2	N/A	x		
29	44.1 - 44.2	515.1	353.0	Dicaffeoylquinic acid derivative (144)		x	x
30	42.1	515.1	353.0	Dicaffeoylquinic acid derivative (144)		x	
31	42.8	515.1	353.0	Dicaffeoylquinic acid derivative (144)		x	
32	44.9	535.1	355.2	N/A			
33	45.0 - 45.2	231.3	213.1	N/A	x		
34	46.5	217.3	171.2	N/A	x		
35	47.3	515.1	353.1	Dicaffeoylquinic acid derivative (144)			x
36	48.7	387.1	342.9	N/A			
37	49.4	677.2	497.2	Tricaffeoylquinic acid derivative (143,147,148)			x
38	49.9 - 50.1	447.3	315.1	N/A	x		

Peak No.	t_R [min][a]	m/z[b]		Tentative Identification	Occurrence in Arnica extracts		
		Precursor	Product		Ferm	Tota	Radix
39	50.7	471.1	425.0	N/A		x	
40	50.8	677.2	497.2	Tricaffeoylquinic acid derivative (143,147,148)			x
41	52.2	677.2	497.2	Tricaffeoylquinic acid derivative (143,147,148)			x
42	53.7	207.2	179.3	Ethyl caffeate (149)		x	
43	54.0	483.1	337.1	N/A			
44	54.2 - 54.8	609.2	485.4	N/A	x	x	x
45	55.3	322.9	254.9	N/A			
46	56.1	583.2	421.0	N/A			x
47	58.3	583.2	421.0	N/A			x
48	58.8 - 59.0	689.3	645.4	N/A	x	x	x
49	61.0 - 61.4	677.2	497.2	Tricaffeoylquinic acid derivative (143,147,148)		x	x
50	64.6 - 65.1	565.4	463.3	N/A		x	x
51	65.5	327.3	229.3	N/A	x	x	
52	65.7 - 65.8	609.2	565.3	Lucenin-2 (147)		x	x
53	66.1	677.2	497.2	Tricaffeoylquinic acid derivative (143,147,148)			x
54	66.4	299.2	284.2	Hispidulin (145)		x	
55	67.2 - 67.5	645.5	543.4	N/A		x	x
56	69.2 - 70.0	745.2	583.0	N/A			x
57	69.1 - 69.2	329.3	229.4	N/A	x	x	
58	71.2	785.5	545.4	N/A		x	
59	72.8	329.3	293.2	N/A	x		
60	73.0	477.2	299.1	N/A		x	
61	74.6 - 75.0	693.2	649.3	N/A		x	x
62	77.0 - 77.6	713.4	681.3	N/A		x	x
63	79.7	649.5	547.3	N/A			x
64	81.4	649.4	547.3	N/A			x
65	82.7	491.2	313.1	N/A		x	
66	83.9	337.0	219.1	N/A			x
67	84.5	601.5	431.2	N/A		x	
68	87.7	351.0	161.1	N/A			x
69	88.8	489.3	474.1	N/A		x	
70	89.9	476.4	279.3	N/A			x
71	90.8	649.2	603.0	N/A			x
72	91.6	564.3	504.2	N/A			x
73	93.0	564.3	504.3	N/A			x
74	94.4	595.4	415.2	N/A			x
75	96.5 - 96.8	461.4	392.8	N/A	x		
76	96.0	595.4	415.2	N/A			x
77	97.3	540.3	480.3	N/A			x
78	99.8	571.4	391.2	N/A			x
79	107.0	433.3	153.1	N/A			x
80	108.0	365.3	297.3	N/A		x	
81	110.6	730.6	326.2	N/A			x
82	112.0	379.4	361.2	N/A			x
83	112.7	N/A	N/A	N/A			
84	113.1	730.6	326.3	N/A			x
85	115.4	339.3	297.3	N/A		x	

[a] Retention times t_R of the respective compounds.

[b] *m/z* of precursor ion (mainly $[M-H]^-$) and a characteristic product ion in negative ionization mode.

3.11 The effects of Arnica extracts on human T cells cannot be mimicked with pure Caffeoylquinic acids

The structural formula of 3-*O*-Caffeoylquinic acid (3-CQA), also known as Chlorogenic acid, is depicted in Figure 30A. Based on literature (150,151), a concentration range of 10 – 100 μM was used and the effect on CD25 and CD69 expression (24 h stimulation) as well as on T cell proliferation (72 h stimulation) was analyzed. In parallel, cell viability was assessed. As summarized in Figure 30B, even the highest test concentration (100 μM) did not reduce cell viability below 90 % after 24 h. However, for concentrations higher than 25 μM, results obtained after 72 h need to be interpreted with caution, since a slight, dose-dependent cytotoxic effect was observed.

Treatment with 3-CQA had no significant effect on PBT activation marker expression (Figure 30C, D). Also, for T cell proliferation the inhibitory effects observed with Arnica extracts (Figure 15B) could not be induced (Figure 30E).

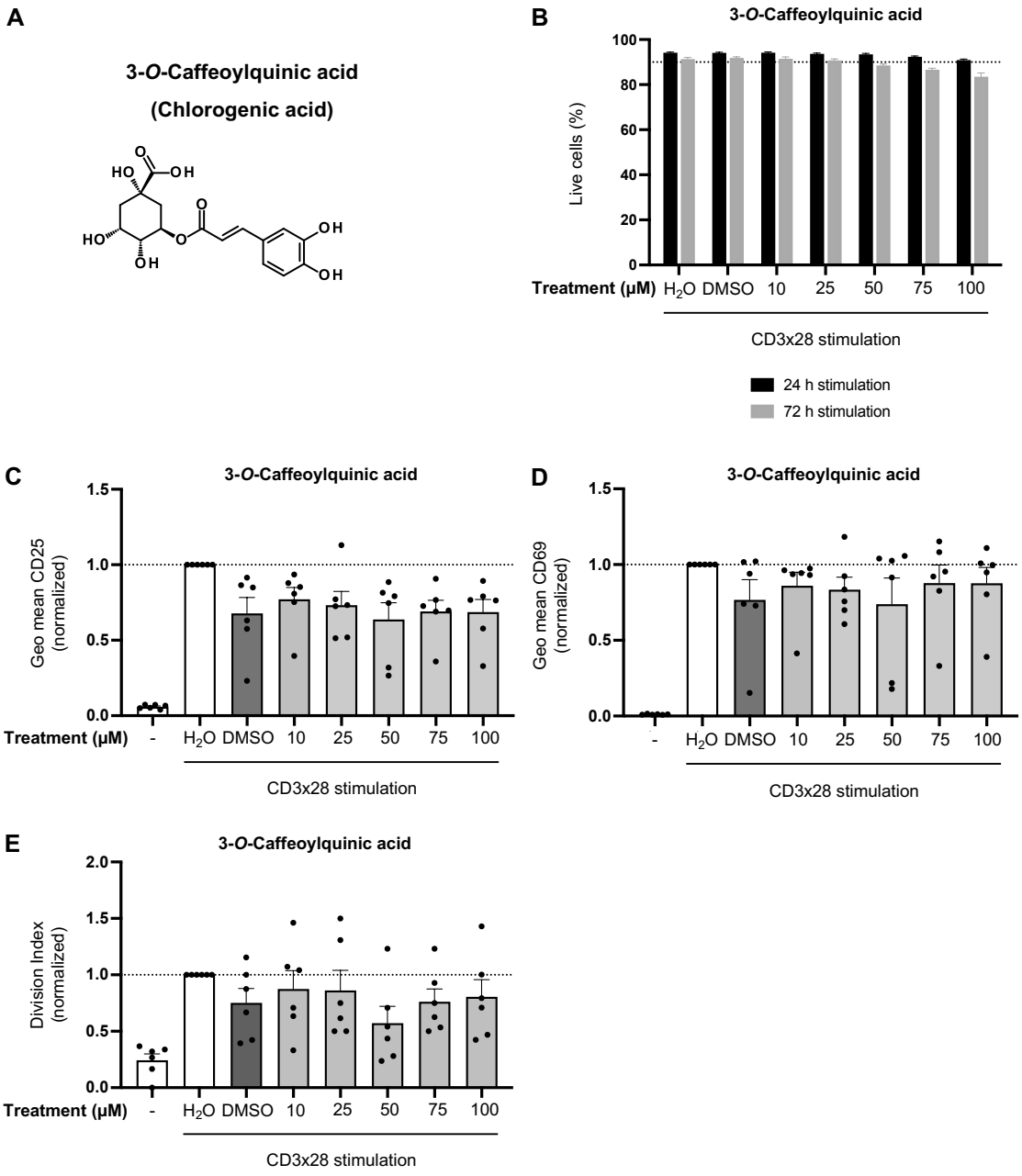

Figure 30: 3-*O*-Caffeoylquinic acid has no effect on T cell activation marker expression and proliferation.
(**A**) Chemical structure of 3-*O*-Caffeoylquinic acid. (**B**) PBTs were pretreated with drug or vehicle for 1 h and subsequently activated with anti-CD3/CD28 antibodies. Cell viability after 24-hour (black) and 72-hour stimulation (grey) was assessed by 7-AAD exclusion in six independent experiments each. (**C**, **D**) PBTs were left unstimulated (left white bar) or pretreated with substance (light grey bars) or vehicle (dark grey bar) for 1 h and subsequently activated with anti-CD3/CD28 antibodies for 24 h. Statistical evaluation of CD25 (**C**) and CD69 (**D**) surface expression analyzed by flow cytometry in six independent experiments. Data were normalized to the H_2O control sample. (**E**) PBTs were labeled with CFSE, left unstimulated (left white bar) or pretreated with substance (light grey bars) or vehicle (dark grey bar) for 1 h and subsequently activated with anti-CD3/CD28 antibodies for 72 h. Statistical evaluation of T cell proliferation assessed by CFSE dilution in six independent experiments. Data were normalized to the H_2O control sample. Each data point represents an individual T cell donor. Data are expressed as mean ± SEM.

The results obtained when treating PBTs with 10 – 100 μM 3,5-Di-*O*-Caffeoylquinic acid (3,5-diCQA) are presented in Figure 31. Figure 31A shows the chemical structure. Again, the effect on T cell viability after 24 h and 72 h treatment was checked. Compared to 3-CQA (Figure 30B), 3,5-diCQA showed to be more toxic (Figure 31B). For 24-hour assays, a concentration up to 75 μM was found to be non-toxic, for longer incubation (72 h) the maximum was only 25 μM otherwise the percentage of live cells dropped below the threshold of 90 %. This has to be kept in mind when interpreting the drug's effect on T cell activation marker expression and proliferation.

While all Arnica extracts diminished CD25 expression (Figure 14D), the opposite effect, namely an increase in the MFI of CD25, was observed upon treatment with 10 μM and 25 μM 3,5-diCQA (Figure 31C). The other test concentrations had no significant influence. Regarding CD69, a significantly increased expression was found with 10 μM, all other concentrations did not show a difference compared to the DMSO control (Figure 31D). After 72 h of stimulation, it was assessed if 3,5-diCQA affects PBT proliferation. This was not the case, as no significant change in the Division Index was found compared to the solvent control (Figure 31E). Thus, the inhibitory effect of Arnica extracts on T cell proliferation (Figure 15B) could not be reproduced with isolated 3,5-diCQA.

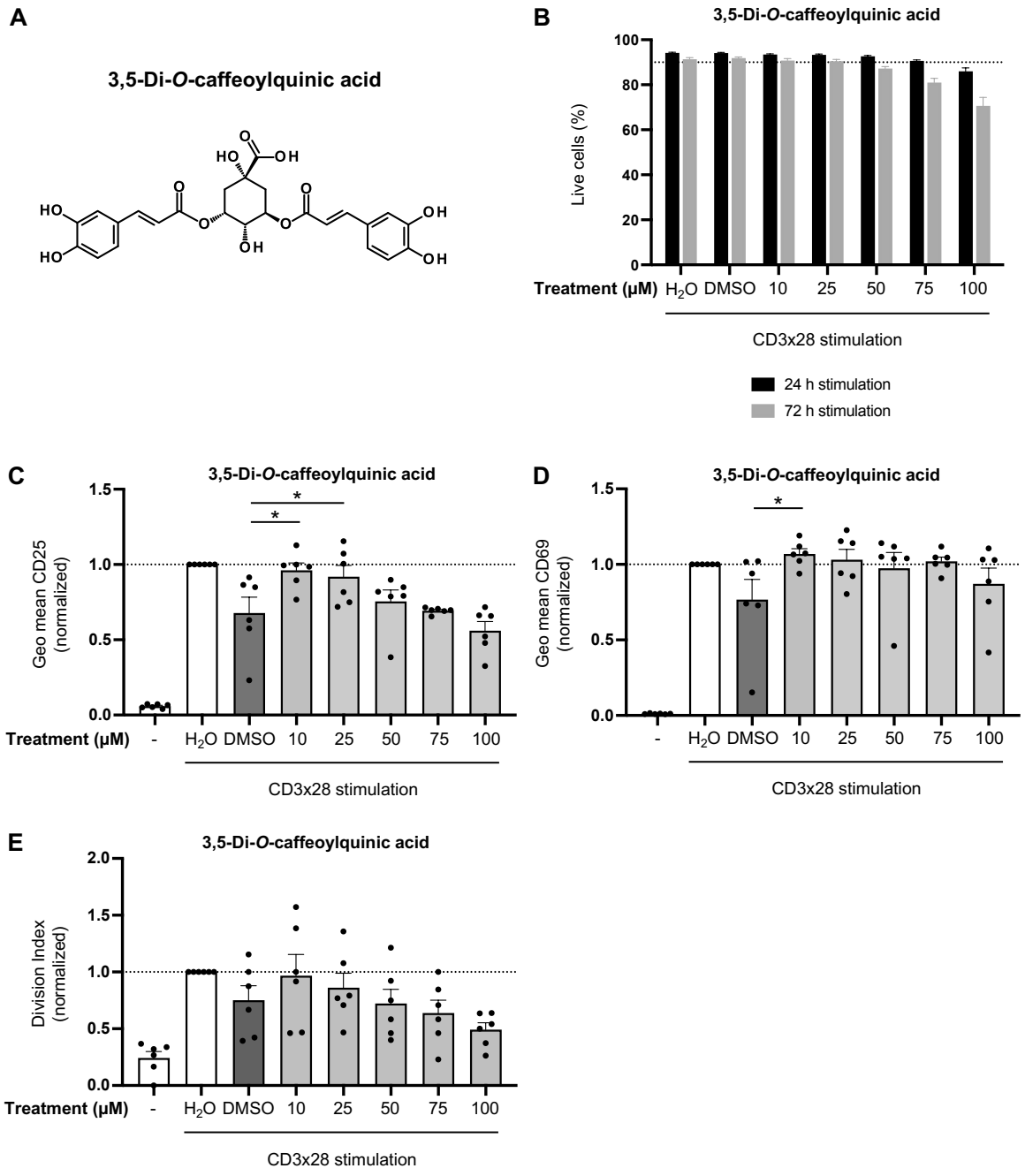

Figure 31: 3,5-Di-*O*-caffeoylquinic acid at lower concentrations promotes CD25 and CD69 expression and has no effect on T cell proliferation.

(**A**) Chemical structure of 3,5-Di-*O*-caffeoylquinic acid. (**B**) PBTs were pretreated with drug or vehicle for 1 h and subsequently activated with anti-CD3/CD28 antibodies. Cell viability after 24-hour (black) and 72-hour stimulation (grey) was assessed by 7-AAD exclusion in six independent experiments each. (**C**, **D**) PBTs were left unstimulated (left white bar) or pretreated with substance (light grey bars) or vehicle (dark grey bar) for 1 h and subsequently activated with anti-CD3/CD28 antibodies for 24 h. Statistical evaluation of CD25 (**C**) and CD69 (**D**) surface expression analyzed by flow cytometry in six independent experiments. Data were normalized to the H_2O control sample. (**E**) PBTs were labeled with CFSE, left unstimulated (left white bar) or pretreated with substance (light grey bars) or vehicle (dark grey bar) for 1 h and subsequently activated with anti-CD3/CD28 antibodies for 72 h. Statistical evaluation of T cell proliferation assessed by CFSE dilution in six independent experiments. Data were normalized to the H_2O control sample. Each data point represents an individual T cell donor. Data are expressed as mean ± SEM. *$p \leq 0.05$

Finally, 3,4,5-Tri-*O*-caffeoylquinic acid (3,4,5-triCQA, structure compare Figure 32A) was tested for an immunomodulatory effect on human PBTs. Initially, the same concentration range (10 - 100 μM) that was used for 3-CQA and 3,5-diCQA was tested and found to be highly cytotoxic. Therefore, the range was adjusted to 0.5 – 5 μM for 3,4,5-triCQA. Even with 5 μM, a toxic effect was observable after 24 h and 72 h (Figure 32B). The maximum non-toxic concentration for 24-hour experiments was 2.5 μM and for 72-hour stimulation the limit was 1 μM. 3,4,5-triCQA did not have any effect on CD25 (Figure 32C) and CD69 expression (Figure 32D) in human PBTs. A significant reduction of T cell proliferation was only observed with the toxic 5 μM concentration (Figure 32E).

In conclusion, the effects of Arnica extracts on human PBTs were not mimicked by isolated (Mono-, di-, and tri-) Caffeoylquinic acids.

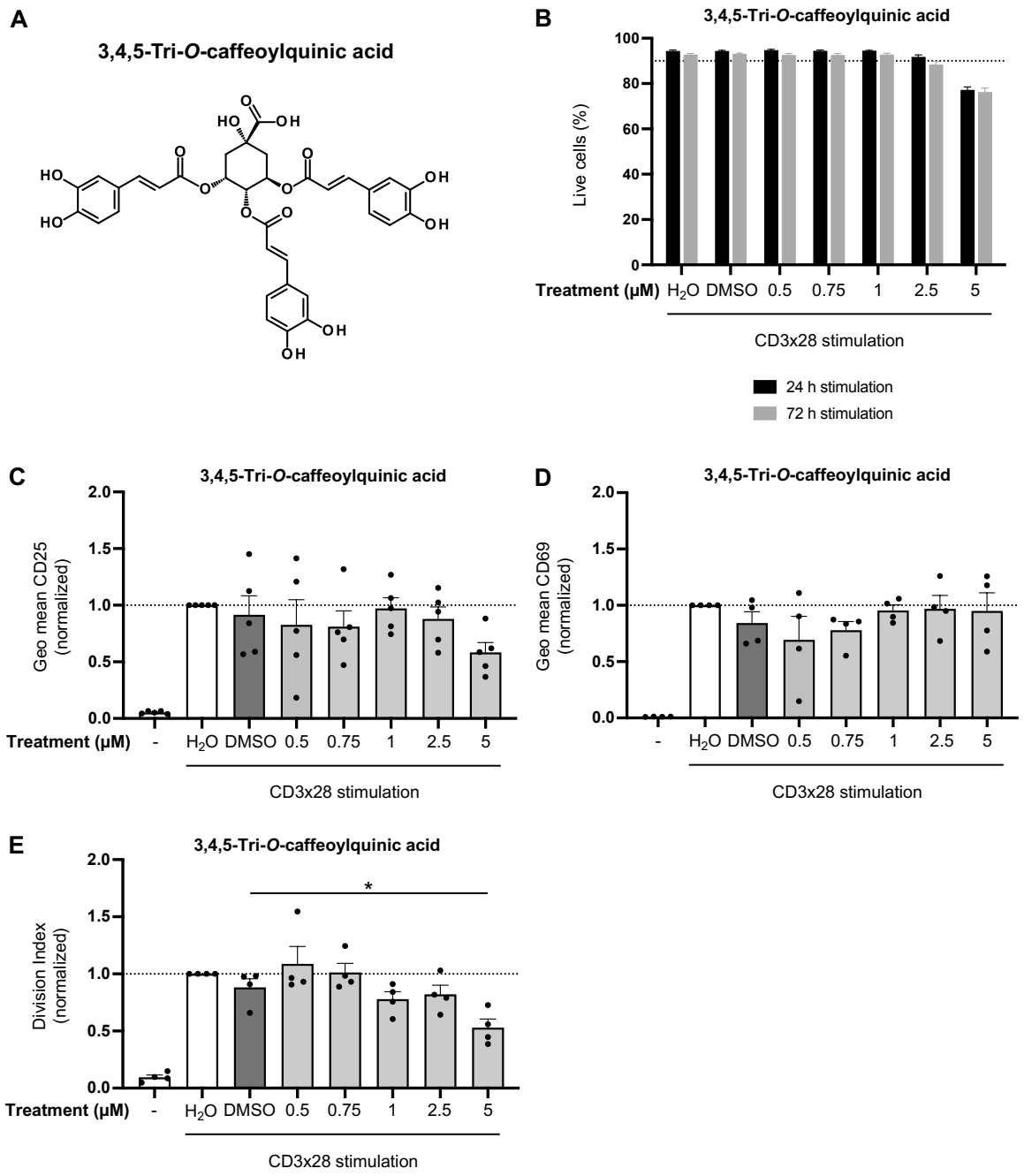

Figure 32: 3,4,5-Tri-*O*-caffeoylquinic acid at non-toxic concentrations does not affect T cell activation marker expression and proliferation.

(**A**) Chemical structure of 3,4,5-Tri-*O*-caffeoylquinic acid. (**B**) PBTs were pretreated with drug or vehicle for 1 h and subsequently activated with anti-CD3/CD28 antibodies. Cell viability after 24-hour (black) and 72-hour stimulation (grey) was assessed by 7-AAD exclusion in six independent experiments each. (**C**, **D**) PBTs were left unstimulated (left white bar) or pretreated with substance (light grey bars) or vehicle (dark grey bar) for 1 h and subsequently activated with anti-CD3/CD28 antibodies for 24 h. Statistical evaluation of CD25 (**C**) and CD69 (**D**) surface expression analyzed by flow cytometry in six independent experiments. Data were normalized to the H_2O control sample. (**E**) PBTs were labeled with CFSE, left unstimulated (left white bar) or pretreated with substance (light grey bars) or vehicle (dark grey bar) for 1 h and subsequently activated with anti-CD3/CD28 antibodies for 72 h. Statistical evaluation of T cell proliferation assessed by CFSE dilution in six independent experiments. Data were normalized to the H_2O control sample. Each data point represents an individual T cell donor. Data are expressed as mean ± SEM. *$p \leq 0.05$

4 Discussion

4.1 Criteria to be considered for establishing an optimal *in vitro* test system to study the effects of plant extracts on human immune cells

Multiple factors need to be taken into consideration when testing drugs, and in particular plant extracts, in a cell culture system.

An important choice to be made at the beginning of each study is about the cell type. Different immortalized or tumor cell lines are available and frequently used as they are easier in handling and compatible with a vast array of assays, which often prove difficult when working with primary cells. Nevertheless, using primary cells should be generally favored since studies in cell lines often do not reflect the situation in primary cells due to differences in signaling. For this thesis, total primary human PBTs, freshly isolated from peripheral blood of healthy donors, were chosen. As PBTs are hard to transfect, the NFAT luciferase reporter assay was exceptionally performed with Jurkat E6.1 cells.

Each cell type can be activated *in vitro* by means of different stimulants. It can be distinguished between stimulating signals initiated at the cell surface, for example via the TCR, and stimulants that induce cellular activation by acting directly on intracellular signaling pathways, such as phorbol 12-myristate 13-acetate (PMA) and Ionomycin. While PMA activates protein kinase C (152), the calcium ionophore Ionomycin enhances calcium influx by direct stimulation of SOCE (153). Inducing T cell activation via the TCR has the advantage that such a system also allows to detect drug effects on early costimulation-induced signaling events. Furthermore, T cell stimulation by TCR engagement more closely resembles the *in vivo* condition and, in general, such a stimulation is not as strong as for example PMA/Ionomycin-mediated stimulation. Therefore, a combination of antibodies against CD3 and CD28 was chosen for induction of T cell activation in this thesis. By titration, the optimal concentration of each antibody was identified to reach robust though not complete activation of T cells. Using this setting, it was possible to identify both, stimulatory as well as inhibitory drug effects on T cell function.

Another important factor to be considered when studying the immunomodulatory potential of drugs is the exclusion of toxic concentrations. This step is essential, as one can otherwise not distinguish between cytotoxicity-related and drug-mediated effects. For previously tested drugs, the concentration range to be tested can be narrowed down based on published literature. However, cell viability analysis needs to be performed for each cell type individually, as results may vary greatly, especially between primary cells and cell lines. In this thesis, treatments that did not lower the percentage of viable cells below a threshold of 90 % were considered as non-toxic.

Apart from that, it is very important to know about the exact solvent composition of each test drug. Plant extracts are commonly aqueous, hydroalcoholic or alcoholic and purified

substances are usually dissolved in the organic solvent DMSO. For both, EtOH and DMSO, a cytotoxic as well as an immunomodulatory potential has been described (154–157). Therefore, the final concentration of these solvents in cell culture needs to be limited by appropriate dilution. In general, a maximum concentration of 0.1 % is considered as safe (158) and was therefore used in this thesis. Drug treated samples were always compared to the respective solvent control for direct comparison.

Lipopolysaccharide (LPS) constitutes a characteristic component of the outer membrane of most gram-negative bacteria that can activate immune cells via TLR4 (159,160). It consists of three structural domains, the O-Antigen, the core oligosaccharide, and lipid A. The latter part represents the endotoxin region of LPS and mediates local and systemic toxicity (161). Since bacteria reside on raw plant materials, plant extracts can naturally contain endotoxins, which are regarded as unwanted contaminant due to their multiple cellular effects (162,163). The endotoxin concentration is specified in endotoxin units (EU) per milliliter (EU/ml) with 1 EU/ml being approximately equal to 0.1 – 0.2 ng/ml of endotoxin. Commercial suppliers of cell culture accessories such as media and recombinant protein products limit the endotoxin content in their products to less than 1 EU/ml. On this basis, the endotoxin concentration of Arnica extracts tested in this thesis was also limited to 1 EU/ml.

Furthermore, changes in the pH value of cell culture medium following drug addition need to be monitored, for example by means of the contained pH indicator phenol red. Arnica extracts were found to be acidic, as higher concentrations induced a color change of the medium towards orange/yellow. *Bosticardo et al.* and others showed that T cell-mediated immunity is inhibited by low extracellular pH (164–166). To prevent studying effects that are actually elicited by the acidic microenvironment and not by bioactive compounds, the tested extracts were diluted at least 1:100.

4.2 Anti-inflammatory effects of Arnica on human T cells

Using the experimental system described in the previous section, the effects of differentially manufactured *Arnica montana* L. extracts and the lead compounds Thymol and Helenalin on primary human T cells have been investigated at a functional and molecular level. Such a side-by-side comparison is beneficial for direct comparability and was not published before.

An anti-inflammatory mode of action of Arnica extracts was so far only shown with a murine macrophage cell line (92) and the Jurkat T cell leukemia cell line (87). However, no studies using primary immune cells and, in particular primary human T cells, are available, underlining the need for more research in this area. In this thesis, an anti-inflammatory effect of the three selected Arnica extracts (Ferm, Tota, Radix) on primary human PBTs was found. Using a physiologically relevant stimulation condition, namely CD3/CD28 costimulation, Arnica extracts inhibited T cell proliferation. A diminished production of the growth factor IL-2 probably contributes to the decreased cell division rate, IL-2 supplementation, however, could not

rescue T cell proliferation. This can be explained by simultaneous reduction of stimulation-induced IL-2Rα (CD25) expression, which is a prerequisite for formation of a high-affinity IL-2 receptor. Interestingly, despite similar functional effects of the extracts, different molecular mechanisms were identified (Figure 33). As a molecular explanation for diminished IL-2 production upon treatment with Arnica Ferm extract, an inhibitory effect on NFAT-dependent gene expression was found. By trend, though not reaching significance, also NFκB DNA binding, but not nuclear translocation or p65 subunit phosphorylation at S529, was found to be diminished. Since TCR-induced calcium influx was not affected, Ferm extract obviously interferes at another step within the Calcium/Calcineurin/NFAT signaling pathway (see section 1.3.2). Similarly, Arnica Tota extract also reduced both, NFAT-dependent gene expression and NFκB DNA binding, however not significantly. Again, no effect on intracellular calcium levels was observable. While the two whole plant extracts appeared to act on both investigated signaling pathways, a selective reduction of NFκB DNA binding was observed for Radix extract (root). Given the completely different raw materials and extraction procedures, these results strengthen the assumed difference in phytochemical compounds.

Using TNF-α-stimulated Jurkat T cells, *Klaas et al.* found diminished NFκB DNA binding upon treatment with hydroalcoholic Arnica flower tincture (87). Furthermore, both tested flower tinctures inhibited NFAT DNA binding in response to PMA/Ionomycin stimulation. The Arnica planta tota extracts tested in this thesis (Ferm and Tota) were prepared from the fresh entire flowering plant and are thus supposed to contain, inter alia, bioactive compounds of the flowers such as sesquiterpene lactones. The results obtained when treating PBTs with Arnica Tota or Ferm extract fit to the data from *Klaas et al.*, even though the effects were in general less prominent and no complete inhibition was reached. This might be explained by the use of only flower heads in the study of *Klaas et al.* versus the whole flowering plant in our study, from which proportionally less flower-derived compounds are extracted. Another difference lies in the used cell type and the mode of stimulation. While *Klaas et al.* used TNF-α and PMA/Ionomycin, respectively, for Jurkat cell stimulation, in this thesis freshly prepared PBTs were stimulated via the TCR (CD3xCD28). Interestingly, the strongest inhibitory effect on NFκB DNA binding in PBTs was observed with the Radix extract prepared from dried roots. How far the extracts differ in their phytochemical composition and how this influences data interpretation will be further discussed in section 4.4. As opposed to LPS-stimulated J774 murine macrophages treated with Arnica whole plant methanolic extract in the study of *Verma et al.* (92), an inhibitory effect on NFκB nuclear translocation was not found in CD3x28-stimulated PBTs with any of the three tested extracts. Although *Verma et al.* also worked with a hydroalcoholic whole plant extract, which would be comparable to Arnica Tota extract used in this thesis, there are still major differences in extract manufacturing and handling. While they used dried plant material as raw material, Weleda used the fresh flowering

plant. Furthermore, the results described in this thesis were generated using diluted mother tincture. *Verma et al.*, however, evaporated the solvent and redissolved the powder in DMSO. An advantage of the latter procedure is that stock solutions with a higher concentration can be prepared. In contrast, using unprocessed mother tincture ensures that all extracted plant components remain in solution, which can prove difficult when dissolving dried powder. Further differences that can contribute to the divergent effects lie in the used cell type (murine macrophage cell line versus primary human PBTs) and the mode of stimulation (LPS/TLR4 versus CD3x28/TCR).

Similar to the Arnica extracts, also Thymol and Helenalin diminished activation, IL-2 production and proliferation of PBTs. Unlike Helenalin, which specifically interfered with NFκB nuclear translocation, the effects mediated by Thymol were less specific, since NFκB as well as Calcium/Calcineurin/NFAT signaling were found to be inhibited at different stages (Figure 33). Besides inhibiting nuclear translocation of NFκB and p65 subunit phosphorylation at S529, Thymol also interfered with calcium signaling and NFAT-dependent gene expression. So far, the effect of Thymol on isolated primary human T cells has not been investigated, but the results obtained in this thesis fit to published data generated with PBLs and Jurkat T leukemia cells, which also proliferated less upon Thymol treatment (130). Another study working with Jurkat T leukemia cells found diminished IL-2 production in response to Thymol treatment (97), which was reproducible in primary PBTs. Furthermore, diminished nuclear translocation of NFAT2 was found in Thymol-treated Jurkat cells, fitting to decreased NFAT-dependent gene expression in PBTs. Divergent data were described for phosphorylation of the NFκB p65 subunit. While Thymol diminished S529 phosphorylation in this thesis, *Gholijani et al.* found no significant influence in Jurkat cells without specifying the phosphorylation site. Thus, potential differences in the analyzed phosphorylation site and the use of nuclear extracts for Western Blotting (*Gholijani et al.*) versus flow cytometric analysis in the entire cell (this thesis) impair direct comparability. Using LPS-stimulated RAW264.7 murine macrophage cells, Thymol proved to be anti-inflammatory, inter alia, by inhibiting TLR4-mediated NFκB p65 subunit phosphorylation (167). Although these data fit to the results described for NFκB p65 S529 phosphorylation in PBTs in this thesis, again, a direct comparison is not possible due to missing information on the specific phosphorylation site investigated by *Wu et al*.

While it was known from studies using non-immune cells that Thymol treatment induces spontaneous calcium influx (138–140), this effect was not described for primary T cells before. Also, the inhibition of stimulation-induced calcium influx, as described for PBTs in this thesis, provides novel insights into the molecular mechanism underlying Thymol's effects. An inhibition of calcium mobilization by Thymol was published before for N-formyl-methionyl-leucyl-phenylalanine (fMLP)-stimulated neutrophils (99). Due to its hydrophobic nature,

Thymol can easily cross cell membranes and was found to act on various ion channels (168–170).

The effect of Helenalin on $CD4^+$ PBTs was studied before (96), however no publications on its effect on total PBTs are available. Fitting to the results published by *Berges et al.*, Helenalin was found to inhibit CD25 expression and proliferation of PBTs. Although also IL-2 production by $CD4^+$ PBTs and other readouts were analyzed, those results cannot be directly compared, as *Berges et al.* focused on the apoptosis-inducing action of Helenalin and worked with a toxic drug concentration.

The molecular mechanism underlying Helenalin's effect on Jurkat cells was published by *Lyss et al.* in 1998 (95). In Jurkat T cells, they found that Helenalin selectively alkylates cysteine sulfhydryl groups in the p65 subunit and thereby inhibits NFκB DNA binding without affecting its nuclear translocation. In this thesis, Helenalin was shown to significantly decrease the percentage of PBTs with nuclear NFκB, which is not in line with the findings described above. Whether Helenalin, in addition, affects NFκB DNA binding in PBTs could not be finally addressed since the applied technique did not allow to distinguish between effects on nuclear translocation and DNA binding. Nevertheless, in a previous publication from 1997, *Lyss et al.* stated that Helenalin does not directly modify NFκB but rather interferes with its release from the inhibitor IκB (94), which would result in inhibited nuclear translocation fitting to the results obtained in this thesis.

No effect on NFAT-dependent gene expression was observed upon Helenalin treatment of PBTs, which supports a specific effect on NFκB signaling. In contrast, *Berges et al.* found significantly diminished nuclear translocation of NFAT1 in $CD4^+$ PBTs in response to Helenalin (96). This finding might be related to the use of a cytotoxic drug concentration, whereas a lower and certainly non-toxic concentration was used for this thesis.

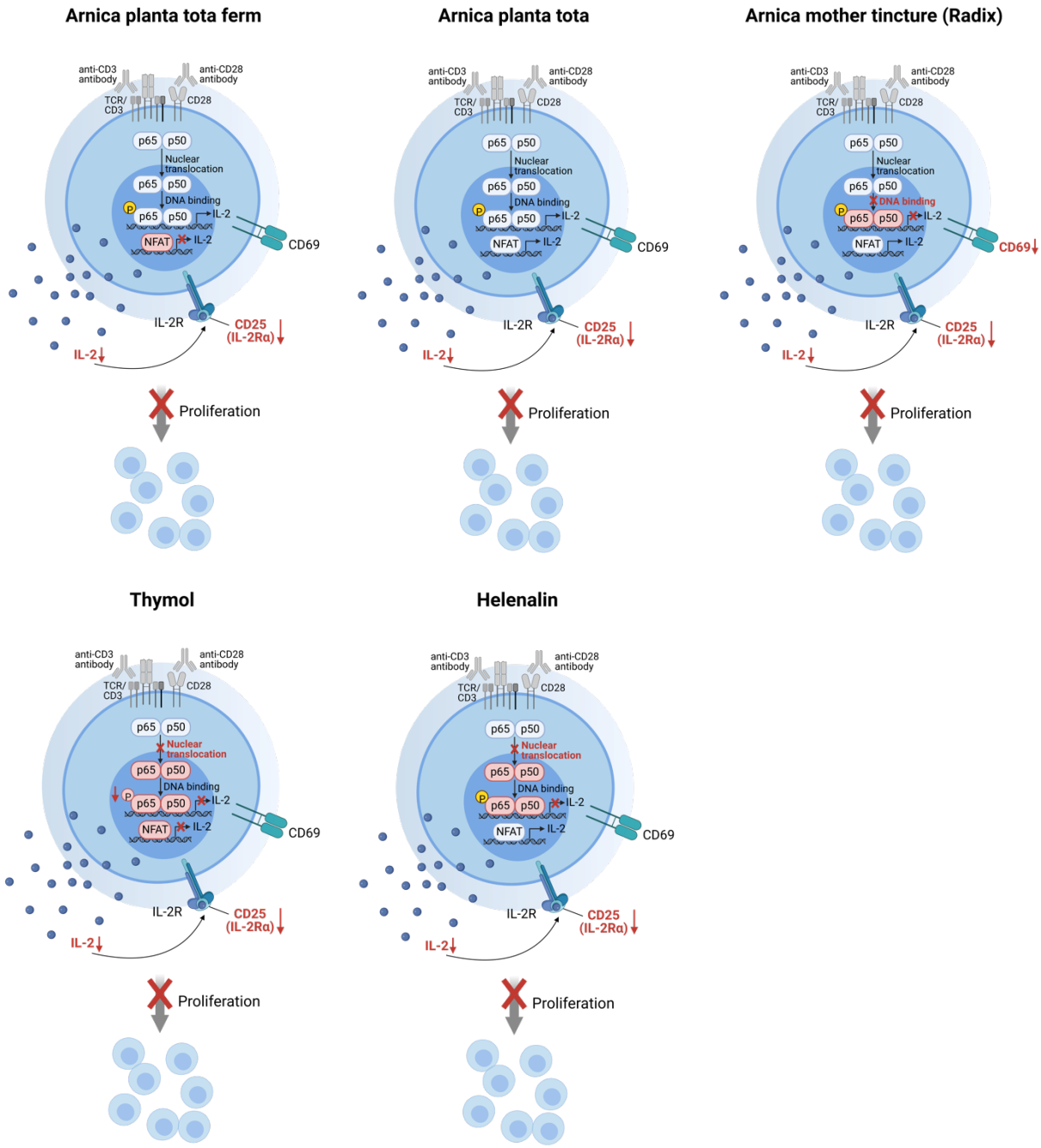

Figure 33: Graphical summary.

Despite similar effects on T cell function, including decreased CD25 expression, diminished IL-2 production and inhibited T cell proliferation, Arnica preparations differ in their molecular mechanism underlying the observed effects. Only statistically significant changes are indicated in this schematic representation. Arnica Ferm extract reduced NFAT-dependent gene expression, while the Radix extract diminished NFκB DNA binding. For Tota extract, the molecular mechanism could not be finally evaluated. Thymol inhibited the NFκB nuclear translocation, p65 subunit phosphorylation and NFAT-dependent gene expression. In contrast, Helenalin had a negative impact specifically on nuclear translocation of NFκB. This figure was created with BioRender.com.

4.3 Arnica and the cellular redox status – ROS as signaling regulator on various levels

While low levels of ROS are critically involved in intracellular signaling, excess ROS induce oxidative stress which can eventually lead to cell death.

In general, Arnica preparations are associated with an antioxidant potential that was proven in different cell-free assays (88). An antioxidant activity of three different Arnica extracts was demonstrated for the first time intracellularly in human PBTs in this thesis. Unlike cell-free systems, results obtained by analyzing intracellular ROS levels provide a higher level of evidence that the test drug indeed might mediate its effect, inter alia, via influencing the cellular redox status. As reactive oxygen species are critically involved in different TCR signaling pathways (see section 1.4), their levels need to be tightly controlled. ROS at lower levels fulfil an important function in promoting cell growth and survival (reviewed by (68)). Therefore, T cell activation and proliferation can be negatively affected under suboptimal ROS levels. This might indeed be the case upon exposure of PBTs to antioxidant Arnica extracts and explain the observed inhibitory influence on T cell function. Of note, T cell viability was not affected.

Opposite to this, *Klemke et al.* found that T cells become hyporesponsive under prooxidative conditions by oxidation of the actin-remodeling protein cofilin (35). Although being mainly described as antioxidant (104,171), Thymol, in contrast to Arnica extracts, increased intracellular ROS levels in PBTs. Therefore, creation of a prooxidative milieu might be one factor mediating Thymol's inhibitory effect on T cell activation and function. Fitting to the negative effect of elevated ROS levels on NFκB and NFAT signaling stated by different studies (compare section 1.4), the ROS-inducing action of Thymol might be responsible for inhibition of these two signaling pathways as described in this thesis. Since Helenalin did not influence intracellular ROS levels in PBTs, its molecular mechanism seems to be independent of the cellular redox status.

4.4 Phytochemical compounds in Arnica extracts – important role of substances other than sesquiterpene lactones

Phytochemical analysis of the tested Arnica extracts by HPLC-MS/MS revealed interesting and unexpected results. Due to the completely different manufacturing processes, differences in the used solvent and the raw plant material, Ferm, Tota and Radix extracts prepared from *Arnica montana* L. were expected to contain varying phytochemical compounds. This was indeed found to be the case. Interestingly, none of the three extracts contained detectable levels of sesquiterpene lactones, such as Helenalin. Since this compound is mainly enriched in the flower heads (172), it was not expected in high concentrations in the Radix extract. However, at least for Ferm and Tota extract prepared from fresh material of the entire flowering plant, Helenalin was supposed to be a prominent component. The only explanation for this

finding is that sesquiterpene lactones probably have degraded during the manufacturing process and therefore could not be detected.

The three tested extracts differentially affected NFκB and/or NFAT signaling in PBTs. So far, the inhibitory influences of Arnica preparations especially on the NFκB pathway were mainly attributed to Helenalin and other sesquiterpene lactones (87). Given the absence of Helenalin and other sesquiterpene lactones in our extracts, the observed effects on PBTs had to be mediated by other compounds or substance groups. Therefore, the results described in this thesis support another perspective that focusses on the interplay and the synergistic effects elicited by various bioactive components which eventually accounts for the cellular effects. That isolated caffeoylquinic acids, which constituted the main identified substance group in all analyzed Arnica extracts, did not show any effect on T cell function, further strengthens this assumption.

4.5 Application of Arnica for muscle healing – it's all a matter of timing

As described in detail in section 1.6, different immune cell types are critically involved in the process of muscle healing and regeneration in response to trauma. Various studies investigated the spatiotemporal distribution of the participating cell populations (reviewed by (107,173)) and thereby essentially contributed to a better and more detailed understanding of this complex process. Only knowing about dysregulated spots within the whole network that ultimately cause delayed tissue remodeling makes it possible to intervene for therapeutic purposes. In this context, prolonged persistence of $CD4^+$ and $CD8^+$ T cells was shown to be a hallmark of impaired muscle healing (123). Having this finding in mind, inhibition of T cell activation upon treatment with Arnica preparations as described in this thesis, could indeed promote resolution of inflammation and facilitate normal muscle healing.

Nevertheless, the timing of Arnica application needs to be well chosen. As outlined in section 1.6.1, T cells also play a major role in the early phase of the normal wound healing process and are critically involved in establishment of a proinflammatory milieu that is required for proper tissue repair. Supporting the importance of T cells for proper muscle healing, *Fu et al.* observed delayed muscle regeneration in *Rag*$^{-/-}$ mice lacking functional T and B cells. Transplantation of activated $CD3^+$ T cells, however, was able to restore normal muscle healing. The positive effect of T cells could be traced back to their release of the pro-inflammatory cytokines IL-1α, IL-13, IFN-γ and TNF-α, which were found to promote muscle stem cell proliferation and inhibit their differentiation (174). Thus, interfering with T cell activation at the wrong time can even have detrimental effects and impair proper muscle regeneration.

All in all, the anti-inflammatory effect on T cells proven in this thesis makes Arnica an interesting drug candidate and underpins its traditional use as herbal remedy. To make conclusive statements on the effectiveness of Arnica in promoting healing of blunt injuries such

as contusions and bruises, its effect on other (immune) cell types needs to be investigated in more detail and solid clinical trials are urgently needed.

4.6 Drug bioavailability – hurdles to overcome

Arnica preparations can be applied either topically (cream, ointment) or systemically (oral drops, globules, injection). As for each drug, it is essential that the bioactive compounds can reach their intended biological destination within the human body in order to be bioavailable. However, there are certain hurdles to be overcome for both, topical and systemic use. Following cutaneous application, therapeutic agents have to overcome the barrier function of the skin, whereas the gastrointestinal tract represents the main obstacle after oral ingestion. *Wagner et al.* studied the penetration kinetics of sesquiterpene lactones using pig skin as a model (175). Compared to the application of isolated SLs, a much higher permeation of SLs through the stratum corneum, the outermost layer of the epidermis, was observed when applying Arnica tinctures prepared from dried flower heads. A recent study on dermal absorption of SLs contained in Arnica flower tincture found that the majority of SLs penetrated porcine and human skin samples after 48 h (176). Skin penetration enhancers like oleic acid, offer the possibility to further promote cutaneous bioavailability of SLs (177).

Due to its hydrophobic nature, Thymol is expected to rather easily cross the skin barrier, which is supported by its use as a skin penetration enhancer in various studies (178–180). Following oral intake, Thymol is readily absorbed in the intestine and metabolized to Thymol sulfate and Thymol glucuronide (181–183). In humans, Thymol was not detectable in plasma or urine after oral application (184).

Taken together, there are only few studies available investigating the bioavailability of bioactive compounds from Arnica preparations. Having in mind that bioactive compounds other than SLs play an important role in mediating Arnica's anti-inflammatory effect (see section 4.4), further bioavailability studies not solely focusing on SLs should be conducted.

4.7 Conclusion and Outlook

The anti-inflammatory effects of different Arnica preparations on freshly isolated primary human T cells described in this thesis will contribute to a critical evaluation of complementary treatment options based on consolidated experimental data. In virtue of these findings, the indication of Arnica could be extended to other T cell-mediated inflammatory processes as described, for example, in psoriasis or arthritis. Since different Th subsets were characterized as drivers of these chronic inflammatory diseases, future studies should investigate if Arnica preparations affect the differentiation process of T cells. Overall, it becomes clear that there is a great need for more research in this field and finally, the results obtained *in vitro* need to be confirmed *in vivo*.

5 Appendix

5.1 Abbreviations

Abbreviation	Description
AP-1	Activator protein 1
APC	Antigen-presenting cell
APS	Ammonium persulfate
Arnica	*Arnica montana* L.
AUC	Area under the curve
BAFFR	B-cell activating factor receptor
BSA	Bovine serum albumin
Ca^{2+}	Calcium
CaM	Calmodulin
CCR	C-C chemokine receptor
CD	Cluster of differentiation
CD3x28 stimulation	Stimulation with anti-CD3 + anti-CD28 antibodies
CFSE	Carboxyfluorescein succinimidyl ester
Ch	Channel
3-CQA	3-*O*-Caffeoylquinic acid
CRAC channels	Ca^{2+} release-activated Ca^{2+} channels
DAG	Diacylglycerol
DAMP	Damage-associated molecular pattern
DC	Dendritic cell
3,5-diCQA	3,5-Di-*O*-caffeoylquinic acid
DMSO	Dimethyl sulfoxide
DNA	Deoxyribonucleic acid
dpi	day(s) post injury
DTT	Dithiothreitol
ECM	Extracellular matrix
EDTA	Ethylenediaminetetraacetic acid

Abbreviation	Description
EGTA	Ethylene glycol-bis(2-aminoethylether)-N,N,N',N'-tetraacetic acid
ER	Endoplasmic reticulum
EtOH	Ethanol
EU	Endotoxin unit
FACS	Fluorescence-activated cell sorting
FBS	Fetal bovine serum
Ferm	*Arnica montana* L. E planta tota ferm 33c (WALA)
fMLP	N-formyl-methionyl-leucyl-phenylalanine
FSC	Forward scatter
GAPDH	Glyceraldehyde-3-phosphate dehydrogenase
Geo mean	Geometric mean
GHP	German Homeopathic Pharmacopeia
Hel	Helenalin
hpi	hour(s) post injury
HPLC	High performance liquid chromatography
HRP	Horseradish peroxidase
IFN	Interferon
IGF1	Insulin-like growth factor 1
IgG	Immunoglobulin G
IgM	Immunoglobulin M
IKK	IκB kinase
IL	Interleukin
Iono	Ionomycin
IP3	Inositol 1,4,5-trisphosphate
ITAM	Immunoreceptor tyrosine-based activation motif
ITK	Interleukin-2-inducible tyrosine kinase
KEGG	Kyoto Encyclopedia of Genes and Genomes
LAT	Linker for activation of T cells

Abbreviation	Description
LCK	Lymphocyte-specific protein tyrosine kinase
LPL	L-plastin
LPS	Lipopolysaccharide
LTßR	Lymphotoxin-ß receptor
MAPK	Mitogen-activated protein kinase
MFI	Mean fluorescent intensity
$MgCl_2$	Magnesium chloride
MHC	Major histocompatibility complex
mRNA	Messenger RNA
MS	Mass spectrometry
mTORC1	Mammalian target of rapamycin complex 1
NAC	N-acetyl-L-cysteine
NaCl	Sodium chloride
NaF	Sodium fluoride
NaN_3	Sodium azide
NES	Normalized enrichment score
NFAT	Nuclear factor of activated T cells
NFκB	Nuclear factor 'kappa-light-chain-enhancer' of activated B cells
NIK	NFκB-inducing kinase
ORAC assay	Oxygen radical absorbance capacity assay
PAGE	Polyacrylamide gel electrophoresis
pAPC	Professional antigen-presenting cell
PBMC	Peripheral blood mononuclear cell
PBS	Phosphate-buffered saline
PBT	Peripheral blood T cell
PDA	Photodiode array
PFA	Paraformaldehyde
PHA	Phytohaemagglutinin

Abbreviation	Description
PI3K	Phosphatidylinositol 3-kinase
PIP2	Phosphatidylinositol 4,5-bisphosphate
PKB	Protein kinase B
PKCθ	Protein kinase Cθ
PLCγ1	Phospholipase Cγ1
p-LPL	Phosphorylated L-plastin
PMA	Phorbol 12-myristate 13-acetate
PMSF	Phenylmethylsulfonyl fluoride
PP	Protein phosphatase
PRR	Pattern recognition receptor
qPCR	Quantitative PCR
Radix	*Arnica montana* L. mother tincture (DHU)
RANK	Receptor activator of NFκB
RE	Response element
RNA	Ribonucleic acid
ROS	Reactive oxygen species
SDF	Stromal cell-derived factor
SDS	Sodium dodecyl sulfate
SL	Sesquiterpene lactone
SLP-76	Leukocyte protein of 76 kDa
SOCE	Store-operated Ca^{2+} entry
TBHP	Tert-Butyl hydroperoxide
TBS	Tris-buffered saline
TBS-T	Tris-buffered saline with Tween®
TCR	T cell receptor
TEAC assay	Trolox equivalent antioxidant capacity assay
TEMED	N,N,N',N'-Tetramethyl ethylenediamine
Tfh cells	T follicular helper cells

Abbreviation	Description
Th	Thymol
Th cells	T helper cells
TIC	Total ion chromatogram
TLR	Toll-like receptor
TNF	Tumor necrosis factor
Tota	*Arnica montana* L. Planta tota ∅ V.2b (Weleda)
TRAF3	TNF receptor-associated factor 3
Treg	Regulatory T cell
3,4,5-triCQA	3,4,5-Tri-*O*-caffeoylquinic acid
ZAP70	Zeta-chain-associated protein kinase 70

5.2 List of Figures

5.3 List of Tables

5.4 Plasmid map

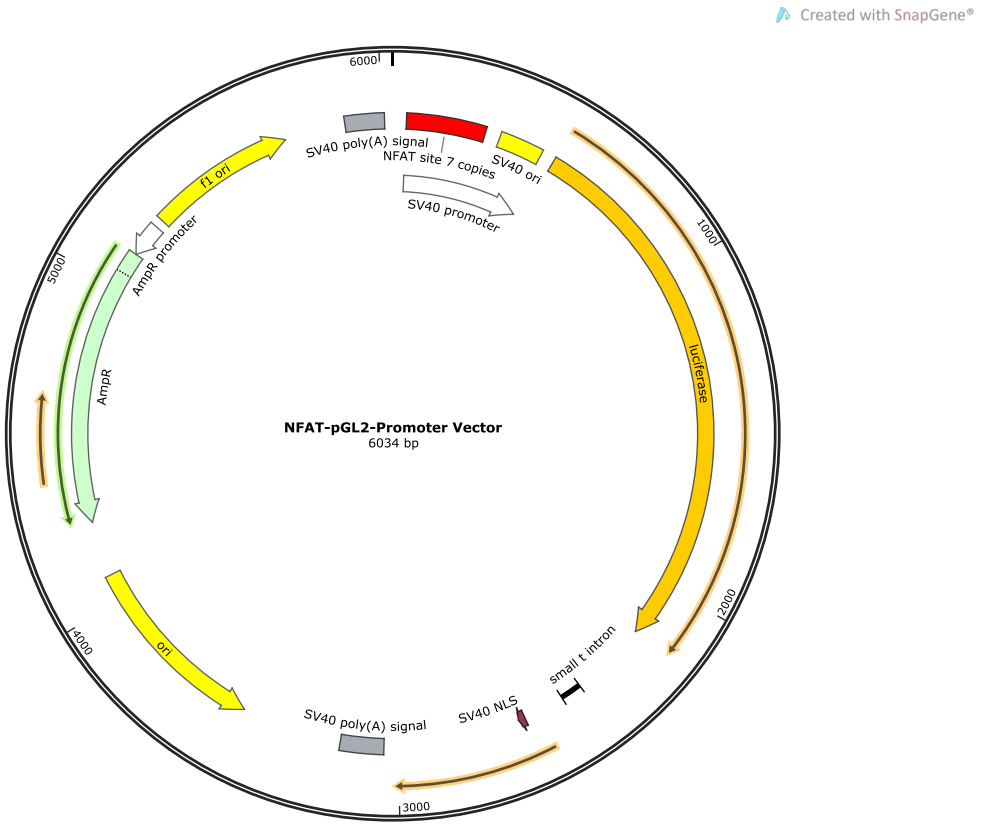

Figure 34: Plasmid map of the NFAT-pGL2-Promoter Vector.

The NFAT-pGL2-Promter Vector plasmid was used to analyze NFAT-dependent gene expression by luciferase reporter assay. Firefly luciferase reporter gene expression is controlled by seven copies of the NFAT site (-290 / -261) of the murine IL-2 promoter. The plasmid was obtained from the Department of Molecular and Developmental Biology (Institute of Medical Science, University of Tokyo, Japan).

6 References

1. Medzhitov R, Preston-Hurlburt P, Janeway CA. A human homologue of the Drosophila Toll protein signals activation of adaptive immunity. Nature. 1997 Jul 24;388(6640):394–7.

2. Rock FL, Hardiman G, Timans JC, Kastelein RA, Bazan JF. A family of human receptors structurally related to Drosophila Toll. Proc Natl Acad Sci. 1998 Jan 20;95(2):588–93.

3. Takeda K, Akira S. Toll-like receptors in innate immunity. Int Immunol. 2005 Jan;17(1):1–14.

4. Brenner MB, McLean J, Dialynas DP, Strominger JL, Smith JA, Owen FL, et al. Identification of a putative second T-cell receptor. Nature. 1986 Jul 10;322(6075):145–9.

5. Caza T, Landas S. Functional and Phenotypic Plasticity of CD4+ T Cell Subsets. BioMed Res Int. 2015;2015:521957.

6. Breitfeld D, Ohl L, Kremmer E, Ellwart J, Sallusto F, Lipp M, et al. Follicular B helper T cells express CXC chemokine receptor 5, localize to B cell follicles, and support immunoglobulin production. J Exp Med. 2000 Dec 4;192(11):1545–52.

7. Russ BE, Prier JE, Rao S, Turner SJ. T cell immunity as a tool for studying epigenetic regulation of cellular differentiation. Front Genet. 2013 Nov 12;4:218.

8. Liu J, Zhang X, Cheng Y, Cao X. Dendritic cell migration in inflammation and immunity. Cell Mol Immunol. 2021 Nov;18(11):2461–71.

9. Jenkins MK, Schwartz RH. Antigen presentation by chemically modified splenocytes induces antigen-specific T cell unresponsiveness in vitro and in vivo. J Exp Med. 1987 Feb 1;165(2):302–19.

10. Schwartz RH. A cell culture model for T lymphocyte clonal anergy. Science. 1990 Jun 15;248(4961):1349–56.

11. Hwang JR, Byeon Y, Kim D, Park SG. Recent insights of T cell receptor-mediated signaling pathways for T cell activation and development. Exp Mol Med. 2020 May;52(5):750–61.

12. Yamasaki S, Takamatsu M, Iwashima M. The kinase, SH3, and SH2 domains of Lck play critical roles in T-cell activation after ZAP-70 membrane localization. Mol Cell Biol. 1996 Dec;16(12):7151–60.

13. Artyomov MN, Lis M, Devadas S, Davis MM, Chakraborty AK. CD4 and CD8 binding to MHC molecules primarily acts to enhance Lck delivery. Proc Natl Acad Sci U S A. 2010 Sep 28;107(39):16916–21.

14. Chan AC, Irving BA, Fraser JD, Weiss A. The zeta chain is associated with a tyrosine kinase and upon T-cell antigen receptor stimulation associates with ZAP-70, a 70-kDa tyrosine phosphoprotein. Proc Natl Acad Sci U S A. 1991 Oct 15;88(20):9166–70.

15. Chan AC, Dalton M, Johnson R, Kong GH, Wang T, Thoma R, et al. Activation of ZAP-70 kinase activity by phosphorylation of tyrosine 493 is required for lymphocyte antigen receptor function. EMBO J. 1995 Jun 1;14(11):2499–508.

16. Zhang W, Sloan-Lancaster J, Kitchen J, Trible RP, Samelson LE. LAT: the ZAP-70 tyrosine kinase substrate that links T cell receptor to cellular activation. Cell. 1998 Jan 9;92(1):83–92.

17. Bubeck Wardenburg J, Fu C, Jackman JK, Flotow H, Wilkinson SE, Williams DH, et al. Phosphorylation of SLP-76 by the ZAP-70 protein-tyrosine kinase is required for T-cell receptor function. J Biol Chem. 1996 Aug 16;271(33):19641–4.

18. Crespo P, Schuebel KE, Ostrom AA, Gutkind JS, Bustelo XR. Phosphotyrosine-dependent activation of Rac-1 GDP/GTP exchange by the vav proto-oncogene product. Nature. 1997 Jan 9;385(6612):169–72.

19. Nobes CD, Hall A. Rho, rac, and cdc42 GTPases regulate the assembly of multimolecular focal complexes associated with actin stress fibers, lamellipodia, and filopodia. Cell. 1995 Apr 7;81(1):53–62.

20. Schaeffer EM, Debnath J, Yap G, McVicar D, Liao XC, Littman DR, et al. Requirement for Tec kinases Rlk and Itk in T cell receptor signaling and immunity. Science. 1999 Apr 23;284(5414):638–41.

21. Noh DY, Shin SH, Rhee SG. Phosphoinositide-specific phospholipase C and mitogenic signaling. Biochim Biophys Acta. 1995 Dec 18;1242(2):99–113.

22. Bell RM, Hannun YA, Loomis CR. Mechanism of regulation of protein kinase C by lipid second messengers. Symp Fundam Cancer Res. 1986;39:145–56.

23. Tognon CE, Kirk HE, Passmore LA, Whitehead IP, Der CJ, Kay RJ. Regulation of RasGRP via a phorbol ester-responsive C1 domain. Mol Cell Biol. 1998 Dec;18(12):6995–7008.

24. Ebinu JO, Bottorff DA, Chan EY, Stang SL, Dunn RJ, Stone JC. RasGRP, a Ras guanyl nucleotide- releasing protein with calcium- and diacylglycerol-binding motifs. Science. 1998 May 1;280(5366):1082–6.

25. Streb H, Irvine RF, Berridge MJ, Schulz I. Release of Ca2+ from a nonmitochondrial intracellular store in pancreatic acinar cells by inositol-1,4,5-trisphosphate. Nature. 1983 Nov 3;306(5938):67–9.

26. Prentki M, Corkey BE, Matschinsky FM. Inositol 1,4,5-trisphosphate and the endoplasmic reticulum Ca2+ cycle of a rat insulinoma cell line. J Biol Chem. 1985 Aug 5;260(16):9185–90.

27. Frauwirth KA, Riley JL, Harris MH, Parry RV, Rathmell JC, Plas DR, et al. The CD28 Signaling Pathway Regulates Glucose Metabolism. Immunity. 2002 Jun 1;16(6):769–77.

28. Henning SW, Meuer SC, Samstag Y. Serine phosphorylation of a 67-kDa protein in human T lymphocytes represents an accessory receptor-mediated signaling event. J Immunol Baltim Md 1950. 1994 May 15;152(10):4808–15.

29. Samstag Y, Bader A, Meuer SC. A serine phosphatase is involved in CD2-mediated activation of human T lymphocytes and natural killer cells. J Immunol Baltim Md 1950. 1991 Aug 1;147(3):788–94.

30. Samstag Y, Henning SW, Bader A, Meuer SC. Dephosphorylation of pp19: a common second signal for human T cell activation mediated through different accessory molecules. Int Immunol. 1992 Nov;4(11):1255–62.

31. Samstag Y, Eckerskorn C, Wesselborg S, Henning S, Wallich R, Meuer SC. Costimulatory signals for human T-cell activation induce nuclear translocation of pp19/cofilin. Proc Natl Acad Sci U S A. 1994 May 10;91(10):4494–8.

32. Lommel MJ, Trairatphisan P, Gäbler K, Laurini C, Muller A, Kaoma T, et al. L-plastin Ser5 phosphorylation in breast cancer cells and in vitro is mediated by RSK downstream of the ERK/MAPK pathway. FASEB J Off Publ Fed Am Soc Exp Biol. 2016 Mar;30(3):1218–33.

33. Wabnitz GH, Honus S, Habicht J, Orlik C, Kirchgessner H, Samstag Y. LFA-1 cluster formation in T-cells depends on l-plastin phosphorylation regulated by P90RSK and PP2A. Cell Mol Life Sci. 2021 Apr 1;78(7):3543–64.

34. Ambach A, Saunus J, Konstandin M, Wesselborg S, Meuer SC, Samstag Y. The serine phosphatases PP1 and PP2A associate with and activate the actin-binding protein cofilin in human T lymphocytes. Eur J Immunol. 2000 Dec;30(12):3422–31.

35. Klemke M, Wabnitz GH, Funke F, Funk B, Kirchgessner H, Samstag Y. Oxidation of cofilin mediates T cell hyporesponsiveness under oxidative stress conditions. Immunity. 2008 Sep 19;29(3):404–13.

36. Balta E, Hardt R, Liang J, Kirchgessner H, Orlik C, Jahraus B, et al. Spatial oxidation of L-plastin downmodulates actin-based functions of tumor cells. Nat Commun. 2019 Sep 9;10(1):4073.

37. Chen Q, Lu X, Zhang X. Noncanonical NF-κB Signaling Pathway in Liver Diseases. J Clin Transl Hepatol. 2021 Feb 28;9(1):81–9.

38. Baeuerle PA, Baltimore D. I kappa B: a specific inhibitor of the NF-kappa B transcription factor. Science. 1988 Oct 28;242(4878):540–6.

39. DiDonato JA, Hayakawa M, Rothwarf DM, Zandi E, Karin M. A cytokine-responsive IkappaB kinase that activates the transcription factor NF-kappaB. Nature. 1997 Aug 7;388(6642):548–54.

40. Wabnitz GH, Kirchgessner H, Jahraus B, Umansky L, Shenolikar S, Samstag Y. Protein Phosphatase 1α and Cofilin Regulate Nuclear Translocation of NF-κB and Promote

Expression of the Anti-Inflammatory Cytokine Interleukin-10 by T Cells. Mol Cell Biol. 2018 Nov 15;38(22):e00041-18.

41. Baeuerle PA, Baltimore D. A 65-kappaD subunit of active NF-kappaB is required for inhibition of NF-kappaB by I kappaB. Genes Dev. 1989 Nov;3(11):1689–98.

42. Schmitz ML, Baeuerle PA. The p65 subunit is responsible for the strong transcription activating potential of NF-kappa B. EMBO J. 1991 Dec;10(12):3805–17.

43. Hou S, Guan H, Ricciardi RP. Phosphorylation of Serine 337 of NF-κB p50 Is Critical for DNA Binding*. J Biol Chem. 2003 Nov 14;278(46):45994–8.

44. Bird TA, Schooley K, Dower SK, Hagen H, Virca GD. Activation of Nuclear Transcription Factor NF-κB by Interleukin-1 Is Accompanied by Casein Kinase II-mediated Phosphorylation of the p65 Subunit. J Biol Chem. 1997 Dec;272(51):32606–12.

45. Wang D, Baldwin AS. Activation of Nuclear Factor-κB-dependent Transcription by Tumor Necrosis Factor-α Is Mediated through Phosphorylation of RelA/p65 on Serine 529*. J Biol Chem. 1998 Nov 6;273(45):29411–6.

46. Sun SC, Ganchi PA, Ballard DW, Greene WC. NF-kappa B controls expression of inhibitor I kappa B alpha: evidence for an inducible autoregulatory pathway. Science. 1993 Mar 26;259(5103):1912–5.

47. Coope HJ, Atkinson PGP, Huhse B, Belich M, Janzen J, Holman MJ, et al. CD40 regulates the processing of NF-kappaB2 p100 to p52. EMBO J. 2002 Oct 15;21(20):5375–85.

48. Claudio E, Brown K, Park S, Wang H, Siebenlist U. BAFF-induced NEMO-independent processing of NF-kappa B2 in maturing B cells. Nat Immunol. 2002 Oct;3(10):958–65.

49. Dejardin E, Droin NM, Delhase M, Haas E, Cao Y, Makris C, et al. The lymphotoxin-beta receptor induces different patterns of gene expression via two NF-kappaB pathways. Immunity. 2002 Oct;17(4):525–35.

50. Novack DV, Yin L, Hagen-Stapleton A, Schreiber RD, Goeddel DV, Ross FP, et al. The IkappaB function of NF-kappaB2 p100 controls stimulated osteoclastogenesis. J Exp Med. 2003 Sep 1;198(5):771–81.

51. Liao G, Zhang M, Harhaj EW, Sun SC. Regulation of the NF-kappaB-inducing kinase by tumor necrosis factor receptor-associated factor 3-induced degradation. J Biol Chem. 2004 Jun 18;279(25):26243–50.

52. Xiao G, Harhaj EW, Sun SC. NF-kappaB-inducing kinase regulates the processing of NF-kappaB2 p100. Mol Cell. 2001 Feb;7(2):401–9.

53. Senftleben U, Cao Y, Xiao G, Greten FR, Krähn G, Bonizzi G, et al. Activation by IKKalpha of a second, evolutionary conserved, NF-kappa B signaling pathway. Science. 2001 Aug 24;293(5534):1495–9.

54. Yamada T, Mitani T, Yorita K, Uchida D, Matsushima A, Iwamasa K, et al. Abnormal immune function of hemopoietic cells from alymphoplasia (aly) mice, a natural strain with mutant NF-kappa B-inducing kinase. J Immunol Baltim Md 1950. 2000 Jul 15;165(2):804–12.

55. Zweifach A, Lewis RS. Mitogen-regulated Ca2+ current of T lymphocytes is activated by depletion of intracellular Ca2+ stores. Proc Natl Acad Sci. 1993 Jul;90(13):6295–9.

56. Gelfand EW, Cheung RK, Mills GB, Grinstein S. Uptake of extracellular Ca2+ and not recruitment from internal stores is essential for T lymphocyte proliferation. Eur J Immunol. 1988 Jun;18(6):917–22.

57. Valeyev NV, Bates DG, Heslop-Harrison P, Postlethwaite I, Kotov NV. Elucidating the mechanisms of cooperative calcium-calmodulin interactions: a structural systems biology approach. BMC Syst Biol. 2008 Jun 2;2(1):48.

58. Li H, Rao A, Hogan PG. Interaction of calcineurin with substrates and targeting proteins. Trends Cell Biol. 2011 Feb 1;21(2):91–103.

59. Lyakh L, Ghosh P, Rice NR. Expression of NFAT-family proteins in normal human T cells. Mol Cell Biol. 1997 May;17(5):2475–84.

60. Okamura H, Aramburu J, García-Rodríguez C, Viola JP, Raghavan A, Tahiliani M, et al. Concerted dephosphorylation of the transcription factor NFAT1 induces a conformational switch that regulates transcriptional activity. Mol Cell. 2000 Sep;6(3):539–50.

61. Jain J, McCaffrey PG, Valge-Archer VE, Rao A. Nuclear factor of activated T cells contains Fos and Jun. Nature. 1992 Apr;356(6372):801–4.

62. Wu Y, Borde M, Heissmeyer V, Feuerer M, Lapan AD, Stroud JC, et al. FOXP3 controls regulatory T cell function through cooperation with NFAT. Cell. 2006 Jul 28;126(2):375–87.

63. Monaco S, Jahraus B, Samstag Y, Bading H. Nuclear calcium is required for human T cell activation. J Cell Biol. 2016 Oct 17;215(2):231–43.

64. Devadas S, Zaritskaya L, Rhee SG, Oberley L, Williams MS. Discrete Generation of Superoxide and Hydrogen Peroxide by T Cell Receptor Stimulation : Selective Regulation of Mitogen-Activated Protein Kinase Activation and Fas Ligand Expression. J Exp Med. 2002 Jan 7;195(1):59–70.

65. Finkel T. Signal transduction by reactive oxygen species. J Cell Biol. 2011 Jul 11;194(1):7–15.

66. Jackson SH, Devadas S, Kwon J, Pinto LA, Williams MS. T cells express a phagocyte-type NADPH oxidase that is activated after T cell receptor stimulation. Nat Immunol. 2004 Aug;5(8):818–27.

67. Los M, Schenk H, Hexel K, Baeuerle PA, Dröge W, Schulze-Osthoff K. IL-2 gene expression and NF-kappa B activation through CD28 requires reactive oxygen production by 5-lipoxygenase. EMBO J. 1995 Aug 1;14(15):3731–40.

68. Kesarwani P, Murali AK, Al-Khami AA, Mehrotra S. Redox Regulation of T-Cell Function: From Molecular Mechanisms to Significance in Human Health and Disease. Antioxid Redox Signal. 2013 Apr 20;18(12):1497–534.

69. Paulsen CE, Truong TH, Garcia FJ, Homann A, Gupta V, Leonard SE, et al. Peroxide-dependent sulfenylation of the EGFR catalytic site enhances kinase activity. Nat Chem Biol. 2012 Jan;8(1):57–64.

70. Kabe Y, Ando K, Hirao S, Yoshida M, Handa H. Redox regulation of NF-kappaB activation: distinct redox regulation between the cytoplasm and the nucleus. Antioxid Redox Signal. 2005 Apr;7(3–4):395–403.

71. Morgan MJ, Liu Z gang. Crosstalk of reactive oxygen species and NF-κB signaling. Cell Res. 2011 Jan;21(1):103–15.

72. Toledano MB, Leonard WJ. Modulation of transcription factor NF-kappa B binding activity by oxidation-reduction in vitro. Proc Natl Acad Sci U S A. 1991 May 15;88(10):4328–32.

73. Toledano MB, Ghosh D, Trinh F, Leonard WJ. N-terminal DNA-binding domains contribute to differential DNA-binding specificities of NF-kappa B p50 and p65. Mol Cell Biol. 1993 Feb;13(2):852–60.

74. Matthews JR, Kaszubska W, Turcatti G, Wells TN, Hay RT. Role of cysteine62 in DNA recognition by the P50 subunit of NF-kappa B. Nucleic Acids Res. 1993 Apr 25;21(8):1727–34.

75. Wu M, Bian Q, Liu Y, Fernandes AF, Taylor A, Pereira P, et al. Sustained oxidative stress inhibits NF-kappaB activation partially via inactivating the proteasome. Free Radic Biol Med. 2009 Jan 1;46(1):62–9.

76. Schreck R, Rieber P, Baeuerle PA. Reactive oxygen intermediates as apparently widely used messengers in the activation of the NF-kappa B transcription factor and HIV-1. EMBO J. 1991 Aug;10(8):2247–58.

77. Sena LA, Li S, Jairaman A, Prakriya M, Ezponda T, Hildeman DA, et al. Mitochondria are required for antigen-specific T cell activation through reactive oxygen species signaling. Immunity. 2013 Feb 21;38(2):225–36.

78. Quintana A, Schwindling C, Wenning AS, Becherer U, Rettig J, Schwarz EC, et al. T cell activation requires mitochondrial translocation to the immunological synapse. Proc Natl Acad Sci. 2007 Sep 4;104(36):14418–23.

79. Flescher E, Ledbetter JA, Schieven GL, Vela-Roch N, Fossum D, Dang H, et al. Longitudinal exposure of human T lymphocytes to weak oxidative stress suppresses transmembrane and nuclear signal transduction. J Immunol Baltim Md 1950. 1994 Dec 1;153(11):4880–9.

80. Namgaladze D, Hofer HW, Ullrich V. Redox Control of Calcineurin by Targeting the Binuclear Fe2+-Zn2+ Center at the Enzyme Active Site*. J Biol Chem. 2002 Feb 22;277(8):5962–9.

81. Wabnitz GH, Goursot C, Jahraus B, Kirchgessner H, Hellwig A, Klemke M, et al. Mitochondrial translocation of oxidized cofilin induces caspase-independent necrotic-like programmed cell death of T cells. Cell Death Dis. 2010 Jul;1(7):e58–e58.

82. Sugier D, Sugier P, Gawlik-Dziki U. Propagation and Introduction of Arnica montana L. into Cultivation: A Step to Reduce the Pressure on Endangered and High-Valued Medicinal Plant Species. Sci World J. 2013 Oct 24;2013:414363.

83. Kriplani P, Guarve K, Baghael US. *Arnica montana L* . - a plant of healing: review. J Pharm Pharmacol. 2017 Aug;69(8):925–45.

84. Kos O, Lindenmeyer MT, Tubaro A, Sosa S, Merfort I. New Sesquiterpene Lactones from Arnica Tincture Prepared from Fresh Flowerheads of Arnica montana. Planta Med. 2005 Oct;71(11):1044–52.

85. Ebert M, Merfort I, Willuhn G. Flavonoid distribution in arnica subgenera Montana and Austromontana. Phytochemistry. 1988 Jan 1;27(12):3849–51.

86. Merfort I. Caffeoylquinic acids from flowers of Arnica montana and Arnica chamissonis. Phytochemistry. 1992 Jun 1;31(6):2111–3.

87. Klaas CA, Wagner G, Laufer S, Sosa S, Della Loggia R, Bomme U, et al. Studies on the anti-inflammatory activity of phytopharmaceuticals prepared from Arnica flowers. Planta Med. 2002 May 1;68(5):385–91.

88. Craciunescu O, Constantin D, Gaspar A, Toma L, Utoiu E, Moldovan L. Evaluation of antioxidant and cytoprotective activities of Arnica montana L. and Artemisia absinthium L. ethanolic extracts. Chem Cent J. 2012 Sep 9;6(1):97.

89. Pljevljakušić D, Rančić D, Ristić M, Vujisić L, Radanović D, Dajić-Stevanović Z. Rhizome and root yield of the cultivated Arnica montana L., chemical composition and histochemical localization of essential oil. Ind Crops Prod. 2012;39:177–89.

90. Weremczuk-Jeżyna I, Wysokińska H, Kalemba D. Constituents of the Essential Oil from Hairy Roots and Plant Roots of Arnica montana L. J Essent Oil Res. 2011 Jan 1;23(1):91–7.

91. Kennedy JF, Stevenson DL, White CA, Lombard A, Buffa M. Analysis of the oligosaccharides from the roots of Arnica montana L., Artemisia absinthium L., and Artemisia dracuncula L. Carbohydr Polym. 1988 Jan 1;9(4):277–85.

92. Verma N, Tripathi SK, Sahu D, Das HR, Das RH. Evaluation of inhibitory activities of plant extracts on production of LPS-stimulated pro-inflammatory mediators in J774 murine macrophages. Mol Cell Biochem. 2010 Mar;336(1–2):127–35.

93. Gertsch J, Sticher O, Schmidt T, Heilmann J. Influence of helenanolide-type sesquiterpene lactones on gene transcription profiles in Jurkat T cells and human peripheral

blood cells: anti-inflammatory and cytotoxic effects. Biochem Pharmacol. 2003 Dec;66(11):2141–53.

94. Lyss G, Schmidt TJ, Merfort I, Pahl HL. Helenalin, an Anti-Inflammatory Sesquiterpene Lactone from Arnica, Selectively Inhibits Transcription Factor NF-κB. Biol Chem. 1997 Sep 1;378(9):951–62.

95. Lyss G, Knorre A, Schmidt TJ, Pahl HL, Merfort I. The anti-inflammatory sesquiterpene lactone helenalin inhibits the transcription factor NF-kappaB by directly targeting p65. J Biol Chem. 1998 Dec 11;273(50):33508–16.

96. Berges C, Fuchs D, Opelz G, Daniel V, Naujokat C. Helenalin suppresses essential immune functions of activated CD4+ T cells by multiple mechanisms. Mol Immunol. 2009 Sep;46(15):2892–901.

97. Gholijani N, Gharagozloo M, Kalantar F, Ramezani A, Amirghofran Z. Modulation of Cytokine Production and Transcription Factors Activities in Human Jurkat T Cells by Thymol and Carvacrol. Adv Pharm Bull. 2015 Dec 31;5(Suppl 1):653–60.

98. Gholijani N, Gharagozloo M, Farjadian S, Amirghofran Z. Modulatory effects of thymol and carvacrol on inflammatory transcription factors in lipopolysaccharide-treated macrophages. J Immunotoxicol. 2016 Mar 3;13(2):157–64.

99. Braga PC, Dal Sasso M, Culici M, Bianchi T, Bordoni L, Marabini L. Anti-Inflammatory Activity of Thymol: Inhibitory Effect on the Release of Human Neutrophil Elastase. Pharmacology. 2006;77(3):130–6.

100. Moldovan L, Gaspar A, Toma L, Craciunescu O, Saviuc C. Comparison of Polyphenolic Content and Antioxidant Capacity of Five Romanian Traditional Medicinal Plants. Rev Chim-Buchar. 2011 Mar 1;62.

101. Hoffmann R, von Schwarzenberg K, López-Antón N, Rudy A, Wanner G, Dirsch VM, et al. Helenalin bypasses Bcl-2-mediated cell death resistance by inhibiting NF-κB and promoting reactive oxygen species generation. Biochem Pharmacol. 2011 Sep 1;82(5):453–63.

102. Jang JH, Iqbal T, Min K jin, Kim S, Park JW, Son EI, et al. Helenalin-induced apoptosis is dependent on production of reactive oxygen species and independent of induction of endoplasmic reticulum stress in renal cell carcinoma. Toxicol In Vitro. 2013 Mar 1;27(2):588–96.

103. Li Y, Zeng Y, Huang Q, Wen S, Wei Y, Chen Y, et al. Helenalin from Centipeda minima ameliorates acute hepatic injury by protecting mitochondria function, activating Nrf2 pathway and inhibiting NF-κB activation. Biomed Pharmacother Biomedecine Pharmacother. 2019 Nov;119:109435.

104. Ündeğer Ü, Başaran A, Degen GH, Başaran N. Antioxidant activities of major thyme ingredients and lack of (oxidative) DNA damage in V79 Chinese hamster lung fibroblast cells at low levels of carvacrol and thymol. Food Chem Toxicol. 2009 Aug 1;47(8):2037–43.

105. Deb DD, Parimala G, Saravana Devi S, Chakraborty T. Effect of thymol on peripheral blood mononuclear cell PBMC and acute promyelotic cancer cell line HL-60. Chem Biol Interact. 2011 Aug 15;193(1):97–106.

106. Krishnan M, Kim DK, Gie Kim S, Kang SC. Thymol exposure mediates pro-oxidant shift by regulating Nrf2 and apoptotic events in zebrafish (Danio rerio) embryos. Environ Toxicol Pharmacol. 2019 Jan 1;65:1–8.

107. Muire PJ, Mangum LH, Wenke JC. Time Course of Immune Response and Immunomodulation During Normal and Delayed Healing of Musculoskeletal Wounds. Front Immunol [Internet]. 2020 [cited 2022 Aug 24];11. Available from: https://www.frontiersin.org/articles/10.3389/fimmu.2020.01056

108. Fielding RA, Manfredi TJ, Ding W, Fiatarone MA, Evans WJ, Cannon JG. Acute phase response in exercise. III. Neutrophil and IL-1 beta accumulation in skeletal muscle. Am J Physiol. 1993 Jul;265(1 Pt 2):R166-172.

109. McLennan IS. Degenerating and regenerating skeletal muscles contain several subpopulations of macrophages with distinct spatial and temporal distributions. J Anat. 1996 Feb;188(Pt 1):17–28.

110. Merly F, Lescaudron L, Rouaud T, Crossin F, Gardahaut MF. Macrophages enhance muscle satellite cell proliferation and delay their differentiation. Muscle Nerve. 1999 Jun;22(6):724–32.

111. Bencze M, Negroni E, Vallese D, Yacoub-Youssef H, Chaouch S, Wolff A, et al. Proinflammatory macrophages enhance the regenerative capacity of human myoblasts by modifying their kinetics of proliferation and differentiation. Mol Ther J Am Soc Gene Ther. 2012 Nov;20(11):2168–79.

112. St Pierre BA, Tidball JG. Differential response of macrophage subpopulations to soleus muscle reloading after rat hindlimb suspension. J Appl Physiol Bethesda Md 1985. 1994 Jul;77(1):290–7.

113. Tonkin J, Temmerman L, Sampson RD, Gallego-Colon E, Barberi L, Bilbao D, et al. Monocyte/Macrophage-derived IGF-1 Orchestrates Murine Skeletal Muscle Regeneration and Modulates Autocrine Polarization. Mol Ther J Am Soc Gene Ther. 2015 Jul;23(7):1189–200.

114. Spadaro O, Camell CD, Bosurgi L, Nguyen KY, Youm YH, Rothlin CV, et al. IGF1 Shapes Macrophage Activation in Response to Immunometabolic Challenge. Cell Rep. 2017 Apr 11;19(2):225–34.

115. Arnold L, Henry A, Poron F, Baba-Amer Y, van Rooijen N, Plonquet A, et al. Inflammatory monocytes recruited after skeletal muscle injury switch into antiinflammatory macrophages to support myogenesis. J Exp Med. 2007 May 14;204(5):1057–69.

116. Pimorady-Esfahani A, Grounds MD, McMenamin PG. Macrophages and dendritic cells in normal and regenerating murine skeletal muscle. Muscle Nerve. 1997 Feb;20(2):158–66.

117. Zhang J, Xiao Z, Qu C, Cui W, Wang X, Du J. CD8 T Cells Are Involved in Skeletal Muscle Regeneration through Facilitating MCP-1 Secretion and Gr1high Macrophage Infiltration. J Immunol. 2014 Nov 15;193(10):5149–60.

118. Stein M, Keshav S, Harris N, Gordon S. Interleukin 4 potently enhances murine macrophage mannose receptor activity: a marker of alternative immunologic macrophage activation. J Exp Med. 1992 Jul 1;176(1):287–92.

119. Tiemessen MM, Jagger AL, Evans HG, van Herwijnen MJC, John S, Taams LS. CD4+CD25+Foxp3+ regulatory T cells induce alternative activation of human monocytes/macrophages. Proc Natl Acad Sci U S A. 2007 Dec 4;104(49):19446–51.

120. Burzyn D, Kuswanto W, Kolodin D, Shadrach JL, Cerletti M, Jang Y, et al. A Special Population of Regulatory T Cells Potentiates Muscle Repair. Cell. 2013 Dec 5;155(6):1282–95.

121. Castiglioni A, Corna G, Rigamonti E, Basso V, Vezzoli M, Monno A, et al. FOXP3+ T Cells Recruited to Sites of Sterile Skeletal Muscle Injury Regulate the Fate of Satellite Cells and Guide Effective Tissue Regeneration. PLoS ONE. 2015 Jun 3;10(6):e0128094.

122. Mann CJ, Perdiguero E, Kharraz Y, Aguilar S, Pessina P, Serrano AL, et al. Aberrant repair and fibrosis development in skeletal muscle. Skelet Muscle. 2011 May 4;1(1):21.

123. Hurtgen BJ, Ward CL, Garg K, Pollot BE, Goldman SM, McKinley TO, et al. Severe muscle trauma triggers heightened and prolonged local musculoskeletal inflammation and impairs adjacent tibia fracture healing. J Musculoskelet Neuronal Interact. 2016 Jun 1;16(2):122–34.

124. Böyum A. Isolation of mononuclear cells and granulocytes from human blood. Isolation of monuclear cells by one centrifugation, and of granulocytes by combining centrifugation and sedimentation at 1 g. Scand J Clin Lab Investig Suppl. 1968;97:77–89.

125. Inkabi S, Fredenburg K, Rodriguez M. Western Blot Comparison of Wet Transfer and Semi-Dry Transfer Methods. 2019 Oct 30;13:54–64.

126. Sergushichev AA. An algorithm for fast preranked gene set enrichment analysis using cumulative statistic calculation [Internet]. bioRxiv; 2016 [cited 2022 Nov 18]. p. 060012. Available from: https://www.biorxiv.org/content/10.1101/060012v1

127. Geistlinger L, Csaba G, Zimmer R. Bioconductor's EnrichmentBrowser: seamless navigation through combined results of set- & network-based enrichment analysis. BMC Bioinformatics. 2016 Jan 20;17(1):45.

128. Lyons AB, Parish CR. Determination of lymphocyte division by flow cytometry. J Immunol Methods. 1994 May 2;171(1):131–7.

129. Gill JE, Jotz MM, Young SG, Modest EJ, Sengupta SK. 7-Amino-actinomycin D as a cytochemical probe. I. Spectral properties. J Histochem Cytochem. 1975 Nov 1;23(11):793–9.

130. Amirghofran Z, Hashemzadeh R, Javidnia K, Golmoghaddam H, Esmaeilbeig A. *In vitro* immunomodulatory effects of extracts from three plants of the *Labiatae* family and isolation of the active compound(s). J Immunotoxicol. 2011 Dec;8(4):265–73.

131. Kavoosi G, Teixeira da Silva JA, Saharkhiz MJ. Inhibitory effects of *Zataria multiflora* essential oil and its main components on nitric oxide and hydrogen peroxide production in lipopolysaccharide-stimulated macrophages: *Z. multiflora* essential oil: bioactivity. J Pharm Pharmacol. 2012 Oct;64(10):1491–500.

132. Zwicker P, Schultze N, Niehs S, Albrecht D, Methling K, Wurster M, et al. Differential effects of Helenalin, an anti-inflammatory sesquiterpene lactone, on the proteome, metabolome and the oxidative stress response in several immune cell types. Toxicol In Vitro. 2017 Apr;40:45–54.

133. Oberlin E, Amara A, Bachelerie F, Bessia C, Virelizier JL, Arenzana-Seisdedos F, et al. The CXC chemokine SDF-1 is the ligand for LESTR/fusin and prevents infection by T-cell-line-adapted HIV-1. Nature. 1996 Aug 29;382(6594):833–5.

134. Bleul CC, Fuhlbrigge RC, Casasnovas JM, Aiuti A, Springer TA. A highly efficacious lymphocyte chemoattractant, stromal cell-derived factor 1 (SDF-1). J Exp Med. 1996 Sep 1;184(3):1101–9.

135. Samstag Y. Actin cytoskeletal dynamics in T lymphocyte activation and migration. J Leukoc Biol. 2003 Jan 1;73(1):30–48.

136. Kanehisa M, Goto S. KEGG: kyoto encyclopedia of genes and genomes. Nucleic Acids Res. 2000 Jan 1;28(1):27–30.

137. Podolin PL, Callahan JF, Bolognese BJ, Li YH, Carlson K, Davis TG, et al. Attenuation of murine collagen-induced arthritis by a novel, potent, selective small molecule inhibitor of IkappaB Kinase 2, TPCA-1 (2-[(aminocarbonyl)amino]-5-(4-fluorophenyl)-3-thiophenecarboxamide), occurs via reduction of proinflammatory cytokines and antigen-induced T cell Proliferation. J Pharmacol Exp Ther. 2005 Jan;312(1):373–81.

138. Yeh JH. Effect of Thymol on Ca^(2+) Homeostasis and Viability in PC3 Human Prostate Cancer Cells. Chin J Physiol. 2017 Feb 28;60(1):32–40.

139. Shen AY, Huang MH, Wang TS, Wu HM, Kang YF, Chen CL. Thymol-evoked Ca^{2+} Mobilization and Ion Currents in Pituitary GH_3 Cells. Nat Prod Commun. 2009 Jun;4(6):1934578X0900400.

140. Hsu SS, Lin KL, Chou CT, Chiang AJ, Liang WZ, Chang HT, et al. Effect of thymol on Ca2+ homeostasis and viability in human glioblastoma cells. Eur J Pharmacol. 2011 Nov;670(1):85–91.

141. Wechsler JB, Hsu CL, Bryce PJ. IgE-mediated mast cell responses are inhibited by thymol-mediated, activation-induced cell death in skin inflammation. J Allergy Clin Immunol. 2014 Jun;133(6):1735–43.

142. Aldini G, Altomare A, Baron G, Vistoli G, Carini M, Borsani L, et al. N-Acetylcysteine as an antioxidant and disulphide breaking agent: the reasons why. Free Radic Res. 2018 Jul 3;52(7):751–62.

143. Lin LZ, Harnly JM. Identification of Hydroxycinnamoylquinic Acids of Arnica Flowers and Burdock Roots Using a Standardized LC-DAD-ESI/MS Profiling Method. J Agric Food Chem. 2008 Nov 12;56(21):10105–14.

144. Sharopov F, Wetterauer B, Gulmurodov I, Khalifaev D, Safarzoda R, Sobeh M, et al. Chlorogenic and 1,5-Dicaffeoylquinic Acid-Rich Extract of Topinambur (Helianthus tuberosus L.) Exhibits Strong Antioxidant Activity and Weak Cytotoxicity. Pharm Chem J. 2020 Oct;54(7):745–54.

145. Clauser M, Aiello N, Scartezzini F, Innocenti G, Dall'Acqua S. Differences in the Chemical Composition of *Arnica montana* Flowers from Wild Populations of North Italy. Nat Prod Commun. 2014 Jan;9(1):1934578X1400900.

146. de Athayde AE, de Araujo CES, Sandjo LP, Biavatti MW. Metabolomic analysis among ten traditional "Arnica" (Asteraceae) from Brazil. J Ethnopharmacol. 2021 Jan;265:113149.

147. Gobbo-Neto L, Lopes NP. Online Identification of Chlorogenic Acids, Sesquiterpene Lactones, and Flavonoids in the Brazilian Arnica Lychnophora ericoides Mart. (Asteraceae) Leaves by HPLC-DAD-MS and HPLC-DAD-MS/MS and a Validated HPLC-DAD Method for Their Simultaneous Analysis. J Agric Food Chem. 2008 Feb 1;56(4):1193–204.

148. Guimarães R, Barros L, Dueñas M, Calhelha RC, Carvalho AM, Santos-Buelga C, et al. Infusion and decoction of wild German chamomile: Bioactivity and characterization of organic acids and phenolic compounds. Food Chem. 2013 Jan;136(2):947–54.

149. Barth C da S, Souza HGT de, Rocha LW, Madeira CR de S, Assis C, Bonomini T, et al. RP-HPLC and LC–MS–MS determination of a bioactive artefact from Ipomoea pes-caprae extract. Rev Bras Farmacogn. 2019 Sep 1;29(5):570–7.

150. Zeng A, Liang X, Zhu S, Liu C, Wang S, Zhang Q, et al. Chlorogenic acid induces apoptosis, inhibits metastasis and improves antitumor immunity in breast cancer via the NF-κB signaling pathway. Oncol Rep. 2021 Feb;45(2):717–27.

151. Socodato R, Portugal CC, Canedo T, Domith I, Oliveira NA, Paes-de-Carvalho R, et al. c-Src deactivation by the polyphenol 3-O-caffeoylquinic acid abrogates reactive oxygen

species-mediated glutamate release from microglia and neuronal excitotoxicity. Free Radic Biol Med. 2015 Feb 1;79:45–55.

152. Boneh A, Mandla S, Tenenhouse HS. Phorbol myristate acetate activates protein kinase C, stimulates the phosphorylation of endogenous proteins and inhibits phosphate transport in mouse renal tubules. Biochim Biophys Acta BBA - Mol Cell Res. 1989 Aug 15;1012(3):308–16.

153. Liu C, Hermann TE. Characterization of ionomycin as a calcium ionophore. J Biol Chem. 1978 Sep 10;253(17):5892–4.

154. Tapani E, Taavitsainen M, Lindros K, Vehmas T, Lehtonen E. Toxicity of ethanol in low concentrations. Experimental evaluation in cell culture. Acta Radiol Stockh Swed 1987. 1996 Nov;37(6):923–6.

155. Galvao J, Davis B, Tilley M, Normando E, Duchen MR, Cordeiro MF. Unexpected low-dose toxicity of the universal solvent DMSO. FASEB J Off Publ Fed Am Soc Exp Biol. 2014 Mar;28(3):1317–30.

156. Huang SH, Wu CH, Chen SJ, Sytwu HK, Lin GJ. Immunomodulatory effects and potential clinical applications of dimethyl sulfoxide. Immunobiology. 2020 May 1;225(3):151906.

157. Goral J, Karavitis J, Kovacs EJ. Exposure - dependent effects of ethanol on the innate immune system. Alcohol Fayettev N. 2008 Jun;42(4):237–47.

158. Holthaus L, Lamp D, Gavrisan A, Sharma V, Ziegler AG, Jastroch M, et al. CD4+ T cell activation, function, and metabolism are inhibited by low concentrations of DMSO. J Immunol Methods. 2018 Dec;463:54–60.

159. Hoshino K, Takeuchi O, Kawai T, Sanjo H, Ogawa T, Takeda Y, et al. Cutting edge: Toll-like receptor 4 (TLR4)-deficient mice are hyporesponsive to lipopolysaccharide: evidence for TLR4 as the Lps gene product. J Immunol Baltim Md 1950. 1999 Apr 1;162(7):3749–52.

160. Schwartz DA. The role of TLR4 in endotoxin responsiveness in humans. J Endotoxin Res. 2001;7(5):389–93.

161. Loppnow H, Brade H, Dürrbaum I, Dinarello CA, Kusumoto S, Rietschel ET, et al. IL-1 induction-capacity of defined lipopolysaccharide partial structures. J Immunol Baltim Md 1950. 1989 May 1;142(9):3229–38.

162. Kawakami H, Fuchino H, Kawahara N. Endotoxin Contamination and Reaction Interfering Substances in the Plant Extract Library. Biol Pharm Bull. 2020;43(11):1767–75.

163. Kruk A, Piwowarski JP, Pawłowska KA, Popowski D, Granica S. High molecular pyrogens present in plant extracts interfere with examinations of their immunomodulatory properties in vitro. Sci Rep. 2021 Jan 12;11:799.

164. Bosticardo M, Ariotti S, Losana G, Bernabei P, Novelli F. Biased activation of human T lymphocytes due to low extracellular pH is antagonized by B7/CD28 costimulation. Eur J Immunol. :10.

165. Fischer K, Hoffmann P, Voelkl S, Meidenbauer N, Ammer J, Edinger M, et al. Inhibitory effect of tumor cell-derived lactic acid on human T cells. Blood. 2007 May 1;109(9):3812–9.

166. Calcinotto A, Filipazzi P, Grioni M, Iero M, De Milito A, Ricupito A, et al. Modulation of microenvironment acidity reverses anergy in human and murine tumor-infiltrating T lymphocytes. Cancer Res. 2012 Jun 1;72(11):2746–56.

167. Wu H, Jiang K, Yin N, Ma X, Zhao G, Qiu C, et al. Thymol mitigates lipopolysaccharide-induced endometritis by regulating the TLR4- and ROS-mediated NF-κB signaling pathways. Oncotarget. 2017 Feb 16;8(12):20042–55.

168. Ortar G, Morera L, Schiano Moriello A, Morera E, Nalli M, Di Marzo V, et al. Modulation of thermo-transient receptor potential (thermo-TRP) channels by thymol-based compounds. Bioorg Med Chem Lett. 2012 May 15;22(10):3535–9.

169. Wang W, Wang H, Zhao Z, Huang X, Xiong H, Mei Z. Thymol activates TRPM8-mediated Ca2+ influx for its antipruritic effects and alleviates inflammatory response in Imiquimod-induced mice. Toxicol Appl Pharmacol. 2020 Nov 15;407:115247.

170. Lee SP, Buber MT, Yang Q, Cerne R, Cortés RY, Sprous DG, et al. Thymol and related alkyl phenols activate the hTRPA1 channel. Br J Pharmacol. 2008 Apr;153(8):1739–49.

171. Braga PC, Sasso MD, Culici M, Galastri L, Marceca MT, Guffanti EE. Antioxidant Potential of Thymol Determined by Chemiluminescence Inhibition in Human Neutrophils and Cell-Free Systems. Pharmacology. 2006;76(2):61–8.

172. Willuhn G, Röttger PM, Matthiesen U. [Helenalin- and 11,13-Dihydrohelenalinester from Flowers of Arnica montana.]. Planta Med. 1983 Dec;49(12):226–31.

173. Ziemkiewicz N, Hilliard G, Pullen NA, Garg K. The Role of Innate and Adaptive Immune Cells in Skeletal Muscle Regeneration. Int J Mol Sci. 2021 Mar 23;22(6):3265.

174. Fu X, Xiao J, Wei Y, Li S, Liu Y, Yin J, et al. Combination of inflammation-related cytokines promotes long-term muscle stem cell expansion. Cell Res. 2015 Jun;25(6):655–73.

175. Wagner S, Suter A, Merfort I. Skin Penetration Studies of *Arnica* Preparations and of their Sesquiterpene Lactones. Planta Med. 2004 Oct;70(10):897–903.

176. Jürgens FM, Herrmann FC, Robledo SM, Schmidt TJ. Dermal Absorption of Sesquiterpene Lactones from Arnica Tincture. Pharmaceutics. 2022 Mar 29;14(4):742.

177. Bergonzi MC, Bilia AR, Casiraghi A, Cilurzo F, Minghetti P, Montanari L, et al. Evaluation of skin permeability of sesquiterpenes of an innovative supercritical carbon dioxide Arnica extract by HPLC/DAD/MS. Pharm. 2005 Jan;60(1):36–8.

178. El-Kattan AF, Asbill CS, Kim N, Michniak BB. The effects of terpene enhancers on the percutaneous permeation of drugs with different lipophilicities. Int J Pharm. 2001 Mar 14;215(1):229–40.

179. Gao S, Singh J. Mechanism of transdermal transport of 5-fluorouracil by terpenes: carvone, 1,8-cineole and thymol. Int J Pharm. 1997 Aug 12;154(1):67–77.

180. Kararli T, Kirchhoff C, Penzotti S. Enhancement of transdermal transport of azidothymidine (AZT) with novel terpene and terpene-like enhancers: In vivo-in vitro correlations. J Controlled Release. 1995 Jan 6;34(1):43–51.

181. Katsuyama K, Hata S. Über die Dichlorthymolglykuronsäure. Berichte Dtsch Chem Ges. 1898;31(3):2583–5.

182. Takada M, Agata I, Sakamoto M, Yagi N, Hayashi N. On the metabolic detoxication of thymol in rabbit and man. J Toxicol Sci. 1979 Nov;4(4):341–50.

183. Pisarčíková J, Oceľová V, Faix Š, Plachá I, Calderón AI. Identification and quantification of thymol metabolites in plasma, liver and duodenal wall of broiler chickens using UHPLC-ESI-QTOF-MS. Biomed Chromatogr BMC. 2017 May;31(5).

184. Kohlert C, Schindler G, März RW, Abel G, Brinkhaus B, Derendorf H, et al. Systemic availability and pharmacokinetics of thymol in humans. J Clin Pharmacol. 2002 Jul;42(7):731–7.

7 Acknowledgements

First of all, I would like to thank my supervisor Prof. Dr. Yvonne Samstag. Yvonne, I am very grateful for getting the opportunity to do my PhD in your section. In the last years, I have learned a lot from you and I thank you for your openness and each individual suggestion for improvement. I really enjoyed working under your guidance!

Many thanks to Prof. Dr. Stefan Wölfl for being the first referee of my thesis and the valuable input during my TAC meetings.

Prof. Dr. Marc Freichel and Dr. Guoliang Cui I would like to thank for their willingness to become examiners in my oral examination.

I am very thankful to Prof. Dr. Beate Niesler and Prof. Dr. Adelheid Cerwenka for joining my TAC meetings and giving valuable suggestions on my project.

A big thank you goes to Dr. Bernhard Wetterauer, who did a great job in characterizing the plant extracts and was always very supportive and helpful in case of questions.
Dr. Michael Schmiech supported me a lot with the presentation and interpretation of the HPLC-MS/MS data. I really appreciate that he was immediately available when I needed help or if there was a need for discussion.

Concerning the nCounter analysis, I have to thank Prof. Dr. Beate Niesler and Ralph Röth from the nCounter Core Facility for their great support.
I also thank Dr. Carsten Sticht for conducting the pathway analysis and being available for discussion of the data.

Many thanks to Anastasiia Zuieva from Professor Wölfl's lab for helping me to establish the Luciferase reporter assays.

Next, I would like to acknowledge the pleasant working atmosphere in our lab created by all my colleagues. A special thank you goes to Christian, from whom I learned a great deal throughout our work together. Sven, Johanna and Henning I would like to thank for their constant helpfulness. Thank you, Guido, for introducing me to the ImageStream system, helping me with the data analysis and being available for discussions. Divya I would like to thank for proofreading my thesis and the valuable discussions we had.

Beate, I don’t have the words to express how thankful I am for your constant support in every condition of life and the friendship we developed! You made the way to reach this goal so much easier!

I also thank all the other members of the institute, especially Antje, Lisa, Julia, and Marzena for the positive spirit they are spreading.

Last but not least, I would especially like to thank my family and friends for supporting and motivating me, particularly in challenging times. I am truly grateful to each one of you for being part of my life!